

Dissertation zur Erlangung des Doktorgrades der Fakultät für Chemie und
Pharmazie der Ludwig-Maximilians-Universität München

Characterization of a myosin transport complex from yeast



Alexander Heuck
aus Rodewisch i.V.
2009

Erklärung

Diese Dissertation wurde im Sinne von § 13 Abs. 3 bzw. 4 der Promotionsordnung vom 29. Januar 1998 von Herrn Prof. Dr. Ralf-Peter Jansen betreut.

Ehrenwörtliche Versicherung

Diese Dissertation wurde selbstständig, ohne unerlaubte Hilfe erarbeitet.

München, den 23. März 2009

Alexander Heuck

Dissertation eingereicht am 24. März 2009
1. Gutachter: Prof. Dr. Ralf-Peter Jansen
2. Gutachter: Prof. Dr. Karl-Peter Hopfner
Mündliche Prüfung am 20. Mai 2009

ABBREVIATIONS	IV
1. INTRODUCTION	1
1.1 The cytoskeleton	1
1.2 The actin cytoskeleton in yeast	2
1.3 Dynein and kinesin motor proteins	3
1.4 Myosin motor proteins	5
1.5 Type-V myosins.....	6
1.5.1 <i>The motor domain and lever arm</i>	7
1.5.2 <i>The tail domain - the coiled-coil rich region</i>	8
1.5.3 <i>The tail domain - cargo complexes on type-V myosins</i>	8
1.6 Regulation of myosin-adaptor interactions	10
1.7 The yeast type-V myosin Myo4p	10
1.7.1 <i>mRNA transport in yeast</i>	11
1.7.2 <i>Inheritance of the cortical endoplasmic reticulum in yeast</i>	13
1.8 Structure of the Myo2p globular-tail domain	14
1.9 Objectives.....	16
2. RESULTS	17
2.1 Expression and purification of the Myo4p-tail and She3p-N	17
2.2 Myo4p and She3p form stable complexes	17
2.3 The Myo4p-tail can be divided into three parts	18
2.4 The Myo4p-tail contains two distinct binding sites for She3p.....	19
2.5 The coiled-coil region stabilizes Myo4p-She3p complexes.....	20
2.6 The residues 1056 and 1057 of Myo4p are required for She3p binding	21
2.7 The Myo4p-tail is strictly monomeric.....	23
2.8 The Myo4p-tail forms homodimers when linked to artificial dimerization domains	25
2.9 Artificially dimerized Myo4p fragments bind to She3p and form stable complexes	26
2.10 Disruption of Myo4p dimerization results in disassembly of complexes with She3p.....	27
2.11 The globular-tail domain of Myo4p is not required for ER inheritance	28
2.13 The Myo4p globular-tail domain is required for localized <i>ASH1</i> -mRNA translation	29
2.14 The globular tail is required to localize Myo4p at the bud tip	30
2.15 Crystallization of the Myo4p globular tail.....	32
2.16 Structure determination and refinement of the Myo4p globular tail.....	33
2.17 Crystal structure of the Myo4p globular tail.....	34
2.18 Structural comparison of the Myo4p and Myo2p globular-tail domain	36
2.19 The globular-tail domain of Myo4p interacts directly with membranes	39
2.20 Identification of a membrane interacting region within the Myo4p globular tail	40
2.22 Quantification of the Myo4p globular-tail-vesicle interaction	42
2.23 Crystallization of the Myo4p-She3p complex	43

3. DISCUSSION	45
3.1 The oligomerization state of Myo4p	45
3.2 Structure of the Myo4p-She3p complex – an experimental outlook.....	49
3.3 Two binding regions of Myo4p interact with She3p.....	49
3.4 Importance of complex stability for directional transport	51
3.5 The Myo4p globular-tail domain is conserved in terms of fold but not function	51
3.6 The globular-tail domain as a peripheral membrane-binding domain	53
3.7 The function of the globular-tail domain	57
3.7.1 <i>On cortical ER inheritance</i>	57
3.7.2 <i>On mRNA transport</i>	58
3.7.3 <i>Anchoring at the bud tip</i>	59
3.8 Summary	61
4. MATERIALS AND METHODS	62
4.1 Consumables	62
4.2 Plasmid DNA	62
4.2.1 <i>Purchased plasmids</i>	62
4.2.2 <i>Plasmids for E. coli expression (biochemical characterization)</i>	62
4.2.3 <i>Plasmids for E. coli expression (crystallization)</i>	63
4.3 <i>E. coli</i> strains	64
4.4 <i>S. cerevisiae</i> strains	64
4.5 Oligonucleotides.....	64
4.6 Antibodies.....	65
4.7 Molecular biology	66
4.7.1 <i>Standard cloning methods</i>	66
4.7.2 <i>Transformation of E. coli and isolation of plasmid DNA</i>	66
4.7.3 <i>Transformation of yeast cells</i>	66
4.7.4 <i>Isolation of yeast genomic DNA</i>	66
4.8 Protein analysis	67
4.8.1 <i>Protein separation by SDS-PAGE</i>	67
4.8.2 <i>Western blot</i>	67
4.9 Protein expression, purification and crystallization	67
4.9.1 <i>Recombinant protein expression in E. coli</i>	67
4.9.2 <i>Selenomethionine labeling</i>	68
4.9.3 <i>Purification of Myo4p fragments</i>	68
4.9.4 <i>Purification of She3p fragments</i>	69
4.9.5 <i>Crystallization and structure determination of the Myo4p-GT</i>	69
4.9.6 <i>Crystallization of the Myo4p-She3p complex</i>	70
4.10 <i>In vitro</i> characterization of the Myo4p-tail function	70
4.10.1 <i>Ni-pull down</i>	70
4.10.2 <i>Surface Plasmon-Resonance</i>	70
4.10.2.1 <i>Myo4p-She3p-N interaction</i>	70
4.10.2.2 <i>Myo4p-GT vesicle interaction</i>	71
4.10.3 <i>Floatation assay with ER-like protein-free liposomes</i>	71
4.10.3.1 <i>Preparation of protein free Liposomes</i>	71
4.10.3.2 <i>In vitro binding and floatation of liposomes</i>	71
4.10.4 <i>Reflectometric Interference Spectroscopy</i>	71

TABLE OF CONTENTS

4.11. Fluorescence microscopy.....	72
4.11.1 <i>Preparation of cells for Immunofluorescence microscopy</i>	72
4.11.2 <i>Preparation of cells for fluorescence microscopy</i>	72
4.11.3 <i>Fluorescence microscopy</i>	72
4.12. Bioinformatics.....	73
4.12.1 <i>Homology searches and alignments</i>	73
4.12.2 <i>Protein parameters</i>	73
4.12.3 <i>Structure visualization and analysis</i>	74
5. LITERATURE	75
ACKNOWLEDGMENT	89
CURRICULUM VITAE	90

Abbreviations

%	per cent	LMU	Ludwig-Maximilian University Munich
°C	degree celsius	M	molar
μ	micro	min	minute
Å	angstrom	mRNA	messenger Ribonucleic acid
A ₂₆₀	absorption at 260 nm	n	nano
aa	amino acid	n.d.	not determined
AUC	analytical ultra centrifugation	NaCl	Sodium Chloride
cm	Centimetre	NCS	NonCrystallographic Symmetry
Conc	Concentration	Ni	Nickel
Da	Dalton	ORF	open reading frame
DAPI	4',6-diamidino-2-phenylindole	PAGE	polyacrylamide gel electrophoresis
DNA	Deoxyribonucleic acid	PEG	Polyethylene glycol
Dr	Doctor	Prof	professor
<i>E.coli</i>	<i>Escherichia coli</i>	Pt	Platine
ER	endoplasmatic reticulum	RfS	Reflectometric Interference Spectroscopy
g	gram	R _{max1/2}	complex half-life time
GFP	Green Fluorescence Protein	RMSD	root-mean-square deviation
GST	Glutathion-S-Transferase	RNA	Ribonucleic acid
GT	globular tail	RU	Response Unit
h	hours	S	Svedberg
H	helix	s	second
His	Histidine	SAD	single anomalous diffraction
I	Intensity	SDS	Sodium Dodecyl Sulfate
ITC	isothermal titration calorimetry	SeMet	Selenomethionine
k	kilo	SPR	surface plasmon resonance
K _d	Equilibrium-dissociation constants	TCA	Trichloroacetic acid
K _{off}	off rates	TLS	Twin Lattice Symmetry#
K _{on}	on rates	WT	wild type
l	litre	σ	sigma
A	Alanine	I	Isoleucine
C	Cysteine	K	Lysine
D	Aspartic acid	R	Arginine
F	Phenylalanine	W	Tryptophane
H	Histidine	Y	Tyrosine

1. Introduction

The cytoskeleton is a cellular key component that ensures cell stability and intracellular organization. It helps to maintain the cell shape and to generate physical robustness, especially in cells lacking a cell wall. Within the cell, the cytoskeleton is required to place organelles at certain positions, to enable directed transport of molecules, or to generate force. Many of these functions require the activity of motor proteins, which travel along the filaments like on railways. Thereby, they are able to transport or position all different kinds of cargoes, even against concentration gradients. The work presented here, aims at a deeper understanding of how such motor proteins specifically recognize their cargoes towards the assembly of transport-complexes.

1.1 The cytoskeleton

In eukaryotic cells, microtubules and actin filaments (also called microfilaments) are the components of the cytoskeleton that serve as tracks for motor proteins. Microtubules are involved in mitotic spindle orientation, in cellular motility, and in intracellular transport processes. In contrast, the majority of actin filaments are accumulated below the plasma membrane, fulfilling mainly stabilizing functions. Furthermore, actin filaments form the contractile ring during cell division, and also participate in intracellular transport (Moseley and Goode 2006).

The architectures of microtubules and actin filaments share some basic properties. Both are formed by a linear array of globular proteins. Heterodimers of alpha- and beta-tubulin form the microtubule protofilaments, while microfilaments are composed of repeating actin units. The filament assembly by a repetition of small subunits guarantees both, a high stability and flexible filament architecture. Spatial flexibility is achieved because the individual subunits can diffuse rapidly throughout the cell, thereby enabling filament formation or elongation at every intracellular region.

It is of great importance for functionality that the microtubules and actin filaments provide an intrinsic asymmetry. Consequently, the protofilaments have distinguishable end points, which are referred to as plus and minus ends. Motor proteins that bind to these filaments recognize the polarity and are able to move specifically towards one of both end points (for details see chapter 1.3 and 1.4) (Alberts *et al.* 2003).

1.2 The actin cytoskeleton in yeast

To understand the special functions and properties of microfilaments in *Saccharomyces cerevisiae* (*S. cerevisiae*), essential information about the specific features of cell growth and division in budding yeast will be summarized below. Budding yeast undergoes an asymmetric cell division, with a smaller daughter cell (the bud) growing out of the mother cell at a distinct region. The bud emerges in late G1 cell-cycle stage, followed by a phase, where cell growth is restricted to the bud tip. Later, in stage G2, the bud starts to grow isotropically along the whole surface, until it reaches the mother-cell size. At this point, the daughter is separated from the mother cell by a septum formed at the bud neck.

In *S. cerevisiae*, microfilaments are enriched in three distinct structures: i) in cortical spots or patches, ii) in a collar-like structure at the bud neck axis (the contractile ring) and iii) in long fibers or cables spanning along the cell axis (figure 1.1) (Moseley and Goode 2006).

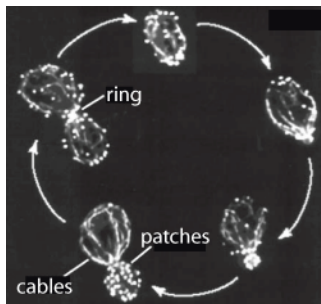


Figure 1.1

Organization of the actin cytoskeleton in *S. cerevisiae*

Three actin structures are visible in yeast cells, when analyzing different cell cycle stages: cortical actin patches, polarized actin cables, and the cytokinetic actin ring. Patches and cables are stable throughout the cell cycle, whereas the ring is only visible during cytokinesis. The figure is taken from (Moseley and Goode (Moseley and Goode 2006) and shows fixed yeast cells, stained with rhodamine phalloidin.

Patches are multi-protein complexes that are involved in endocytosis and accumulate at sites of polarized growth (Ayscough 2005). In endocytosis, actin patches play an active role in vesicle budding. This process requires the actin nucleation complex formed by Arp2/3p (Huckaba *et al.* 2004), but is independent of myosin-motor proteins (Smith *et al.* 2001, Waddle *et al.* 1996). It is likely that the filament motility directly helps to separate vesicles from the plasma membrane (Kaksonen *et al.* 2003). Subsequently, the vesicles are transported towards endosomal sorting compartments. This transport is also linked to actin filaments but seems to be independent of motor-protein activity (Huckaba *et al.* 2004, Kaksonen *et al.* 2003, Pelham and Chang 2001).

The second actin structure found in budding yeast is the contractile ring that spans around the bud-neck axis. Contractile rings are conserved throughout all animals and fungi and help to separate mother and daughter cells during cytokinesis (Moseley and Goode 2006). In yeast the contractile-ring formation depends on the accumulation of a septin scaffold (Lippincott and Li 1998), which recruits most of the factors required for cytokinesis, including actin (Longtine and Bi 2003). During cytokinesis the contractile ring seems to contract actively in a motor-protein (Myo1p) dependent manner (Lippincott and Li 1998), which narrows the bud neck border and

supports cytokinesis. However, contracting the ring does not seem to be essential to complete cytokinesis (Bi *et al.* 1998).

Finally, the third microfilaments-containing structure present in budding yeast is actin cables. The actin cables reach from the bud deep into the mother cell. Each cable is composed of multiple actin filaments, organized into bundles of uniform polarity. To maintain this structure, the cables are covered with bundling proteins (Asakura *et al.* 1998, Drubin *et al.* 1988). Actin cables serve as tracks for myosin-motor proteins. During budding, they travel towards the filaments plus ends at the bud tip. Among their several cargoes, these motors transport vesicles, mRNAs and organelles from the mother cell into the bud (Moseley and Goode 2006). Later in cell cycle, the cables appear to be rearranged, so that their ends are pointing towards the bud neck. This supports cell-wall formation to divide both mother and daughter cell to complete cytokinesis.

Actin cables are generated when polarity factors assemble at the future bud site and form the cable-generating complex (Moseley and Goode 2006). Once the complex is formed, it locates at the bud tip and neck. Essential components of the complex are formins (Sagot *et al.* 2002), and profilin (Evangelista *et al.* 2002, Sagot *et al.* 2002). These proteins bind to the fast growing ends of actin filaments and support their polymerization. However, cable elongation seems to be independent of the Arp2/3p complex (Evangelista *et al.* 2002).

1.3 Dynein and kinesin motor proteins

In total there are three different classes of motor proteins: dynein, kinesins and myosins. In terms of the molecular weight, cytoplasmic dynein is the largest among all motor proteins. Dynein forms homodimers and travels towards the minus end of microtubules (Hirokawa 1998, Hook and Vallee 2006, Vale 2003). The core of the dynein-motor protein is formed by the dynein-heavy chain (DHC), which includes the entire motor domain (figure 1.2). This motor domain contains four ATP-binding domains, whose ATPase activities are coupled. Consequently, there are several possibilities to regulate the motor activity (Kon *et al.* 2004, Mallik and Gross 2004). Furthermore, the DHC binds to additional regulatory light chains (Hirokawa 1998, Kini and Collins 2001, Vallee *et al.* 2004, Vaughan *et al.* 2001). Cytoplasmic dynein is not only the largest among all motor proteins, but also the most complex one. There are numberless possibilities for regulation, making the identification of general principles, how this motor protein binds to its cargo molecules, very difficult.

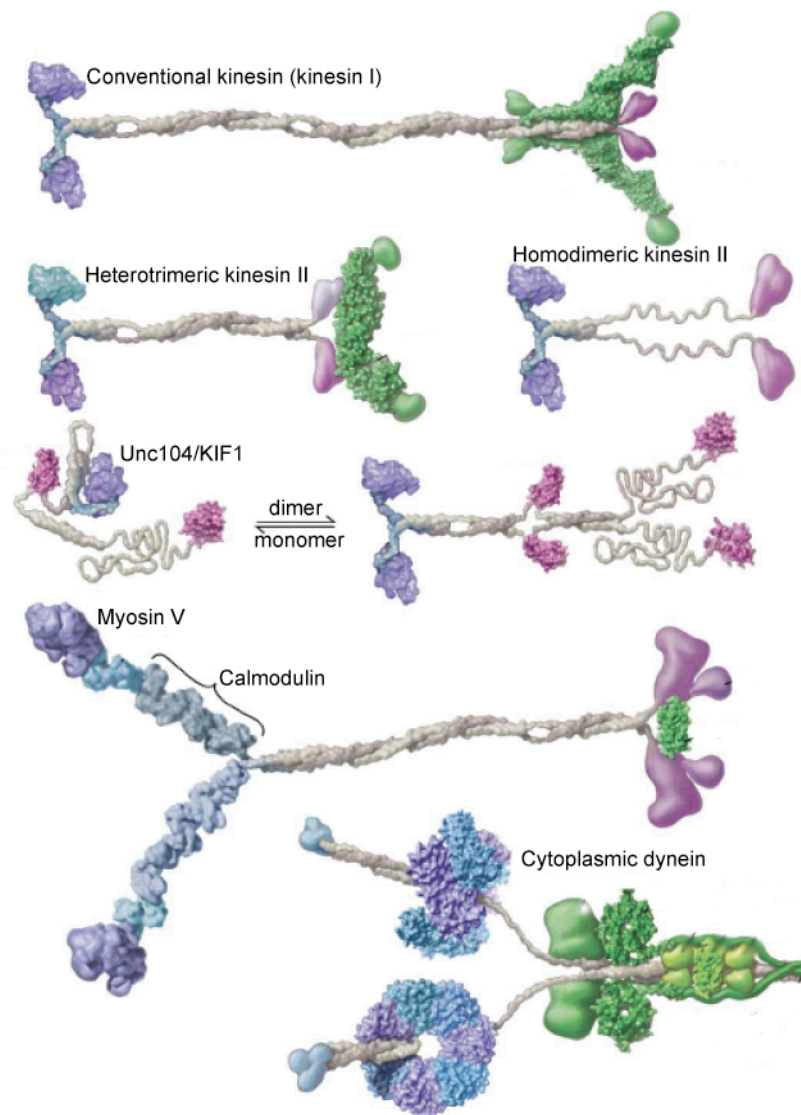


Figure 1.2

Selection of cargo-transporting motor proteins

The picture is taken from Vale 2003 (Vale 2003). Generally, catalytic motor domains are shown in blue, mechanical amplifiers such as light chains in light blue, coiled-coil regions in beige and tail domains that are implicated in cargo attachment are shown in purple. The kinesin motor Unc014/KIF1 can exist as a monomer and dimer.

Kinesin motor proteins represent the second class of microtubule-dependent motor proteins. Over the time, many different kinesin genes have evolved, which are classified into 14 subclasses (Lawrence *et al.* 2004). Kinesins contain a motor domain, a filamentous stalk region and a globular tail. In general, the motor represents the domain with the highest conservation. Most kinesin subclasses form homodimers, but there are also exceptions, which act as monomers or heterodimers with other kinesin subclasses (figure 1.2) (Miki *et al.* 2005).

The motor domain can be located at different positions in the polypeptide chain and the position of the motor domain defines the directionality of the motor protein. However, the majority of the kinesin subclasses have their motor at the N-terminus and travel towards the

microtubules plus-end (Miki *et al.* 2005). Kinesins bind their respective cargo mainly with the help of their globular-tail domain or rather indirectly by additional light chains (Hirokawa *et al.* 1989, Miki *et al.* 2005).

1.4 Myosin motor proteins

Myosin-motor proteins are highly conserved within eukaryotic cells and fulfill a vast number of different functions. The first myosin proteins had been isolated from muscle tissue (Warrick and Spudich 1987). This filament-forming myosin subclass is referred to as conventional myosin. The later identified, non-muscular and non-filamentous myosins are called unconventional myosins (Warrick and Spudich 1987). Since the present work analyzes myosin-mediated transport, it focuses on unconventional myosins only.

Myosins consist of three distinct regions: an N-terminal motor domain mediating the interaction with actin filaments and catalyzing ATP hydrolysis, a regulatory neck region, and a C-terminal tail that is responsible for cargo recognition and/or motor dimerization (figure 1.2). In contrast to the motor domain, which is conserved throughout all myosin classes, the tail domains are highly divergent in their sequence and domain composition (Krendel and Mooseker 2005). The myosin superfamily is divided into approximately 20 classes, mainly dependent on differences and similarities in their tail organization. The majority of these classes can be found within almost all eukaryotic cells and just a few exceptions with a specialized occurrence are known. For example the myosin classes III and VI are exclusively found in metazoans, and the classes X and XVI are restricted to vertebrates. Myosin VIII, XI, and XIII are solely expressed in plants (Berg *et al.* 2001, Krendel and Mooseker 2005).

In terms of directionality it was shown that almost all myosins, except those from class VI (Myo-VI), "walk" towards the plus ends of actin filaments. The reason why Myo-VI travels to the filaments minus end is not depending upon its motor domain but on a short insertion in the lever arm (Park *et al.* 2007, Wells *et al.* 1999). Furthermore, also for the myosin class IX an anomalous directionality was observed. This myosin subclass is capable to travel towards both ends of the actin filament (Inoue *et al.* 2002, O'Connell and Mooseker 2003).

The myosin tail is generally formed by a coiled-coil dimerization- and a globular part at the very C-terminus. The potential of the coiled-coil region to dimerize the myosin (heavy) chains varies between the different subclasses. Some classes like Myo-V are described to form stable dimers by their coiled-coil domains, while members of classes -I, -VI or -IX were shown to be single headed, although they also contain regions predicted to form coiled-coils (Krendel and Mooseker 2005, Reck-Peterson *et al.* 2000, Warrick and Spudich 1987). In contrast, Myo-VII forms homodimers, but this interaction is independent from the coiled-coil region (Inoue and Ikebe 2003). Some of the myosin subclasses, which were identified to be monomeric, can dimerize with the help of additional factors. In the case of Myo-VI it was shown that the motor

dimerizes as a consequence of cargo binding. Although monomeric Myo-VI is not processive, this cargo-dependent dimerization results in processive movement of Myo-VI motors along actin filaments, (Iwaki *et al.* 2006, Park *et al.* 2006). Nevertheless, some other myosins do not require dimerization for processivity. Myo-IX for example is a strictly single-headed motor that catalyzes processive movement along actin filaments (Inoue *et al.* 2002, Post *et al.* 2002).

The C-terminal tails of the various myosin subclasses differ not only in regard to their coiled-coil region, but also with respect to their globular domains, which also evolved individual functions and properties. The globular-tail domains generally mediate protein-protein interactions (Krendel and Mooseker 2005). Within the myosin superfamily, additional functions have emerged for the globular tail. For example, the globular tail of the *Drosophila* Myo-III has an intrinsic kinase activity (Komaba *et al.* 2003), and may fulfill a direct role in signal transduction. Similarly, Myo-IX was shown to contain a GTPase-activating domain for Rho coupled G-proteins (Post *et al.* 1998, Reinhard *et al.* 1995, Vreugde *et al.* 2006). Myo-VI is involved in a large number of different functions. This myosin motor is active in the nucleus, where it enhances polymerase-II transcription (Vreugde *et al.* 2006). Furthermore it interacts directly with membranes, as a peripheral membrane protein. The binding to membranes is mediated by specific interactions of the globular tail with Phosphatidylinositol-4, 5-bisphosphate (PtdIns(4,5)P₂) (Spudich *et al.* 2007).

1.5 Type-V myosins

Type-V myosins are conserved from yeast to human. Different organisms carry a varying number of Myo-V genes. While the *S. cerevisiae* genome contains two homologs (*MYO2* and *MYO4*), vertebrates have even up to three distinct genes (*MYOVa*, *MYOVb*, and *MYOVc*) (Reck-Peterson *et al.* 2000). The respective expression pattern of these three distinct vertebrate genes is different, albeit with some overlap (Bement *et al.* 1994). Besides the myosin classes -I and -II, type-V myosin is the best characterized class of myosin proteins and was the first example for processive actin-based motors (Mehta *et al.* 1999). In the cell, type-V myosins catalyze the continuous transport of organelles, membranous cargoes, secretory vesicles, mRNA, and lipids (Reck-Peterson *et al.* 2000). All type-V myosins share a common architecture, containing an N-terminal motor domain, a regulatory lever arm and a C-terminal cargo interaction domain. Beside these unifying features, they also show considerable differences, for example regarding their cargo binding and processivity (Mehta *et al.* 1999, Reck-Peterson *et al.* 2001).

1.5.1 The motor domain and lever arm

Type-V myosins have an N-terminal motor domain, with one ATP- and one actin- binding site (Cope *et al.* 1996), and the motor domain includes variable loop regions, which may define the processivity of the motor protein (Reck-Peterson *et al.* 2000). Linked to the motor is a regulatory neck region with six IQ-motifs that serve mainly as binding sites for calmodulin (CaM) (Espreafico *et al.* 1992, Mercer *et al.* 1991). CaM binding regulates the stiffness of the neck region, which has a direct influence on the motors step length along the actin filament (Uyeda *et al.* 1996). Furthermore, CaM binding is necessary for catalytic activity (Krementsov *et al.* 2004). CaM binds to the neck domain at low Ca^{2+} levels or even in absence of Ca^{2+} . However, in a Ca^{2+} free situation the tail domain of chicken MyoVa binds to the motor domain and thereby generates an inactive, compact conformation (figure 1.3) (Krementsov *et al.* 2004, Liu *et al.* 2006, Wang *et al.* 2004). This inhibition becomes released at Ca^{2+} concentrations in the lower micromolar (μM) range, leading to an activation of the motor. On the other hand, exceeding Ca^{2+} concentrations in the millimolar (mM) range lead to a dissociation of CaM from the motor, which in turn acts as a break to stop the motor activity (Krementsov *et al.* 2004, Lu *et al.* 2006). Equally important is an activation mechanism where the motor inhibition by the tail domain is released upon cargo binding (Thirumurugan *et al.* 2006).

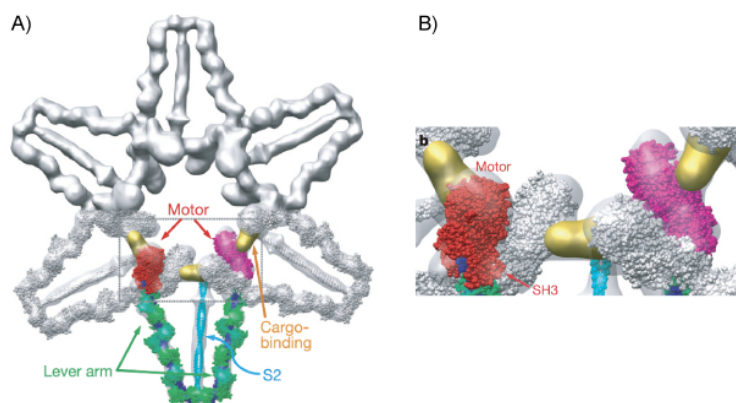


Figure 1.3

Low-resolution structure of the inhibited state of MyoVa

A) Averaged electron micrographs of MyoVa in the inhibited state. The picture is taken from Liu *et al.* (Liu *et al.* 2006). The lower part represents the MyoVa atomic model rendered in space filling. The color scheme is the following: motor domains red and magenta, light chains green, heavy chain component of the lever arm blue, the coiled-coil domain cyan and density envelopes for the cargo-binding domain yellow. Adjacent molecules are shown in gray. B) The interaction surface of the motor domain and the tail domain are shown with higher magnification. The resolution of the shown structure was calculated to be 24 Å.

A) Averaged electron micrographs of MyoVa in the inhibited state. The picture is taken from Liu *et al.* (Liu *et al.* 2006). The lower part represents the MyoVa atomic model rendered in space filling. The color scheme is the following: motor domains red and magenta, light chains green, heavy chain component of the lever arm blue, the coiled-coil domain cyan and density envelopes for the cargo-binding domain yellow. Adjacent molecules are shown in gray. B) The interaction surface of the motor domain and the tail domain are shown with higher magnification. The resolution of the shown structure was calculated to be 24 Å.

1.5.2 The tail domain - the coiled-coil rich region

Most cargo molecules bind type-V myosins at the C-terminal tail domain. Structurally, the tail domain consists of a coiled-coil region of varying length, followed by a globular domain. It is generally assumed that the coiled-coil region is responsible for the formation of myosin dimers. Consistently, Myo-V dimerization was directly observed by electron microscopy (Cheney *et al.* 1993).

In higher eukaryotes, the coiled-coil region of type-V myosins is alternatively spliced. The tail domain of mice MyoVa is composed of the exons A to G (Au and Huang 2002). From these exons, the exons B, D and F are tissue dependently spliced (Seperack *et al.* 1995). The resulting splice forms have different cargo specificities. For example, the presence of exon B is a prerequisite for dynein light chain (DLC) binding to mouse MyoVa. DLC association stabilizes MyoVa dimers (Hodi *et al.* 2006) and generates additional interaction sites for regulatory proteins, like the pro-apoptotic protein Bmf (bcl-2-modifying factor) and the postsynaptic scaffolding protein GKAP (guanylate kinase associated protein) (Naisbitt *et al.* 2000, Puthalakath *et al.* 2001). Additionally, exon F forms one out of two binding sites for melanophilin, which links the motor protein to melanosomes (Fukuda and Kuroda 2004, Wu *et al.* 2002). The binding of melanophilin to MyoVa is further described in the next chapter (chapter 1.5.3).

1.5.3 The tail domain - cargo complexes on type-V myosins

Over the years, several cargoes of type-V myosins have been identified and great progress has been made in the understanding of how these cargoes are connected to the motor protein. First insights, which described the role of the myosin-tail domains in cargo binding, came from dilute mutant mice. These mice show a pale, or "dilute", hair color and neurological defects (Mercer *et al.* 1991). The observed color phenotype could be backtracked to failures in melanosome transport, leading to melanosomes clustering around the nucleus (Provance *et al.* 1996, Wei *et al.* 1997). Several lines of evidence confirmed a direct role of the globular-tail domain in melanosome transport. Overexpression of the MyoVa-tail domain results in the dilute phenotype, as do some specific mutations within this domain (Huang *et al.* 1998, Wu *et al.* 1998). Furthermore, individually expressed tail domains were observed to localize together with melanosomes (Wu *et al.* 1998). Today, the architecture of the melanosome translocation complex is well characterized. MyoVa binds directly to the adapter protein melanophilin. For this interaction melanophilin binds to two distinct regions in the MyoVa tail. One of these regions is located in the coiled-coil region and the other within the globular-tail domain (Fukuda and Kuroda 2004). Melanophilin itself links the motor protein to melanosomes by the interaction with Rab27a (Kukimoto-Niino *et al.* 2008), a peripheral membrane protein, which is

anchored at melanosomes via a di-geranylgeranyl modification (Gomes *et al.* 2003). The interaction of Rab27a with melanophilin depends on the binding of GTP to Rab27a, which regulates the whole transport event (Wu *et al.* 2002). The basic translocation complex of MyoVa, melanophilin, and Rab27a could be reconstituted *in vitro* and was shown to move processively along actin filaments (Wu *et al.* 2006).

Another Rab protein, which is involved in Myo-V dependent transport, is Rab11a. Rab11a was shown to associate with both mice MyoVa and -Vb, and with all their splice variants (Roland *et al.* 2009). The association of Rab11a to MyoVa is necessary for the transport of AMPA receptors into dendritic spines (Correia *et al.* 2008). Furthermore Rab11a is linked to the recycling of endosomes, one cargo of MyoVb. In this complex, the linkage of MyoVb with Rab11a is mediated via the adapter protein Rab11-FIP2 (Hales *et al.* 2002, Lapierre *et al.* 2001). Recently, a homologue of the Rab11 class of proteins, termed Ypt32p, was found to interact directly with Myo2p in budding yeast. The interaction of Ypt32p with the motor is a requirement for the transport of secretory vesicles into the bud. Ypt32p binds to the globular tail of Myo2p at a region, which was earlier identified as the secretory vesicles binding region (Casavola *et al.* 2008, Lipatova *et al.* 2008, Pashkova *et al.* 2006). This region is conserved from yeast Myo2p to mammalian MyoVa, and it is tempting to speculate that also Rab11a binds to MyoVa at this region.

In *S. cerevisiae*, Myo2p also transports the vacuole into the emerging bud. For vacuole inheritance, Myo2p binds with its globular-tail domain to the adapter protein Vac17p, which links the myosin motor to Vac8p, a peripheral membrane protein in the vacuole membrane (Ishikawa *et al.* 2003, Tang *et al.* 2003). Furthermore, Myo2p is involved in the transport of peroxisomes, a mechanism that requires the adapter protein Inp2p (Fagarasanu *et al.* 2006). Myo2p also helps to position the mitotic spindle. For this function, the Myo2p globular tail binds to Kar9p. Kar9p in turn interacts with Bim1p that links the myosin complex to microtubules (Beach *et al.* 2000). Other cargoes moved by Myo2p are mitochondria (Altmann *et al.* 2008) and large ribonucleic acid-protein complexes (Chang *et al.* 2008). However, the exact mechanism of how all these proteins are associated to Myo2p is still poorly understood.

Besides Myo2p, an additional type-V myosin is present in yeast, Myo4p. Myo4p translocates several mRNAs into the bud. This leads among other effects to the establishment of different mating types between daughter and mother in haploid yeast cells. Furthermore, Myo4p is responsible for the inheritance of the cortical endoplasmic reticulum (ER) (Estrada *et al.* 2003, Jansen *et al.* 1996). Both functions will be described in more detail in chapter 1.7.

1.6 Regulation of myosin-adapter interactions

So far, two regulatory mechanisms were described for the interaction of type-V myosins with their adapters, phosphorylation and protein turnover. In budding yeast, the transport of almost all Myo2p cargoes depends on the protein phosphatase Ptc1p, which seems to have a stabilizing effect on the Myo2p adapter proteins (Jin *et al.* 2008). Furthermore, for the Myo2p-dependent vacuole transport it was shown that a phosphorylation of the adapter stabilizes the vacuole-motor association (Peng and Weisman 2008). The Myo2p tail domain is also a direct target for phosphorylation. However, phosphorylation of Myo2p does not seem to have a direct influence on its catalytic activity (Legesse-Miller *et al.* 2006). In addition, Ptc1p has a regulatory effect on Myo4p-dependent transport. However, the detailed mechanism underlying the regulation of Ptc1p on mRNA and cortical-ER transport remains elusive.

A phosphorylation-dependent regulation could also be observed for MyoVa from *Xenopus* oocytes. In these oocytes, phosphorylated MyoVa dissociates from melanosomes, while a significantly reduced phosphorylation level enables efficient binding (Rogers *et al.* 1999).

Besides phosphorylation, type-V myosin-dependent transport is also regulated by protein turnover. Several adapter proteins contain so-called PEST sequences. These are regions with an enriched occurrence of the residues proline, glutamate, serine, threonine and to a lower extent aspartate. PEST sequences represent signals for rapid protein degradation (Rogers *et al.* 1986). The vacuole adapter protein Vac17p contains PEST sequences and degradation of Vac17p is necessary to remove the motor from the vacuole (Tang *et al.* 2003). Melanophilin also contains multiple PEST sequences in the MyoVa binding domain. Mutations of these sequences lead to an increased protein stability (Fukuda and Itoh 2004). Furthermore, PEST sequences are present in the tail domain of almost all vertebrate Myo-V genes. In chicken MyoVa it could be shown that this site is sensitive to proteolysis (Espindola *et al.* 1992, Nascimento *et al.* 1997). For Myo4p from yeast, a PEST site is even found in the motor domain (Haarer *et al.* 1994).

1.7 The yeast type-V myosin Myo4p

The yeast type-V myosin Myo4p represents an excellent model to investigate the molecular mechanisms underlying motor-adapter protein interactions. Myo4p directly binds to the adapter protein She3p and their interaction is fundamental for all functions of the motor protein, especially since other adapter proteins have not been identified for Myo4p. The following chapters give a short introduction into the biological importance of Myo4p and She3p.

1.7.1 mRNA transport in yeast

Today, one of the best characterized examples for motor-protein dependent mRNA translocation is the transport of the *ASH1 mRNA* in budding yeast. *ASH1* codes for Ash1p, a transcription inhibitor that specifically suppresses the expression of the HO endonuclease. This nuclease catalyzes the recombination of genomic DNA at the *MAT* locus, thereby promoting the mating-type switch in haploid yeast cells (Cosma 2004). *ASH1* mRNA is transcribed in the mother nucleus. From there it is actively transported into the bud. During the transport, the mRNA is translationally silenced and becomes activated just after the anchoring at the bud tip (Deng *et al.* 2008, Paquin *et al.* 2007). As a consequence, Ash1p is exclusively present in the bud repressing the HO endonuclease (Bobola *et al.* 1996, Jansen *et al.* 1996, Sil and Herskowitz 1996). Thus, although *ASH1* mRNA is synthesized in the mother nucleus, mating-type switching only occurs in the mother cell.

Mutational experiments and studies disrupting the actin cytoskeleton revealed that *ASH1*-mRNA transport requires actin cables and the activity of the type-V myosin Myo4p (Jansen *et al.* 1996, Long *et al.* 1997, Takizawa *et al.* 1997). The mRNA translocation machinery mainly depends on three core components: the motor protein Myo4p, providing the motile activity, She2p, a specific RNA-binding protein, and She3p, the adapter protein linking Myo4p with She2p (figure 1.4) (Böhl *et al.* 2000, Jansen *et al.* 1996, Long *et al.* 2000, Munchow *et al.* 1999, Takizawa and Vale 2000). These three proteins form the basis of the transport complex, which transports besides *ASH1* mRNA up to 30 additional transcripts into the bud. Several of these transcripts encode for trans-membrane proteins (Shepard *et al.* 2003). Selectivity for transported mRNAs is achieved by She2p, which recognizes distinct stem-loop structures on its RNA targets (Böhl *et al.* 2000, Chartrand *et al.* 2002, Olivier *et al.* 2005). These stem-loop structures are termed localization or zip-code elements.

Besides the composition of the translocation particle, no detailed information is available on how the *ASH1*-mRNA-translocation particles are assembled. Recently, it was found that the RNA binding protein She2p shuttles through the nucleolus of the mother cell, and that this shuttling is necessary to guarantee translational silencing of the mRNA transcript during the transport (Du *et al.* 2008, Shen *et al.* 2009). It is thought that She2p recognizes its target mRNA within the mother cell nucleus. After the complex is exported from the nucleus, the adapter protein She3p binds She2p. The binding region for She2p is located in the C-terminal half of She3p, while the N-terminal part of the adapter interacts with the tail domain of Myo4p (Böhl *et al.* 2000). Finally, the assembled complex translocates into the bud and is subsequently anchored at the bud tip. The binding of She3p to Myo4p is a prerequisite for the transport. Cells lacking She3p show a random distribution of all components of the translocation complex, including Myo4p (Jansen *et al.* 1996).

Furthermore, the nucleolar protein Loc1p was identified to bind to *ASH1* mRNA and to be involved in ribosome biogenesis (Long *et al.* 2001, Urbinati *et al.* 2006). Cells lacking Loc1p show failures in translational repression of *ASH1* mRNA in the mother cell (Komili *et al.* 2007). The exact mechanism how Loc1p controls translation remains unknown. But it was hypothesized that Loc1 helps to generate a certain ribosome subtype, which may be necessary for translation regulation (Komili *et al.* 2007). Other factors, found to be involved in the translational control of *ASH1* mRNA are the cytoplasmic RNA-binding proteins Khd1p and Puf6p (Deng *et al.* 2008, Gu *et al.* 2004, Hasegawa *et al.* 2008, Irie *et al.* 2002). These proteins directly interfere with ribosomal initiation factors and their function in translational control is regulated via phosphorylation (Deng *et al.* 2008, Paquin *et al.* 2007). These findings represent the first concrete example of how *Ash1p* synthesis is regulated by intracellular signaling.

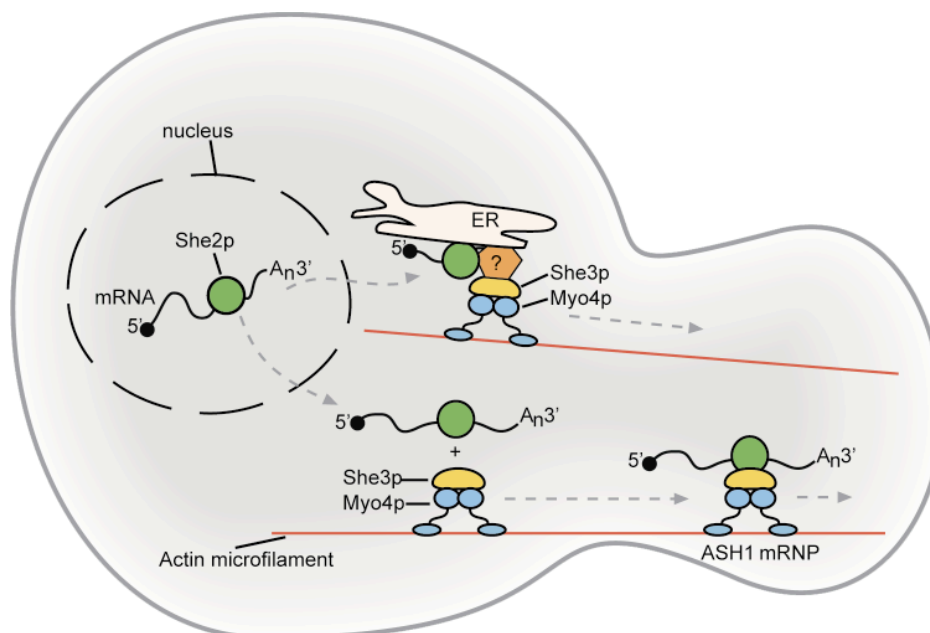


Figure 1.4
Functions of Myo4p

Shown is a dividing yeast cell with the outgrowing bud at the right side. The motor protein Myo4p (in blue) travels along actin filaments towards the bud tip. Within the cytoplasm, Myo4p is attached to the adapter protein She3p (in yellow). For mRNA transport, She3p binds to the RNA binding protein She2p (in green). The complex of all three proteins together with the mRNA is transported towards the bud. After reaching the bud tip, the complex becomes anchored and translationally activated (Böhl *et al.* 2000, Deng *et al.* 2008, Gonzalez *et al.* 1999, Jansen *et al.* 1996, Long *et al.* 2000, Munchow *et al.* 1999, Paquin *et al.* 2007, Takizawa and Vale 2000). Furthermore, Myo4p is involved in cortical-ER inheritance. For this transport, Myo4p also interacts with She3p, but it is unknown in which way the motor complex is attached to the cortical ER. However, She2p is not necessary for the ER inheritance although it directly associates with the ER membranes (Aronov *et al.* 2007, Estrada *et al.* 2003, Schmid *et al.* 2006).

Besides their function in mRNA transport, Myo4p and She3p are also responsible for the inheritance of the endoplasmic reticulum. This transport is independent of She2p but functions in parallel to mRNA transport (Estrada *et al.* 2003).

1.7.2 Inheritance of the cortical endoplasmic reticulum in yeast

The ER in budding yeast is distributed in two different structures: the perinuclear and the cortical ER (Estrada de Martin *et al.* 2005). As the name suggests, perinuclear ER is located around the nucleus and it is continuous with the nuclear envelope. In contrast, the cortical ER is localized at the cell periphery, just below the plasma membrane. It forms an interconnected tubular network, which shares structural similarity to the ER in higher eukaryotes. Both ER subtypes are connected by large tubules that span through the cytoplasm, forming a single intraluminal space (Koning *et al.* 1993). In contrast to higher eukaryotes, the ER dynamics in yeast depend mainly on the actin cytoskeleton (Prinz *et al.* 2000) and Myo4p catalyzes the inheritance of the cortical ER (Estrada *et al.* 2003). This transport takes place shortly after the bud appears during the early S-phase. The ER migrates towards the bud in elongated tubules that are referred to as “ER segregation structures” (Schmid *et al.* 2006). These structures align along the mother-bud axis before they are actively transported into the daughter cell. After reaching the bud tip, the cortical ER becomes anchored at the plasma membrane, from where it extends throughout the bud and forms a polygonal cortical ER network (Estrada de Martin *et al.* 2005).

In yeast, several proteins were described to be required for the inheritance of the cortical ER and the mechanisms of how these proteins influence the whole process are manifold. It was shown that a knock-out of *ICE2*, coding for an integral membrane protein, strongly affects the overall ER structure and leads to a defective cortical-ER inheritance (Estrada de Martin *et al.* 2005). It seems likely that the observed ER-inheritance defects are rather indirect, due to failures in the ER organization. Similar effects are observed for mutations in *SEC27* that is involved in the membrane exchange between ER and golgi, and for *SRP101* and *SRP102*, both factors targeting proteins into the ER-lumen (Prinz *et al.* 2000). For these three mutants, a defective ER structure was described, accompanied with failures in ER inheritance.

In cells with a deficiency in vesicle anchoring, cortical-ER inheritance is also disturbed (Wiederkehr *et al.* 2003). The exocyst is a complex that was shown to be necessary for tethering secretory vesicles to the plasma membrane (TerBush *et al.* 1996). As a consequence, factors of the exocyst like Sec3p, Sec5p, Sec8p and Exo70p are associated with defects in vesicle anchoring as well as in the cortical-ER inheritance (Wiederkehr *et al.* 2004, Wiederkehr *et al.* 2003). Furthermore, in screens searching for disturbances in ER inheritance, *AUX1* was identified. Since C-terminal deletions in Aux1p lead to vacuole fragmentation and membrane accumulation, this protein seems to have several functions in the structural

maintenance of organelles. A loss of Aux1p does not impair the overall ER structure, but disrupts cortical ER inheritance. The mechanism of how *aux1* mutations are connected to ER inheritance is still unclear (Du *et al.* 2004).

MYO4 knock-out strains as well as strains carrying Myo4p mutants with an inactive motor domain showed defects in ER inheritance and resulted in reduced bud ER levels (Estrada *et al.* 2003). In addition, the transport of cortical ER by Myo4p depends on the presence of the adapter protein She3p (figure 1.4). So far it is unclear, how Myo4p is linked to the ER, but both Myo4p and She3p co-fractionate with the ER membrane, indicating a close association (Estrada *et al.* 2003). In contrast to mRNA transport (see section 1.7.1), neither the RNA-binding protein She2p nor the C-terminus of She3p (the She2p-binding region) are required for cortical ER transport (Estrada *et al.* 2003). However, She2p and its associated mRNAs bind independently from Myo4p and She3p to ER membranes, and the transport of ER and She2p is catalyzed simultaneously (Aronov *et al.* 2007, Schmid *et al.* 2006).

1.8 Structure of the Myo2p globular-tail domain

While this thesis was performed, the laboratory of Lois Weisman published the crystal structure of the Myo2p globular tail (Pashkova *et al.* 2006). This represents the only high-resolution structure of a globular tail from type-V myosins. The structure led to interesting insights into how Myo2p mediates specific cargo interactions. The Myo2p globular tail (figure 1.5) consists of the subdomains I and II, which are connected by a long linker helix. Furthermore, the two subdomains are enclosed by a prominent loop, forming a bracket around the entire globular-tail domain.

Previous mutational analyses identified individual cargo-binding regions within the Myo2p globular tail. The adapter protein for the vacuole transport binds to residues located in subdomain I (Catlett *et al.* 2000), while secretory vesicles are associated with subdomain II (figure 1.5) (Lipatova *et al.* 2008, Pashkova *et al.* 2005, Schott *et al.* 1999). It is interesting to note that the areas for vacuole and secretory-vesicle binding are located at opposite sides of the globular-tail domain. This arrangement allows in principle a simultaneous cargo binding to both binding sites (figure 1.5).

Interference experiments with the Myo2p globular tail revealed interesting insights into the mechanism underlying cargo binding by this domain. In these experiments, the entire globular tail or the respective subdomains were overexpressed in yeast cells. If these overexpressed domains bind efficiently to selected cargo molecules, these cargoes should no longer be available for the binding to endogenous, full-length Myo2p motor and should subsequently not be incorporated in functional transport complexes.

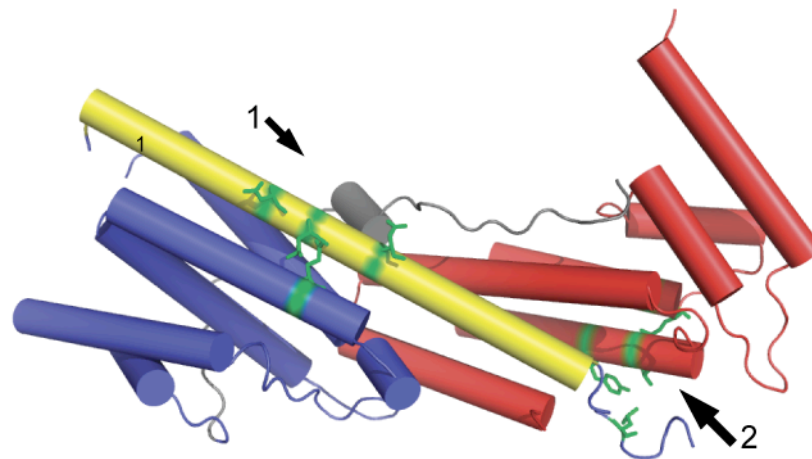


Figure 1.5

Crystal structure of the Myo2p globular-tail domain

Cylinder representation of the globular-tail domain of Myo2p (PDB code 2F6H, Pashkova et al. 2006). The structure is mainly formed by alpha-helical regions. Two subdomains can be distinguished. Subdomain I is highlighted in blue and subdomain II in red, each forming a compact five-helical bundle. Both subdomains are connected by a long linker helix (highlighted in yellow) and a long loop (in gray) that clamps both subdomains together. Residues that were identified to be involved in vacuole binding (arrow 1) and secretory vesicle binding (arrow 2) are highlighted in green (Catlett et al. 2000, Lipatova et al. 2008, Pashkova et al. 2005, Schott et al. 1999). The picture was generated using the program Pymol (DeLano 2002).

The overexpression of the entire globular-tail domain resulted in cell lethality. This is most likely due to failures in the transport of secretory vesicles (Reck-Peterson *et al.* 1999). More interesting were results from experiments, in which both subdomains I and II were overexpressed simultaneously. In contrast to the overexpression of the entire globular-tail domain these cells are viable, indicating a different cargo-binding pattern of the entire globular tail compared with the individual subdomains. This result was rather surprising since the two subdomains were shown to interact closely *in vitro* (Pashkova *et al.* 2005). However, these cells were defective in the transport of the vacuole but not of secretory vesicles. Surprisingly, the vacuole transport was not affected by an exclusive overexpression of subdomain I, although this domain contains all vacuole binding sites identified so far (Pashkova *et al.* 2005). Together, these experiments suggest that the connection of the two subdomains, forming the Myo2p globular tail is important for the binding to the vacuole and the secretory vesicles. However, it is still not possible to comprehend the exact mechanisms of cargo binding by the globular-tail domain of type-V myosins.

1.9 Objectives

Motor protein dependent transport represents a conserved mechanism that is important to establish cell polarity, the generation and maintenance of cell morphology and motility (Lopez de Heredia and Jansen 2004, Vale 2003). The interaction of motor proteins with the cytoskeleton filaments and their force generation towards the catalysis of movement is well understood. However, only little is known about the mechanisms that guarantee specific cargo recognition by these motor proteins. In higher eukaryotes, transport complexes are composed of dozens to hundred different components (mainly mRNAs and proteins) and thus have a rather complex architecture (Angenstein *et al.* 2005, Kanai *et al.* 2004, Villace *et al.* 2004). This high complexity makes the identification of general mechanisms concerning the complex formation very complicated. The present study investigates general principles underlying the generation of specific cargo complexes with the help of a comparable simple and well-defined model system from yeast.

Today, the Myo4p-dependent transport in budding yeast represents one of the best-characterized translocation events. Within this complex Myo4p and its adapter She3p are the essential components for the transport of cortical-endoplasmic reticulum and mRNAs during asymmetric cell division (chapter 1.7 and figure 1.4). Here, the binding of Myo4p to She3p represents a crucial step towards the formation of specific translocation particles. Thus, studying the interaction of Myo4p and She3p might help to obtain detailed insights into general processes of type-V myosin-cargo recognition.

The main focus of this work was the characterization of molecular principles underlying Myo4p-mediated complex assembly with the adapter protein She3p. This study involved biochemical, biophysical, and structural experiments as well as functional studies in living cells. The choice of such a multidisciplinary approach was designed to generate a detailed understanding of the motor-adapter interaction and to provide cross-validation of mechanistic insights from different experimental angles.

2. Results

2.1 Expression and purification of the Myo4p-tail and She3p-N

This study aims to understand the assembly of the intracellular transport complex formed by Myo4p and She3p in budding yeast. Previous studies identified the domains, which mediate the motor-adapter interaction, as the C-terminal tail domain of Myo4p (Myo4p-tail; aa 978-1471) and the N-terminal domain of She3p (She3p-N; aa 1-243) (Böhl *et al.* 2000). In order to characterize their interaction in detail, these fragments were studied with biochemical and biophysical approaches. Recombinant protein fragments of the Myo4p-tail and the N-terminus of She3p were expressed in *Escherichia coli* (*E. coli*) and purified to 95 % purity using standard chromatographic techniques. All details on the purification and the protein constructs used in this study are summarized in the chapters 4.2.2, 4.2.3 and 4.9.

2.2 Myo4p and She3p form stable complexes

For a quantitative assessment of complex formation, the Myo4p-She3p interaction was characterized using Surface Plasmon Resonance. For an SPR experiment, one interaction partner is immobilized to a chip surface (the ligand), and a second protein is floated over the prepared surface (the analyte). Binding of the analyte to the immobilized ligand results in an increase of the response signal that can be traced online. When the equilibrium between complex formation and dissociation is reached, the response signal stops increasing and stabilizes at a certain level. After injection stops, the surface is washed with buffer, resulting in dissociation of the complexes. The dissociation reaction can be traced by the reduction of the response signal over time. Under good experimental conditions, on-rates (K_{on}) and off-rates (K_{off}) can be deduced from these binding experiments. Equilibrium-dissociation constants (K_d) of binding reactions can either be calculated directly from these on- and off-rates ($K_d = K_{off}/K_{on}$) or be deduced from steady state response signals after repeated injections with increasing analyte concentrations and the plot of the equilibrium response signals versus protein concentration (figure 2.1-B and C).

The interaction of the Myo4p-tail fragment (figure 2.1-A) and She3p-N was studied using SPR experiments with She3p-N immobilized to the chip surface and Myo4p-tail as the analyte. Experiments were performed in three replicates and revealed an average K_d of 58 ± 16 nM, indicating a strong interaction (figure 2.1-B and C).

The stability of Myo4p-tail-She3p-N complexes was also assessed. From the dissociation reaction no K_{off} could be calculated, most probably because the complex formation represents a multi step process. Instead, the half-life of the complex was deduced directly from the time point at which the response level dropped to the half-maximal value. For the Myo4p-tail-She3p-N

complex an average half-life time ($R_{\max 1/2}$) of 52 ± 26 s was measured (figure 2.1-D). It has to be mentioned that in these experiments the measured half-life was dependent on the analyte concentration. In order to determine a representative value for the complex stability, dissociation curves from varying concentrations were analyzed, resulting in a relatively large standard deviation.

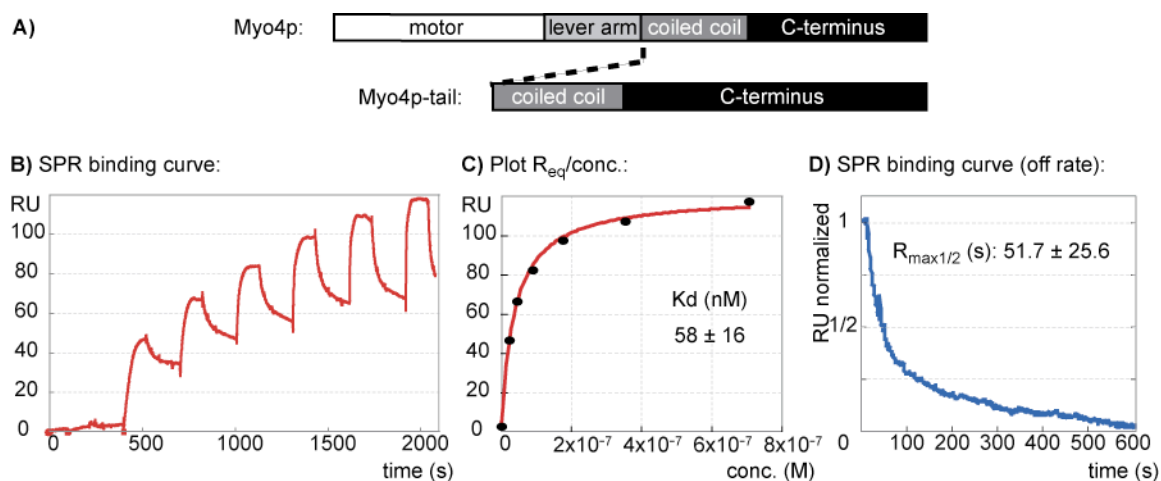


Figure 2.1

SPR analysis of the Myo4p-tail-She3p-N interactions

A) Cartoon representation of the Myo4p-tail fragment used in the experiment. B) Representation of a typical SPR response curve of She3p-N and Myo4p-tail interaction from a multi-injection experiment. RU indicates the measured SPR signal in response units. C) Plot of the response units at equilibrium against the respective Myo4p-tail concentrations. The curve was fitted using the langmuir isotherm (red curve) to obtain the equilibrium-dissociation constant of the interaction. The depicted dissociation constant ($K_d = 58 \pm 16$ nM) indicates the mean value of three independent experiments. D) The response signal over time during complex dissociation is shown. Response units were normalized and used to determine the time point, at which half the complexes were disassembled ($R_{\max 1/2}$). The complex-half-life time of 51.7 ± 25.6 s represents the mean value from three independent experiments. \pm is indicating the standard deviation.

2.3 The Myo4p-tail can be divided into three parts

Previous studies identified the globular, C-terminal tail domain of Myo2p as the main binding site for several adapter proteins (see chapter 1.5.3, 1.6 and 1.8). Since a similar behavior is also assumed for Myo4p, the corresponding globular domain of the Myo4p-tail was identified.

For this, purpose a limited proteolysis experiment was performed with 50 μ g of the Myo4p-tail and 0.5 μ g of the endoproteinase Glu-C (figure 2.2-A). The reaction revealed a stable, protease resistant fragment of approximately 45 kDa. EDMAN sequencing identified the N-terminus of this cleavage product as residue 1091 of the Myo4p sequence. Combining this result with secondary-structure predictions revealed that the Myo4p-tail can be subdivided into three parts, a potential N-terminal coiled-coil domain, the C-terminal cleavage product (the globular tail) and a rather unstructured region (the rod domain), linking the coiled-coil with the globular tail (figure 2.2-B).

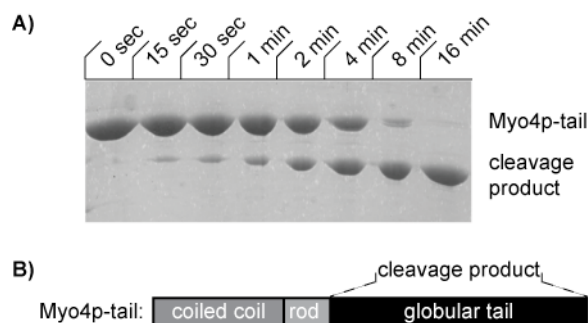


Figure 2.2

Limited proteolysis of the Myo4p-tail

A) After proteolysis with the protease Glu-C, a stable cleavage product of approximately 45 kDa was observed by SDS-PAGE. B) Subsequent EDMAN sequencing revealed the N-terminus of the cleavage product as residue 1091 of the Myo4p sequence. Given that the coiled-coil region is predicted to range from residues 978-1042, the Myo4p-tail can be subdivided into the three domains: the coiled-coil, a protease sensitive rod region, and the protease resistant cleavage product, indicated as the globular tail.

2.4 The Myo4p-tail contains two distinct binding sites for She3p

To locate the She3p binding region within the Myo4p-tail, different Myo4p constructs were generated and tested for their ability to interact with She3p-N. Constructs consisting of the isolated coiled-coil domain (Myo4p-CC; aa 978-1042), the globular-tail domain (Myo4p-GT; aa 1091-1471), or the globular tail and rod region (Myo4p-RGT; aa 1042-1471) were generated. To test if any of these fragments are able to bind to She3p, they were used in SPR experiments with immobilized She3p-N (figure 2.3-A).

In a first set of experiments, the interaction of the Myo4p-GT to She3p-N was analyzed. Surprisingly, even at Myo4p-GT concentrations exceeding 5 μ M no interaction was detected.

In contrast, efficient binding to She3p-N was observed for the Myo4p-CC and the Myo4p-RGT with respective binding constants of $K_d = 423 \pm 26$ nM and $K_d = 605 \pm 115$ nM (figure 2.3-B). Because both fragments do not overlap in their sequence, it can be concluded that She3p binds to Myo4p at two non-overlapping regions. Since the globular tail alone does not bind to She3p, one of these regions may be localized within the rod region. The other region is situated in the coiled-coil domain of Myo4p. Furthermore, both interaction sites have a reduced affinity to She3p compared to the entire Myo4p-tail (figure 2.1-B and C).

In summary, two non-overlapping She3p binding regions could be identified within the Myo4p-tail. Both have a lower affinity to She3p than the entire tail domain. Therefore, it is likely that the simultaneous She3p binding to both regions is necessary to achieve full binding efficiency. The finding that the Myo4p-GT is not involved in cargo binding was rather unexpected and contrasts observations for Myo2p and type-V myosins from higher eukaryotes, where the globular-tail domain is the main cargo interaction site.

half-life of $R_{\max 1/2} = 5.0 \pm 1.2$ s compared to complexes with the Myo4p-tail ($R_{\max 1/2} = 51.7 \pm 25.6$ s, figure 2.4-C). The different complex stabilities might explain why no interaction of the Myo4p-RGT and She3p-N could be observed in the pull down reactions. It is likely that a significant proportion of Myo4p-RGT simply gets lost during the individual washing steps.

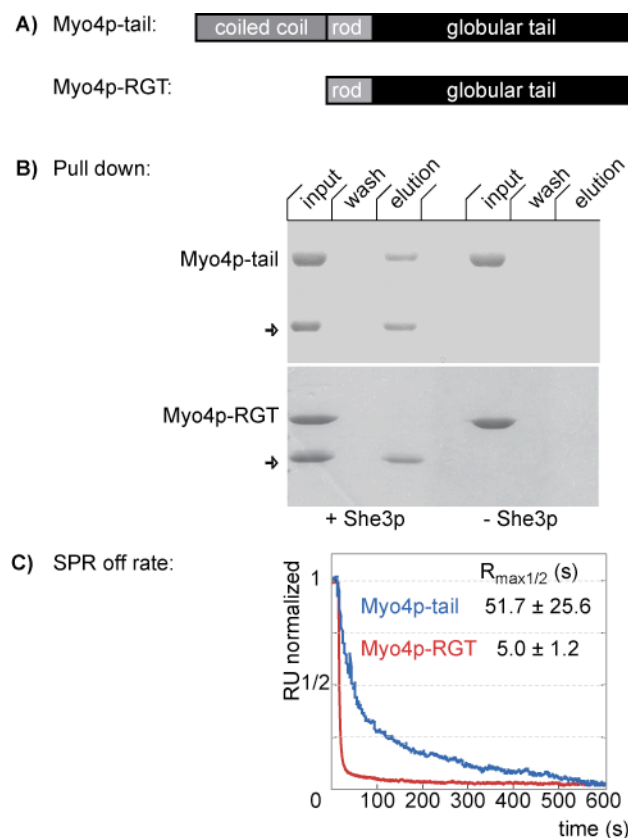


Figure 2.4

Complexes of the She3p-N with the Myo4p-tail and the Myo4p-RGT have different stabilities

A) Cartoon representation of the Myo4p fragments used in the experiment. B) Ni-sepharose pull-down reactions of His-tagged She3p-N and Myo4p fragments. The label input indicates the proteins added to the reaction, wash represents the final wash step and elution indicates the elution fraction after incubating the beads with imidazole. The analysis revealed an elution of the Myo4p-tail together with She3p-N (indicated by the arrow). In contrast, the Myo4p-RGT failed to co-elute with She3p-N. The right half of the PAGE shows control reactions without She3p-N. C) Normalized SPR response signals during complex dissociation of She3p-N with the Myo4p-tail (blue) and the Myo4p-RGT (red). The table quotes the time-point at which 50 % of the complexes have dissociated ($R_{\max 1/2}$).

The observed higher stability of the She3p-Myo4p-tail complex might be explained by a synergistic binding of She3p-N to both regions, the coiled-coil and the rod. Consequently, the coiled-coil lacking Myo4p-RGT does not form stable complexes with She3p. However, the increased complex stability might also be a result of Myo4p-tail dimerization by the coiled-coil region within the complex. If She3p binds to two Myo4p-tail molecules simultaneously, the dissociation from one of them will not necessarily result in complex disassembly. In contrast, the Myo4p-RGT contains no coiled-coil domain and would therefore be unable to form dimers. This aspect will be investigated in more detail in the chapters 2.7 and 2.9.

2.6 The residues 1056 and 1057 of Myo4p are required for She3p binding

Chapter 2.5 showed that the interaction between the Myo4p-tail and She3p-N is detectable in pull-down reactions. This approach offers the possibility to characterize potential effects of varying buffer conditions on the Myo4p-She3p complex formation. Performing the pull-down reaction in the presence of 0.1 % Triton X-100 revealed that the Myo4p-tail (figure 2.5-A) did not

co-elute with She3p-N in detergent-containing buffer (compare figure 2.5-B and C). This result suggests a hydrophobic character of the interaction. If the Myo4p-She3p complex is indeed formed by hydrophobic interactions, repeating the pull down assay under high salt conditions should not disrupt complex formation. Although reduced, an interaction of the Myo4p-tail and She3p-N could still be detected when the pull-down reaction was performed with 1 M NaCl present in the reaction buffer (figure 2.5-D), indicating a hydrophobic contribution for the interaction.

Subsequently, the Myo4p coiled-coil and rod region was analyzed for hydrophobic regions using the program “ProtScale” from the ExPASy Proteomics Server (Kyte and Doolittle 1982). This investigation revealed an accumulation of hydrophobic residues around residue 1060 of the Myo4p sequence (figure 2.5-F). If this region participates in She3p binding, the mutation of one or more hydrophobic residues should have a detectable effect upon complex formation. Therefore, two mutations were introduced into the Myo4p-tail (F1056R and I1057R), both replacing hydrophobic against charged residues (figure 2.5-A). In the pull down reaction, the mutated fragment (Myo4p-tail_{F1056R,I1057R}) failed to interact with She3p-N under standard conditions (figure 2.5-E).

In summary, these results indicate a hydrophobic contribution for the protein interaction, involving a distinct region of the rod. Furthermore, the experiments with the mutated fragment Myo4p-tail_{F1056R, I1057R} revealed that the coiled-coil domain alone is not sufficient to form stable complexes in the pull-down reactions.

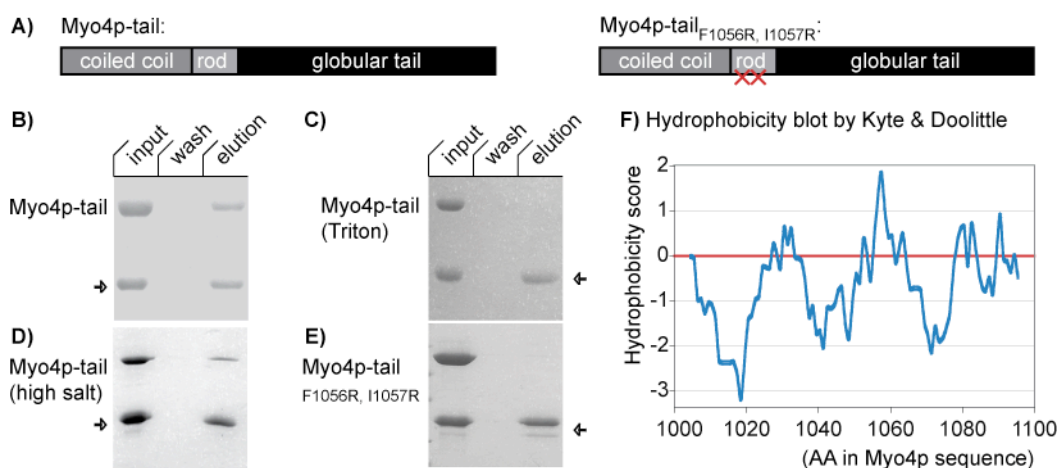


Figure 2.5

She3p binds to a hydrophobic region of the rod

A) Cartoon representation of the Myo4p fragments used in the experiment. B-E) Pull-down reactions between immobilized She3p-N and Myo4p-tail fragments at varying buffer conditions. While the Myo4p-tail bound efficiently to She3p-N at standard conditions (B), no binding of the Myo4p-tail was detected in detergent containing buffer (0.1 % Triton-X 100; C). Under high salt conditions (1 M NaCl) an interaction between the She3p-N and the Myo4p-tail was observed (D). In contrast, the reactions with the Myo4p-tail_{F1056R,I1057R} and She3p-N under standard conditions did not reveal binding (E). F) A hydrophobicity blot according to Kyte and Doolittle (Kyte and Doolittle 1982) indicates a hydrophobic region around position 1060 in the Myo4p sequence.

2.7 The Myo4p-tail is strictly monomeric

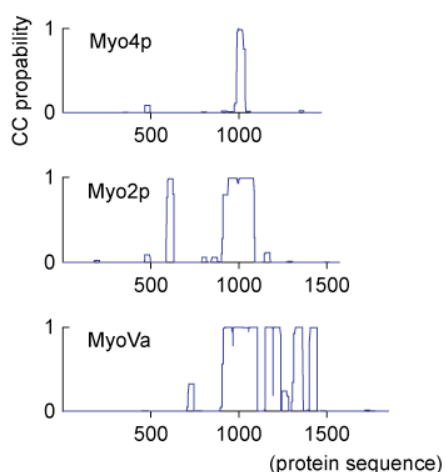
Analytical ultracentrifugation experiments (AUC) were performed in collaboration with Dr. Klaus Richter from the department of Chemistry of the Technical University of Munich, who also performed the data analysis. AUC results are described here because they are important for the understanding of this study.

The Myo4p coiled-coil domain contains one binding site for She3p and is important for the Myo4p-She3p complex stability. On the other hand, pull-down experiments with the mutant Myo4p-tail_{F1056R, I1057R} fragment revealed that the coiled-coil domain alone is not sufficient to form stable complexes with She3p-N. Besides the obvious possibility that both interaction regions have to bind synergistically, a second, more indirect scenario is imaginable, in which the coiled-coil domain might affect She3p binding by promoting dimerization of the motor protein. If the presence of dimeric Myo4p is important for stable complexes with She3p, a deletion of the coiled-coil dimerization domain might not only affect direct She3p binding. It would also destroy the correct oligomeric state required for complex formation.

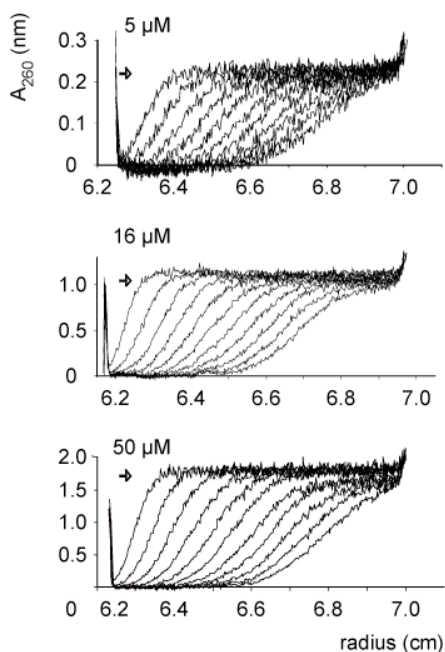
Type-V myosins were described to form constitutive, dimeric motor proteins. Therefore, most of the type-V myosin sequences contain a theoretical coiled-coil region, which include several hundred residues. However, a prediction of coiled-coil regions in the Myo4p sequence with the “Coils” algorithm from the ExPASy Proteomics Server (Lupas *et al.* 1991) revealed an unusually short coiled-coil region, especially when compared to the predicted coiled-coil regions of other type-V myosins like Myo2p or MyoVa (figure 2.6-A). This short predicted coiled-coil domain in Myo4p of only 31 amino acids length raised the question whether Myo4p is indeed able to form stable dimers (as generally expected for type-V myosins). To characterize the oligomeric state of Myo4p, AUC experiments were performed with the Myo4p-tail, using concentrations from 5 to 50 μM .

In sedimentation velocity experiments with the Myo4p-tail (figure 2.6-B), one single oligomeric species was detected (figure 2.6-C). The sedimentation profiles from three different concentrations, in which the protein distribution is blotted against the radius of the measuring cell at different time points, revealed just one single reversal point. This indicates that for all measured concentrations only one oligomeric species of the Myo4p-tail was present (figure 2.6-C). Subsequently, the sedimentation profiles were used to determine the sedimentation coefficients for the Myo4p-tail. This calculation revealed one common sedimentation coefficient of 3.7 Svedberg (S) for all three concentrations, indicating that the Myo4p-tail forms one stable, oligomeric species at all concentrations.

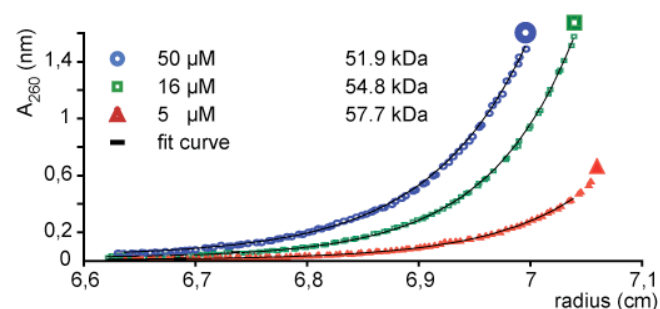
A) coiled coil prediction

B) Myo4p-tail: coiled coil rod globular tail

C) sedimentation velocity experiment



D) sedimentation equilibrium experiment

**Figure 2.6****Determination of the oligomerization state of the Myo4p-tail**

A) Coiled-coil prediction for the type-V myosins Myo4p, Myo2p and MyoVa. The plot indicates the coiled-coil probability against the protein sequence (Lupas *et al.* 1991). B) Cartoon representation of the Myo4p-tail fragment used in the AUC experiment. C) Protein distribution during sedimentation velocity experiments with three different concentrations. The absorption is plotted against the radius of the measuring cell. The curves from left to right represent the protein distribution at increasing time points. The arrows highlight the reversal point within the curves. The Svedberg coefficient calculated from the curves was 3.7 S for all concentrations D) The sedimentation profile after sedimentation equilibrium experiments. The graphs indicate the absorption against the radius of the measuring cell at equilibrium. The different concentrations are highlighted by different symbols and colors. The profiles from all three concentrations represent an exponential distribution and could be fitted to molecular weights between 51.9 and 57.7 kDa.

In sedimentation equilibrium experiments the molecular weight of the Myo4p-tail was determined (figure 2.6-D). The experiments were performed at a low centrifugal speed, so that the sedimentation is balanced by diffusion throughout the entire column, resulting in a protein distribution that fits an exponential distribution (Golemis and Adams 2005). Since the sedimentation velocity experiments revealed one single oligomeric species, the sedimentation profiles at equilibrium could be used to fit the molecular weight of the Myo4p-tail directly. This analysis revealed a molecular weight of approximately 55 kDa, which is almost identical to the calculated mass of the monomeric Myo4p-tail of 56.3 kDa. From these experiments it can be concluded that the Myo4p-tail is strictly monomeric in solution.

2.8 The Myo4p-tail forms homodimers when linked to artificial dimerization domains

Except Myo4p, all type-V myosins studied by now form stable dimers via their coiled-coil regions. A stable myosin dimerization is required to catalyze processive movement as shown for mouse and chicken type-V myosins (Sellers and Veigel 2006). Generally, dimeric myosins travel along the actin filament by a hand-over-hand mechanism, ensuring a permanent attachment to the filament by at least one motor domain. Therefore, Myo4p dimerization may take place after binding to She3p. Such a mechanism would be consistent with the prolonged complex stability of the Myo4p-tail compared to the Myo4p-RGT (figure 2.4). However, if this hypothesis is false, and She3p does not mediate a dimerization of Myo4p, an artificial dimerization of Myo4p would be likely to result in sterical hindrance and thus would interfere with complex formation. To test whether Myo4p dimerization is compatible with complex formation, heterologous dimerization domains were used to replace the coiled-coil region of the Myo4p-tail. Subsequently, it was tested if these dimeric Myo4p fragments are able to interact with She3p. The dimerization domains used in this study were the leucine zipper region of Gcn4p (Myo4p-GCN4) and the Glutathion-S-Transferase (Myo4p-GST, figure 2.7-A). Both domains have been described to mediate stable homodimerization.

To test, whether the introduced domains are capable to dimerize the RGT domain of Myo4p, size exclusion chromatography was performed (figure 2.7-B). The Myo4p-tail and the Myo4p-RGT elute from size-exclusion chromatography at the expected volumes for monomeric proteins (figure 2.7-B), suggesting that the Myo4p-RGT is present in a monomeric state like the Myo4p-tail (chapter 2.7). A comparison of the elution volumes of the Myo4p-GCN4 and the Myo4p-tail revealed that the Myo4p-GCN4 eluted at a considerably lower volume, indicating a higher molecular weight (figure 2.7-B). Since both fragments share an almost identical calculated molecular weight (56.3 kDa and 55.2 kDa respectively, figure 2.7-A), this shift most likely indicates efficient dimerization of the Myo4p-GCN4. The Myo4p-GST possesses a higher molecular weight compared to the other fragments used in the assay. Monomeric Myo4p-GST has a molecular weight of 75 kDa and the monomeric protein should elute at a volume between the dimeric Myo4p-GCN4 dimer and the monomeric Myo4p-tail. However, in size-exclusion

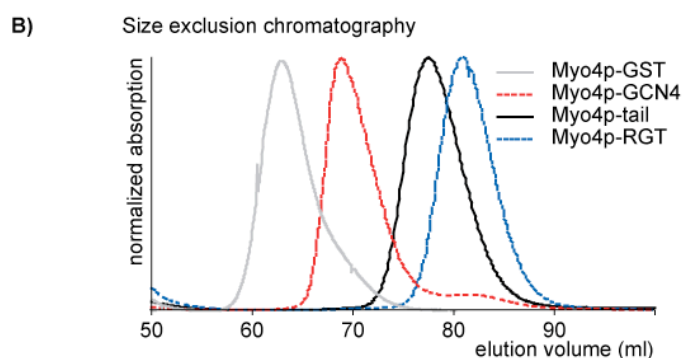
chromatography Myo4p-GST elutes at the lowest volume of all Myo4p-fragments tested, indicating a stable dimeric state of Myo4p-GST.



Figure 2.7

Heterologous dimerization domains force the Myo4p-tail into a dimeric state

A) A cartoon representation of the engineered Myo4p fragments, including their calculated molecular weight. B) The comparison of the elution profiles from size-exclusion chromatography of the Myo4p-GCN4 and the Myo4p-GST with the monomeric Myo4-tail and Myo4p-RGT revealed a dimeric state for both engineered Myo4p-hybrid fragments.



2.9 Artificially dimerized Myo4p fragments bind to She3p and form stable complexes

To test if the artificially dimerized Myo4p fragments can be incorporated into complexes with She3p, the potential interaction of the Myo4p-GCN4 and the Myo4p-GST with She3p-N was analyzed by SPR. Therefore, She3p-N was immobilized as ligand as described in chapter 2.2. In these experiments, both artificially dimerized constructs efficiently bound to She3p-N with a K_d of approximately 300 nM (Myo4-GCN4: $K_d = 281 \pm 66$ nM and Myo4p-GST: $K_d = 330 \pm 31$ nM; figure 2.8). Surprisingly, these K_d values were slightly lower than the value measured for Myo4p-RGT ($K_d = 602$ nM, figure 2.3-B), which contains the same She3p interaction site. Thus, artificial dimerization of Myo4p is not only compatible with the formation of complexes with She3p but even increases their affinity.

In addition, complexes formed by She3p-N and artificially dimerized fragments revealed complex half lives that were longer ($R_{max1/2} = 133 \pm 31$ s for Myo4p-GCN4 and 57 ± 26 s for Myo4p-GST; figure 2.8-A) than for the complex of She3p-N and the Myo4p-tail ($R_{max1/2} = 52$ s; figure 2.4-C). In summary, dimeric Myo4p fragments are incorporated into complexes with She3p-N. Furthermore, these complexes turned out to be even more stable than complexes formed by She3p-N and the Myo4p-tail (compare figure 2.1-D). This finding is rather surprising, since these Myo4p fragments lack the second She3p binding site within the coiled-coil region. It furthermore demonstrates that homo-dimerization of Myo4p might play an important role for the formation of stable complexes.

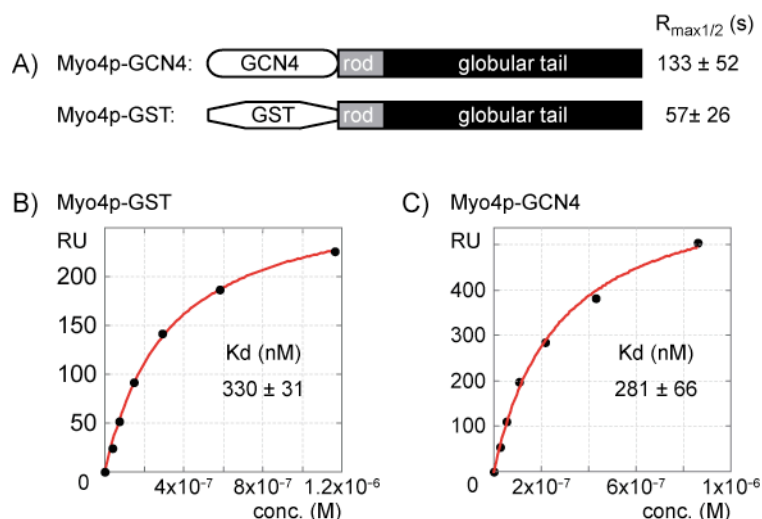


Figure 2.8

SPR analysis for the interaction of She3p-N with artificially dimerized Myo4p fragments

A) Indicated are the fragments used for steady-state binding experiments with artificially dimerized Myo4p-fragments and immobilized She3p-N. Both fragments interact with She3p-N and the resulting complexes have half-life times in the range of one to two minutes (for details, see text). B) and C) Representative plots of the response signals at equilibrium against the concentration are shown for Myo4p-GST and Myo4p-GCN4. RU indicates response unit. The red line indicates the fit curve when applying the langmuir isotherm. The highlighted equilibrium dissociation constants (K_d) represent the average from three independent experiments, with \pm indicating the standard deviation.

2.10 Disruption of Myo4p dimerization results in disassembly of complexes with She3p

AUC experiments revealed that Myo4p alone is strictly monomeric in solution (figure 2.6). However, artificially dimerized Myo4p-fragments are capable to form stable complexes with She3p-N, having half-life times that are comparable to observations for the native Myo4p-tail (compare figure 2.1-C and figure 2.8-A). This complex-stabilizing effect is likely due to Myo4p dimerization within the complexes. To confirm this assumption, pull-down experiments with the Myo4p-GST were performed (figure 2.9). The experiments revealed a stable interaction of Myo4p-GST with the She3p-N (figure 2.9-A). Since the Myo4p-RGT fragment did not show an interaction with the She3p-N in pull down reactions (figure 2.4-B), the binding observed for the Myo4p-GST is likely to depend on the dimerization mediated by GST.

Subsequently, the experiment was repeated, but with a site-specific protease added to the reaction, 30 minutes after mixing the samples. The protease specifically cleaves between GST and the Myo4p-RGT fragment, thereby generating monomeric Myo4p-RGT and free GST. If Myo4p dimerization is required within the complex, the generation of monomeric Myo4p-RGT after complex formation should result in a disassembly of already formed complexes. But if dimerization is instead needed to form complexes and is dispensable afterwards, stable complexes should still be observed. After elution of this protease-treated reaction, no interaction of She3p-N with the Myo4p fragment was observed (figure 2.9-B).

In summary, the protease cleavage experiment suggests that dimerization of Myo4p via GST is necessary to form stable complexes with She3p. This result further indicates a requirement of dimeric Myo4p within the Myo4p-She3p complex.

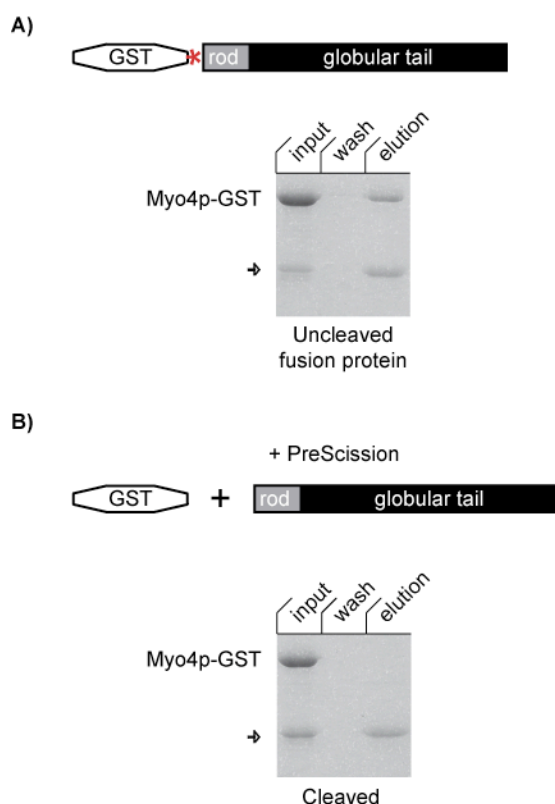


Figure 2.9

Myo4p is dimeric in complexes with She3p

A) Cartoon showing the Myo4p-GST fragment used in the pull down experiment. The red asterik indicates a protease-cleavage site. In pull down experiments, the Myo4p-GST fragment binds efficiently to She3p-N. B) The cartoon highlights the situation when the same reaction as shown in A) is repeated, but a site-specific protease is added after pre-incubation. Protease cleavage generates free GST and the Myo4p-RGT. Here, the Myo4p-RGT is not visible in the elution fraction after PAGE. Therefore, the already assembled complexes may fall apart after cleavage of GST. Furthermore, the lack of GST in the elution fraction ensures that free GST does not interact with She3p-N in the pull down reaction.

2.11 The globular-tail domain of Myo4p is not required for ER inheritance

Type-V myosins are thought to interact with their adapter proteins mainly through binding to the globular-tail domain. However, She3p binds to Myo4p at two individual regions, both outside of the globular tail (figure 2.3). Since no further adapter proteins for Myo4p are known, the role of the globular tail for the two Myo4p functions, namely ER inheritance and mating type switch, remains unclear.

To test the role of the globular-tail domain in ER inheritance, yeast cells carrying a Myc-tagged-Myo4p fragment with a globular-tail deletion were generated (Myo4p Δ GT, figure 2.10-A) and analyzed to what extent these cells are capable to mediate ER inheritance *in vivo*.

For the analysis, yeast cells expressing the Myo4p Δ GT were compared with cells expressing Myc-tagged-full-length Myo4p (Myo4p-WT, figure 2.10-A). The expression of the Myo4p fragments was confirmed by western-blot analysis (figure 2.10-B). To visualize the ER inheritance directly, the yeast strains additionally expressed a GFP fusion of the ER marker protein Hmg1p, which allowed for the analysis of the ER distribution by fluorescence microscopy. To assess ER inheritance, the amount of cells carrying defined, strong bud-localized fluorescence signals was determined (figure 2.10-C). For this purpose, only dividing, pre-

anaphase yeast cells were investigated, since in later stages the ER migrates into the bud by a Myo4p-independent mechanism. Surprisingly, cells carrying full length Myo4p and those lacking the globular tail showed no difference in ER-bud localization (figure 2.10-D, Myo4p-WT: 81.1 ± 1 % and Myo4p Δ GT: 81.7 ± 1 %, $n = 3 \times \geq 80$ cells each). In both cases, strong ER-localized GFP signals were detected in approximately 80 % of all cells, indicating efficient ER inheritance within both cell types. In summary, no difference between cells carrying Myo4p-WT or Myo4p Δ GT could be observed, excluding a potential role of the globular tail in the inheritance of cortical ER. In contrast, cells with a knock-out for MYO4 show no ER-bud localization at all (Schmid *et al.* 2006). Finally, the results show that a Myo4p fragment lacking the globular tail represents a motor with full motile activity.

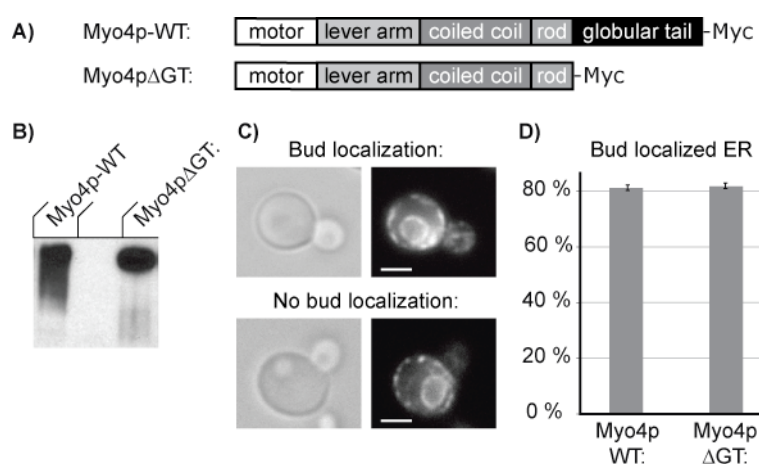


Figure 2.10

The globular tail of Myo4p has no function in ER inheritance

A) The cartoon shows the Myc-tagged Myo4p constructs expressed in yeast cells. B) The expression of the Myo4p fragments was verified by western blot analysis against the Myc-tag. C) Representative images taken with transmission light- and fluorescence-microscopy showing dividing yeast cells. Here, examples for bud localized and not localized ER signals are shown. Scale bars indicate a length of 2 μ m. D) The amount of cells with bud-localized ER is identical in cells expressing Myo4p-WT and Myo4p Δ GT. Error bars represent the standard deviation after analyzing $n = 3 \times \geq 80$ cells for each experiment.

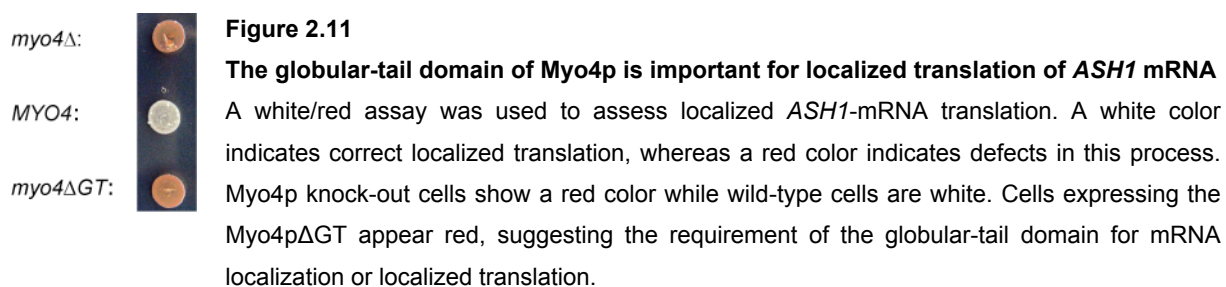
2.13 The Myo4p globular-tail domain is required for localized *ASH1*-mRNA translation

To test if the transport of localized mRNAs depends on the presence of the globular-tail domain, the localized translation of *ASH1* mRNA was investigated in cells expressing the Myo4p Δ GT fragment (figure 2.10-A). Translation of the *ASH1*-mRNA leads to the accumulation of Ash1p, a specific transcription repressor for the *HO*-promoter. During budding, the *ASH1* mRNA is transported towards the bud tip, and this transport results in an exclusive expression of Ash1p within the daughter cell. As a consequence, the *HO*-promoter is active in the mother but not the daughter nucleus. Here, a yeast strain was used in which the *ADE2* gene was controlled by the *HO*-promoter and thereby by Ash1p (Jansen *et al.* 1996). The *ADE2* gene was chosen, because

yeast cells lacking *ADE2* accumulate a red colored pigment (P-ribosylamino imidazole) when they grow under adenine-deficient conditions.

If *ASH1* mRNA is transported properly, no Ash1p is expressed within the mother cell. Consequently, the *HO*-promoter is active and the *ADE2* gene is expressed in these cells, leading to a complete destruction of the red pigment and the formation of white colored colonies. In contrast, cells that are deficient in *ASH1*-mRNA transport express Ash1p in the mother and the daughter cell. These cells are unable to express the *ADE2* gene and colonies appear red.

This assay was used to analyze three different yeast strains for their ability to localize *ASH1* mRNA correctly: i) a Myo4p knock out strain (*myo4Δ*), ii) a wild-type strain expressing full-length Myo4p (*MYO4*), and iii) a strain expressing the Myo4pΔGT (*myo4ΔGT*). As expected, colonies from the *myo4Δ* strain appeared red, whereas wild type cells showed a white color when grown under adenine deficient conditions. Cells expressing the Myo4pΔGT show a red color (figure 2.11). Thus, *MYO4* mutants lacking the globular tail showed defects in the localized translation of the *ASH1*-mRNA. This effect is unlikely to result from a reduced motor activity, since no transport defects were observed for the cortical ER (chapter 2.12).



2.14 The globular tail is required to localize Myo4p at the bud tip

In *myo4ΔGT* cells, the localized translation of *ASH1* mRNA is impaired (chapter 2.13). This effect could either be explained by i) a reduced mRNA-transport efficiency, ii) insufficient translational control or iii) a defective anchoring of the transport complex, caused by the lack of the globular-tail domain. The wild-type like ER inheritance observed for *myo4ΔGT* cells (figure 2.10-D) clearly argues against decreased mRNA-transport efficiencies (i) through impaired motor activity. Since the globular tail of Myo4p is not involved in She3p binding, the transport efficiency is also unlikely to be impaired at the level of a reduced She3p binding and complex assembly. Also, a potential role of the globular-tail domain in translational control (ii) is rather unlikely, since none of the proteins that are involved in translational silencing of the *ASH1*-mRNP (Khd1p, Puf6p) were shown to interact with the globular tail directly. Thus, impaired mRNP anchoring (iii) might be the most likely reason for the observed defects in Ash1p distribution.

Myo4p localizes at the bud tip in dividing yeast cells (Jansen *et al.* 1996). To analyze whether the Myo4p fragment lacking the globular tail shows the same localization as wild-type Myo4p,

genomically Myc-tagged Myo4p constructs were generated (figure 2.12-A) and their localization was investigated in dividing, pre-anaphase cells by immunofluorescence. For a better interpretation, the intracellular Myo4p localization was subdivided into three classes: i) bud tip localization, ii) bud enrichment and iii) random distribution (figure 2.12-B). In wild-type cells, Myo4p localized at the bud tip in 30.7 ± 12.0 % of all cells, while it was enriched within the bud in 39.1 ± 6.8 % (figure 2.12-C, $n = 3 \times \geq 250$ cells each). In total, Myo4p accumulated within the bud in 70 % of all cells. In contrast, total accumulation of the motor in the bud or at the bud tip dropped to 40 % for cells carrying the Myo4p Δ GT (bud-tip localization 8.8 ± 3.8 % and bud enrichment 28.3 ± 3.8 %; figure 2.12-C).

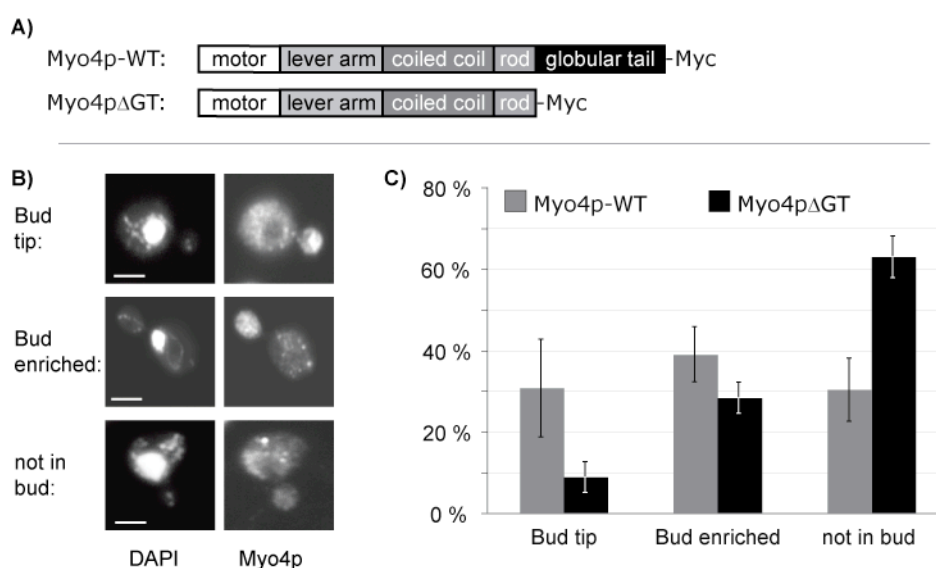


Figure 2.12

Efficient bud-tip localization of Myo4p depends on the globular-tail domain

A) The cartoon shows the Myo4p constructs used in the *in vivo* study. B) Images for the localization of Myc-tagged Myo4p fragments are depicted, showing the nucleus by DAPI staining and the Myo4p localization by immunofluorescence with anti-Myc antibodies. The intracellular Myo4p distribution was distinguished between bud tip, bud enriched and not in bud localized. Scale bars indicate distances of 2 μ m. C) Graphical representation of the Myo4p distribution. Error bars represent the standard deviation of three independent experiments with $n = 3 \times \geq 250$ cells each.

The laboratory of Prof. Jansen (Eberhard-Karls University, Tübingen) previously found a consistent result in a related experiment. They detected a bud localization of wild-type Myo4p in approximately 80 % of all cells, compared to 20 % in cells lacking a C-terminal region that includes the globular tail (C. Kruse & R.-P. Jansen: personal communication). However, the Myo4p fragment used in this experiment contained a stop codon after residue 1073 (compared to 1091 in the present study) and the exact statistics are unknown. In the present study, the recombinant expression of this Myo4p construct, carrying a stop codon at position 1073 resulted in unstable protein. Therefore, it is not possible to determine how She3p interacts with such a fragment compared to the Myo4p Δ GT.

In summary, these experiments confirm that the globular-tail domain of Myo4p plays an important role in accumulating the motor protein within the bud. Furthermore, a similar amount of cells with a bud enriched motor localization (Myo4p-WT and Myo4p Δ GT) indicates that the Myo4p Δ GT motor is indeed active in terms of transport.

2.15 Crystallization of the Myo4p globular tail

The only previously published crystal structure of a globular tail from a type V myosin is the Myo2p-GT. The structure revealed new insights into how type-V myosins mediate specific interactions with different adapter proteins (Pashkova *et al.* 2006). Since for Myo4p no binding protein could be identified, which is associated with the globular-tail domain, this domain seems to fulfill a different function. Therefore, it is interesting to compare the structure of both globular-tail domains and to identify differences that may explain their specificity. The globular-tail domains of Myo2p and Myo4p share a sequence identity of 28 %. Since this is not sufficient to generate a trustable three-dimensional model of the Myo4p globular-tail domain, crystallization experiments were performed to solve the structure of the Myo4p-GT.

Initial crystallization trials were set up using a crystallization robot with commercially available crystallization screens in the 96-well sitting drop format. Crystal growth in 500 nl drops was observed after 24 hours in various conditions, mainly containing 15-30 % PEG (2000-8000), pH 3.5-8.5 and 200 mM of a variety of salts (figure 2.13-A). Several of these conditions were refined, by varying the pH, the concentrations of PEG and salts, or by changing their respective type. The best crystallization condition could be achieved on the basis of Hampton PEG suite #41 with a final composition of 100 mM Hepes pH 8.5, 20 % PEG 3350, 150 mM Sodium-Formate and 10 mM Potassium-tetracyanoplatinate-II ($K_2Pt(CN)_4$). With this condition, plate shaped crystals with a maximum size of 200 μ m x 100 μ m x 10 μ m were obtained (figure 2.13-B). Cryo-protection was achieved by the addition of 20 % ethylene glycol to the refinement solution. The crystals belonged to space group $P2_12_12_1$ with unit cell constants: $a=43.46$ Å, $b=120.99$ Å, $c=157.68$ Å. From the unit cell a Matthews's coefficient of 2.38 Å³/dalton of protein was calculated (Kantardjieff and Rupp 2003, Matthews 1968) with a solvent content of 48.99 % and two molecules per asymmetric unit. The crystals showed high-quality diffraction up to 2.3 Å at the beamline ID14-1 (ESRF, Grenoble, France) and were used for data set recording. Selenomethionine (SeMet) containing crystals grew under the same condition as the native, but lacking the Pt-derivate. Diffraction data of SeMet crystals were collected at beamline X12 (DESY, Hamburg, Germany) with a resolution of 3.0 Å, and significant anomalous signals to 4 Å.

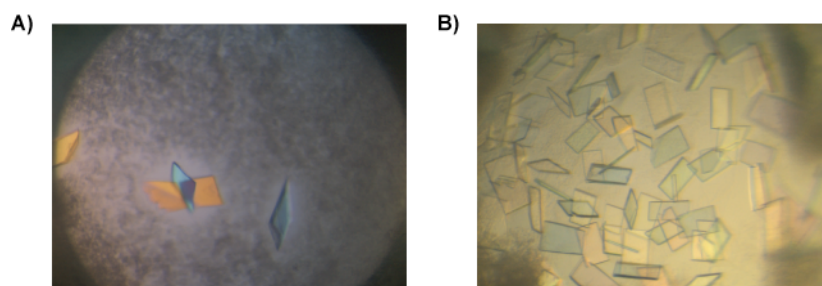


Figure 2.13

A) Representative images of Myo4p-GT crystals that were grown in Hampton PEG suite # 41: 0.2 M Lithium Chloride, 20 % w/v PEG 3350. B) Refined crystals grew in a condition containing: 100 mM Hepes pH 8.5, 20 % PEG 3350 and 150 mM Sodium-Formate 10 mM Potassium-tetracyanoplatinate-II.

2.16 Structure determination and refinement of the Myo4p globular tail

For phase angle determination, molecular replacement approaches with the Myo2p-GT structure as template were tried. Unfortunately, these attempts failed to produce a reasonable solution. Therefore single anomalous diffraction (SAD) experiments were performed.

The data from the derivatized crystal were processed, indexed and scaled with XDS and XSCALE to space group $P2_12_12_1$ (Kabsch 1993). The Myo4p-GT contains 9 methionines and using SHELXD (Collaborative Computational Project 1994, Schneider and Sheldrick 2002) 14 out of 18 selenomethionine positions could be located within the asymmetric unit. Phases were calculated with SHARP (Bricogne *et al.* 2003) and extended to 2.3 Å using the native data set. The resulting electron density allowed partial automated model building with ARPwarp (Perrakis *et al.* 1999) for approximately 60 % of the sequence. Subsequent manual model building was performed with COOT. Refinement was mainly performed using restrained refinement, including TLS (Twin-Lattice Symmetry) and NCS (Non-Crystallographic Symmetry), with the program Refmac (Murshudov *et al.* 1997, Terwilliger 2002). Solvent molecules were introduced using COOT and verified manually. The final model of the Myo4p-GT includes 343 out of 380 amino acids and 200 solvent molecules. It has an R-factor of 23.3 ($R_{\text{free}} = 26.0$), and the Ramachandran plot shows 99.9 % of the residues in the allowed or additional allowed regions (figure 2.14). Crystallographic statistics are listed in table 2.1.

Data collection			Refinement	
Data set	Native	SeMet K Peak		
X-ray source	ID 14 (ESRF)	X12 (DESY)		
Wavelength (Å)	0.933	0.978	Data range (Å)	96.0-2.3
Data range (Å)	96-2.3	20-3.2	Reflections F>0	36093
Observations	286493	202888	R _{work}	0.233
(unique)	(37418)	(26406)	(R _{free})	(0.26)
I/σ	23.16	18.37	RMS bond length (Å)	0.022
(last shell)	(4.88)	(6.85)	RMS bond angles (deg)	(2.016)
Completeness (%)	98.1	98.5		
(last shell)	(94.7)	(95.7)		
R _{sym}	0.06	0.11		
(last shell)	(0.46)	(0.29)		

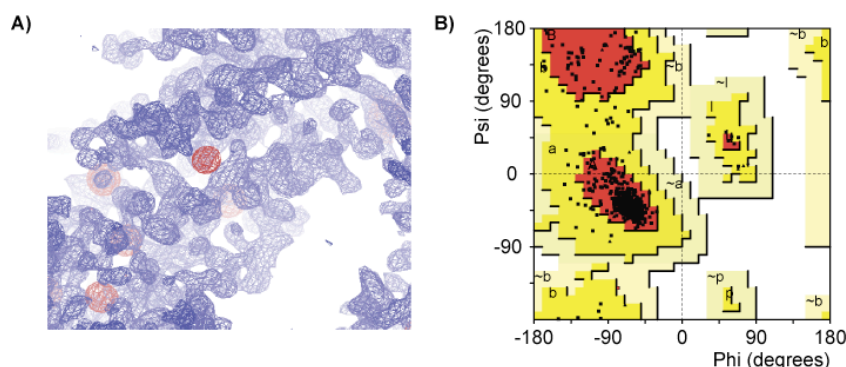
Table 2.1**Data collection and refinement statistics**

cell symmetry: (P2₁2₁2₁) cell constants (Å): a=43.46, b=120.99, c=157.68

R_{sym} is the un-weighted R-value on I between symmetry mates.

$R_{work} = \sum_{hkl} |F_{obs}(hkl) - F_{calc}(hkl)| / \sum_{hkl} |F_{obs}(hkl)|$ for reflections in the working data set.

R_{free} = cross validation R-factor for 5 % of reflections against which the model was not refined.

**Figure 2.14****Structure determination of the Myo4p globular tail**

A) Caption from the 1 σ contoured SAD map of the Myo4p-GT at 2.3 Å after phase extension (blue mesh), together with the superimposed anomalous difference fourier map from SeMet phasing at 3 σ (red mesh). B) Ramachandran plot derived from the Myo4p-GT structure.

2.17 Crystal structure of the Myo4p globular tail

The structure of the Myo4p-GT includes amino acids 1101 to 1468, lacking disordered loop regions in the positions 1208-1213, 1400-1402, and 1446-1457. Furthermore, no structural information was obtained for the very N-terminal 10 and C-terminal 3 residues. The non-resolved residues are most likely located within flexible loop regions.

The overall structural arrangement of the Myo4p-GT is similar to the structure of the Myo2p-GT and is mainly composed of alpha helices, which are organized in two globular domains (figure 2.15-A, B and C). Subdomain I reaches from helix H1 to the first half of helix H6. The helices H2 to H6 form a compact five-helix bundle, which represents the globular core of subdomain I.

Helix H6 connects subdomain I with II, and is part of a second five-helical bundle, formed by the residues from the distal part of helix H6 to helix H10. In addition to this bundle, subdomain II comprises a three-helical extension consisting of helices H11 to H13. From helix H13 an extended loop region emerges, which clamps both subdomains I and II together. This loop connects the helices H13 with H14 and is only partially resolved in the electron density. Helix H14 interacts with the helices H1 and H2 and generates a discrete three-helical region at the tip of subdomain I. However, helix H14 is not an integral part of subdomain I.

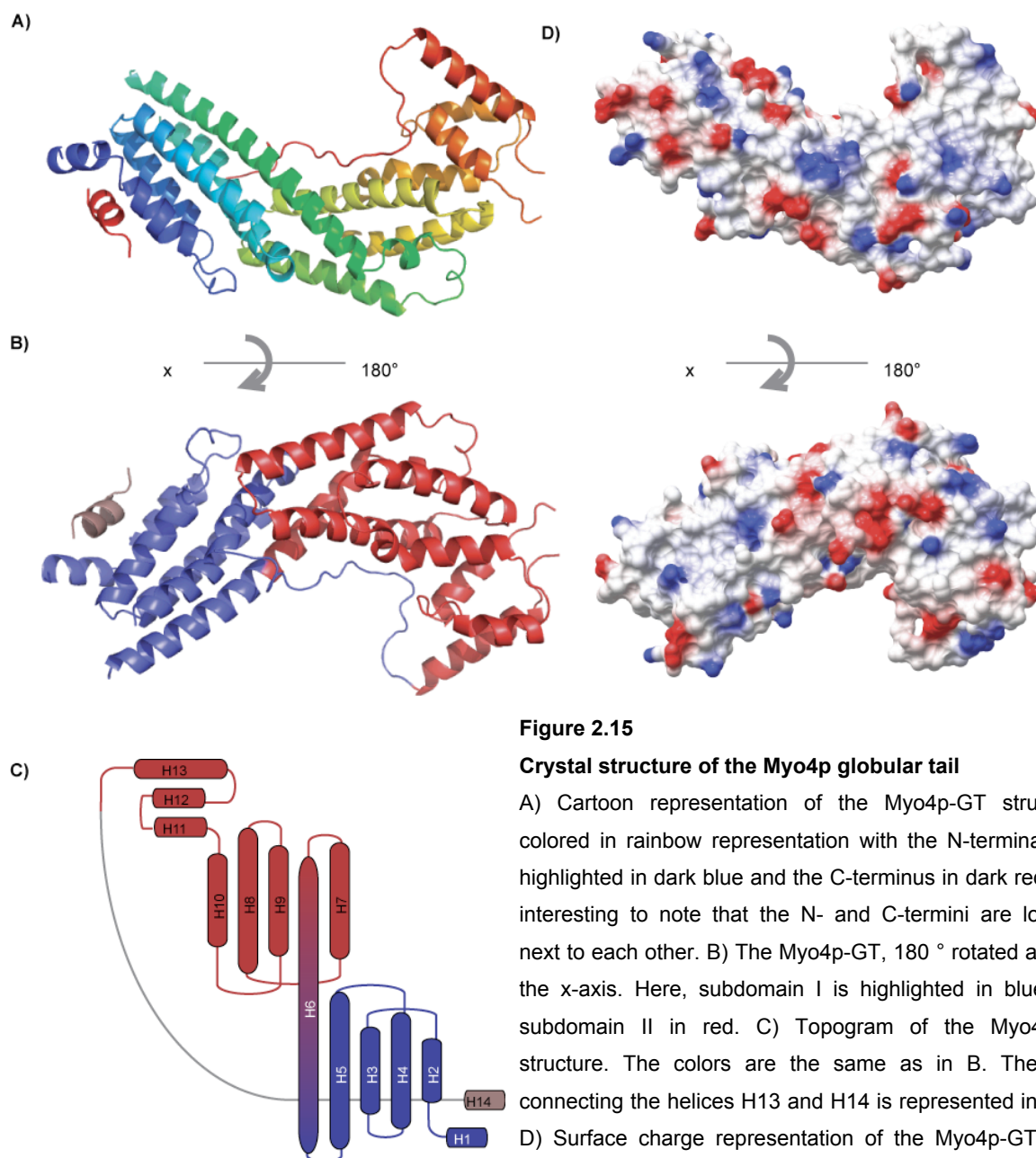


Figure 2.15

Crystal structure of the Myo4p globular tail

A) Cartoon representation of the Myo4p-GT structure, colored in rainbow representation with the N-terminal end highlighted in dark blue and the C-terminus in dark red. It is interesting to note that the N- and C-termini are located next to each other. B) The Myo4p-GT, 180 ° rotated around the x-axis. Here, subdomain I is highlighted in blue and subdomain II in red. C) Topogram of the Myo4p-GT structure. The colors are the same as in B. The loop connecting the helices H13 and H14 is represented in gray. D) Surface charge representation of the Myo4p-GT, with positively (blue) and negatively (red) charged areas. Figures A) and B) were generated with the program Pymol (DeLano 2002), surface charges representations in figure D) were calculated with CCP4MG (Potterton *et al.* 2002).

Assessment of the electrostatic surface potential of the Myo4p-GT reveals a rather uncharged overall surface (figure 2.15-D). Often patches with a defined, non-random surface charge distribution correlate with a special function or a protein-interaction region (Ma *et al.* 2003). Therefore, the random-like surface charge distribution observed for the Myo4p-GT is consistent with the observation that this domain is not involved in She3p binding.

2.18 Structural comparison of the Myo4p and Myo2p globular-tail domain

The crystal structures of the globular-tail domains from Myo4p and Myo2p show a similar overall fold, with almost identical domain architectures. The most obvious difference in both structures is the orientation of the subdomains I and II relative to each other (figure 2.16-A to C). This difference is responsible for the relatively large root-mean-square deviation (RMSD) of 8.4 Å (figure 2.16-A), calculated only for the helical regions. The different subdomain orientation also explains why molecular replacement approaches with Myo2p-GT failed to determine phase angles for the Myo4p-GT. A closer look at the interface of both subdomains explains the structural basis for this difference. The long linker helix H6 represents the connection between subdomain I and II (figure 2.15-C). While helix H6 is just slightly curved in Myo2p, it is bent by an angle of almost 90 ° in Myo4p (figure 2.16-D). The different geometry of helix H6 is then translated into distinguishable orientations of both subdomains and might explain the difference in the overall shape of the Myo2p and Myo4p globular-tail domain. In Myo4p, this 90 ° kink in the helix H6 allows for a shorter length of the loop, connecting helices H6 and H7. In Myo2p this loop is significantly prolonged compared to the one in Myo4p and had to be cleaved for crystal growth (Pashkova *et al.* 2006). Besides their relative orientation, the individual subdomains I and II are structurally highly conserved, resulting in an almost identical geometry and RMSD values of 1.5 Å and 3 Å, respectively (figure 2.16-B and C).

To visualize, which areas are conserved within the globular tails of type-V myosins, a sequence alignment of Myo4p, Myo2p, and human MYOVIa was performed and blotted on the surface of the Myo4p structure (figure 2.16-E and figure 2.17). The surface-conservation plot reveals that just a few of the conserved residues are exposed to the surface. Quantification revealed that 11.3 % of all residues buried within the core of the structure are highly conserved between all three type-V myosins (table 2.2). These conserved residues contribute most likely to the similar structural fold. In contrast, only 3.5 % of the surface exposed residues are highly conserved among all three sequences. This low surface conservation is consistent with the different cargo specificities of Myo2p and Myo4p. It is tempting to speculate that the low amount of surface conservation is a prerequisite for the observed large differences in cargo specificity for type-V myosins.

Both globular-tail domains from Myo4p and Myo2p show a long loop at their C-terminus, spanning around the entire globular-tail domain and connecting subdomain I and II. In Myo2p,

this loop is eventually involved in Vac17p binding (Pashkova *et al.* 2005) but its potential role for Myo4p function remains unclear. However, this loop is important for protein stability. C-terminally shortened Myo4p-tail fragments with a deletion of helix H14 are severely degraded (data not shown). Therefore, this bracket loop might be a general feature to guarantee stability of type-V myosin tail domains.

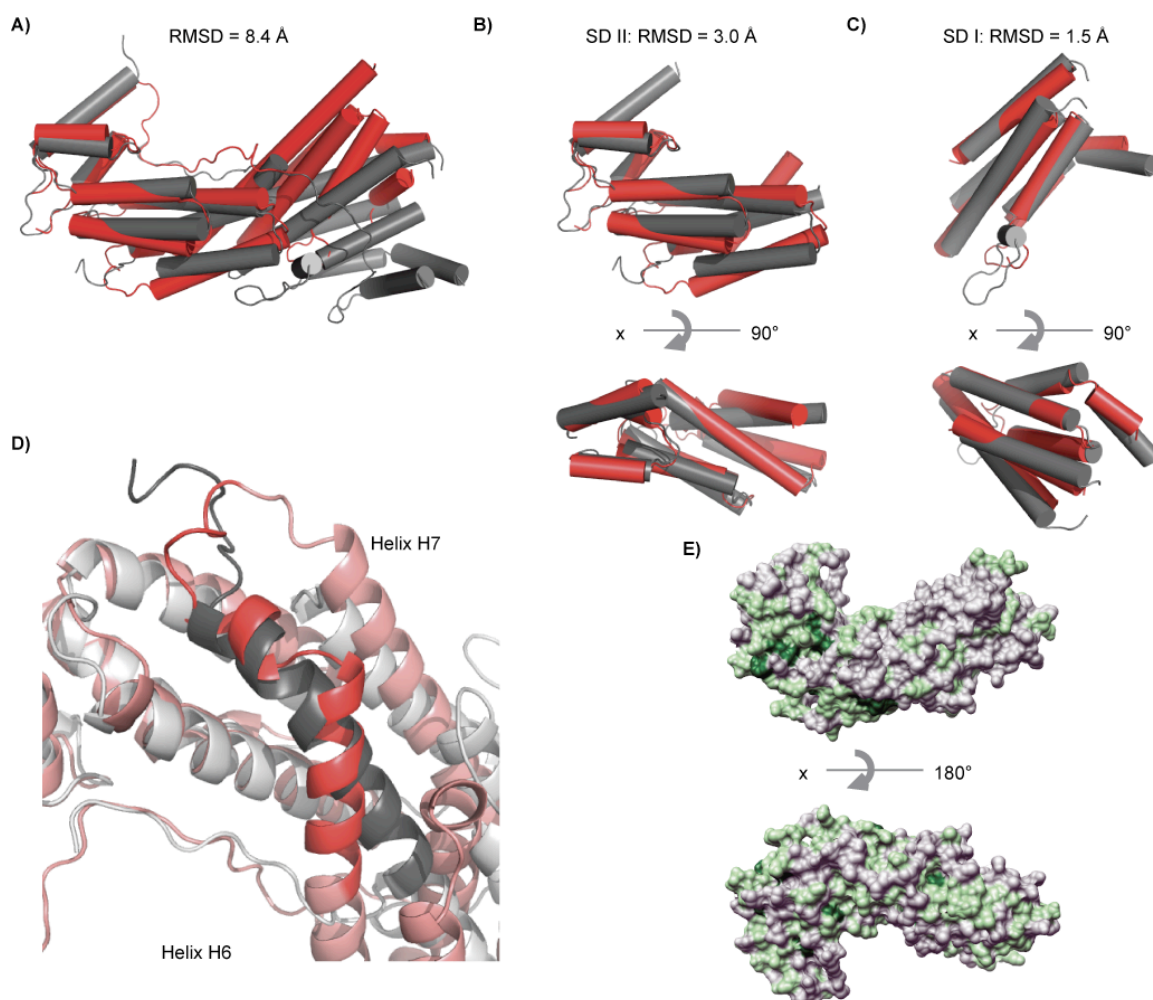


Figure 2.16

Structural comparison of the Myo4p and Myo2p globular-tail domains

A) Overlay of the globular-tail domains from Myo4p (in red) and Myo2p (in gray). The structure of the Myo4p-GT is aligned as in figure 2.15-A. and the RMSD value is indicated above. B) and C) Overlay of the subdomains (SD) II and I, respectively. Both structures are also shown rotated by 90 ° around the x-axis. D) A close up of the intersection of subdomain I and II. Myo4p is shown in red and Myo2p in gray. Dark red and gray colors indicate for both structures the C-terminal part of helix H6 and the first residues of the loop connecting helix H6 with H7. In Myo4p, helix H6 is kinked by approximately 90 °. E) Surface-conservation plot of the globular-tail domain between Myo4p, Myo2p, and human MYOVa. Colors are used as follows: non-conserved residues in gray, highly conserved residues in dark green. Figures A-D) were generated with the program Pymol (DeLano 2002), the representation of the surface conservation in E) was generated with the program CHIMERA (Pettersen *et al.* 2004).

	Residues	Number (percentage) of highly conserved residues (Myo4p, Myo2, Myo5a)
total	343	25 (8.3 %)
surface exposed	175	6 (3.5 %)
buried	168	19 (11.3 %)

Table 2.2**Conservation of the Myo4p globular tail divided into surface-exposed and buried amino acids**

In the table, the amounts of highly conserved residues that are exposed to the surface and that are buried in the core of the structure are compared.

2.19 The globular-tail domain of Myo4p interacts directly with membranes

Investigations of the intracellular localization of Myo4p (see chapter 2.14) suggest a role of the globular-tail domain in anchoring of the transport complex. One potential mechanism how the Myo4p-GT helps associating the transport complex at the bud tip is a direct membrane binding by the globular-tail domain. To test whether the globular-tail domain of Myo4p has a membrane binding capability, floatation assays with synthetic, protein free liposomes containing a yeast-membrane-like composition were performed (for details see materials and methods chapter 4.10.3). The proteins were incubated with the liposomes, mixed with a buffer containing 70 % sucrose, overlaid with a sucrose gradient and centrifuged for 16 hours to equilibrium (figure 2.18-A). During centrifugation, vesicles float up the gradient and accumulate at the interphase between 0 and 40 % sucrose. If proteins bind to the membranes, they will co-migrate with the vesicles, otherwise they remain at the bottom. Following centrifugation, the gradients were fractionated from top to bottom and the individual fractions were precipitated using TCA and analyzed by SDS-PAGE. The second fraction from top generally contained the floated membranes (figure 2.18-A).

For Myo4p-GT a protein signal is visible in fraction 2, indicating a co-migration with the vesicles and therefore a direct membrane association. In contrast, neither for She3p-N nor for the Myo2p-GT (aa 1084-1575) membrane binding could be observed (figure 2.18-B). If the Myo4p-GT indeed helps to anchor the motor complex at the bud tip, Myo4p would need to bind simultaneously to membranes and to She3p. Therefore, the She3p binding sites-containing Myo4p-tail should in principle bind simultaneously to vesicles and She3p-N and tether She3p-N to vesicles. In floatation experiments, a considerable fraction of She3p-N indeed co-migrated Myo4p-tail-dependently with vesicles (figure 2.18-C).

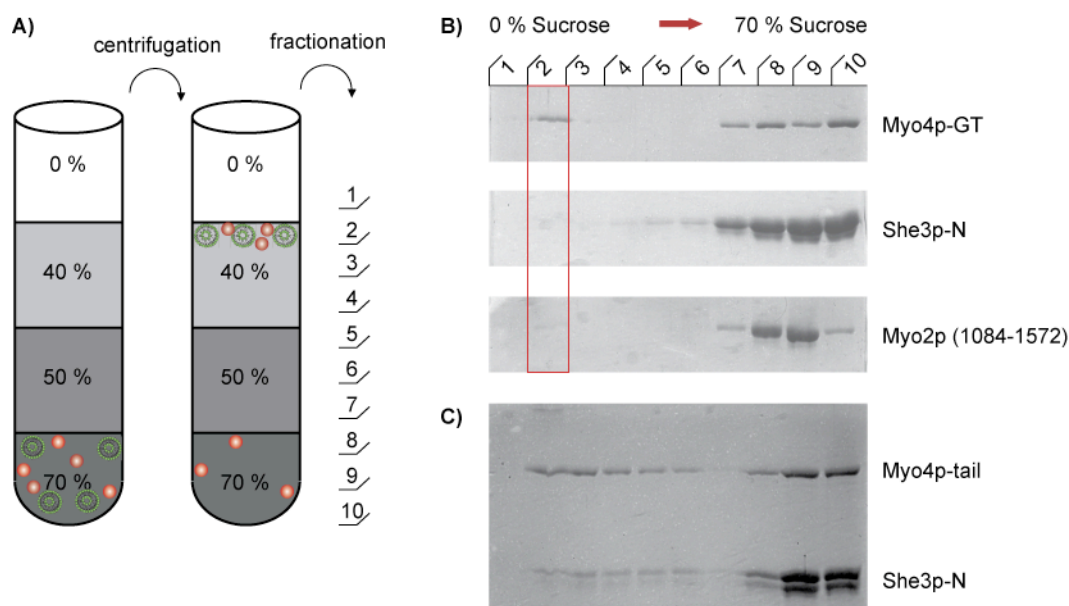


Figure 2.18

Floatation assay to test for direct membrane associations

A) Schematic representation of the floatation assay: The protein of interest (red circles) and synthetic vesicles (green) are mixed in 70 % sucrose and covered by a sucrose gradient. After centrifugation to equilibrium, vesicles float up the gradient. Vesicle-bound proteins co-migrate to the upper layers of the gradient, while proteins that do not bind to membranes remain at the bottom. After centrifugation, the gradients were fractionated from top to bottom and the individual fractions were prepared for SDS-PAGE. Fraction 2 generally contains the floated membranes. B) Subsequent SDS-PAGE with coomassie staining after the floatation assay for Myo4p-GT, She3p-N, and Myo2p-(1084-1572). Only for the Myo4p-GT a protein signal is detectable in the floated fractions (red box). In contrast, neither She3p-N nor the Myo2p-(1084-1572) bound to vesicles. C) When the Myo4p-tail and She3p-N were used in the floatation assay simultaneously, both proteins can be detected in the floated fractions.

2.20 Identification of a membrane interacting region within the Myo4p globular tail

For a molecular characterization of the membrane binding by the Myo4p-GT domain, its structure was analyzed to identify potential membrane-associated regions. Often, peripheral membrane binding regions are characterized by a local enrichment of hydrophobic or positively charged residues. Such regions were identified and analyzed for their involvement in membrane association. The strategy was to exchange surface-exposed positive or uncharged residues with aspartic acids. The negatively charged aspartic acid should mediate an electrostatic repulsion with the negatively charged lipid surface and therefore actively interfere with membrane binding. For instance the Myo4p-GT_{F1379D,Y1381D}, in which the hydrophobic residues F1379 and Y1381 were exchanged, was analyzed for membrane binding (figure 2.19-A). Although this mutant fragment was only weakly expressed and therefore less protein was used in the reactions, a considerable amount of protein associated with membranes. This result shows that the introduction of negatively charged residues does not generally interfere with membrane binding. In contrast, the mutant protein Myo4p-GT_{W1325D,Y1329D} showed no association with membranes

(figure 2.19-A). Thus, the two hydrophobic residues W1325 and Y1329, located within helix H9 in subdomain II (figure 2.19-B), potentially mediate direct lipid interactions that are disrupted upon mutation.

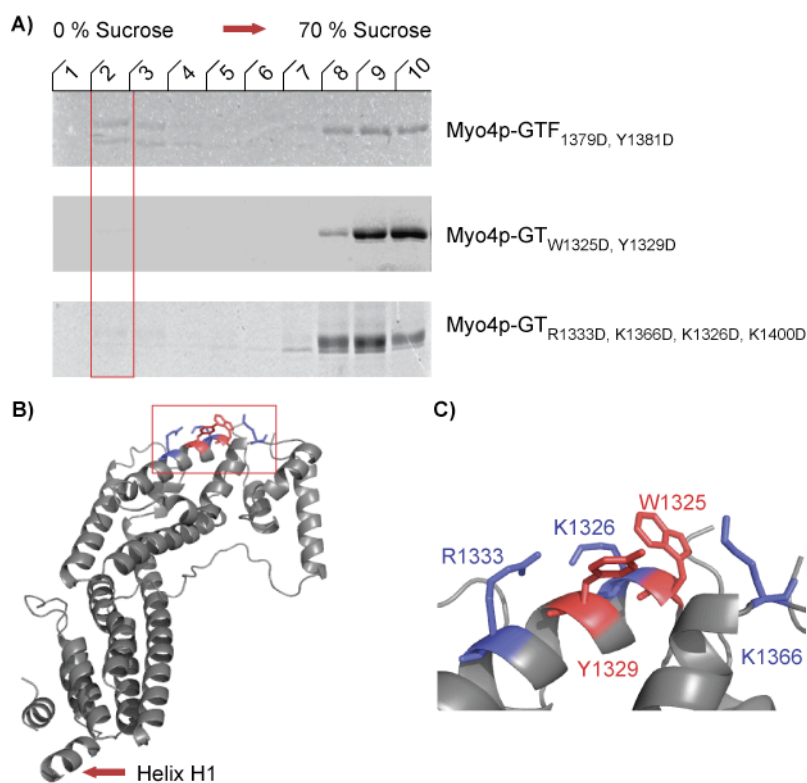


Figure 2.19

Tryptophane 1325 and tyrosine 1329 of the Myo4p-tail are required for membrane binding

A) SDS-PAGE with subsequent coomassie staining after the floatation assay for the Myo4p-GT_{F1379D, Y1381D}, Myo4p-GT_{W1325D, Y1329D} and Myo4p-GT_{K1326D, R1333D, K1366D, K1400D}. Membrane association was only observed for Myo4p-GT_{F1379D, Y1381D} (indicated by the protein signal in fraction two, red box). B) The area, which is important for membrane association is highlighted within the Myo4p-GT structure (red box) and resolved residues are displayed with side chains. The two aromatic residues W1325 and Y1329 are highlighted in red, the positively charged residues K1326D, R1333D, K1366D, surrounding the hydrophobic core, are highlighted in blue. For a better understanding where the membrane-binding region is localized in the globular-tail domain, the N-terminal helix H1 is highlighted. C) Close-up of the membrane-binding region. The aromatic residues W1325 and Y1329 are located on top of helix H9 encircled by positively charged residues.

The positively charged residues K1326, R1333 and K1366 surround the described hydrophobic residues. These basic residues potentially mediate ionic interactions with the negatively charged vesicle surface. In addition, residue K1400 is located within the loop region connecting helix H12 with H13, and is therefore in close proximity to the two aromatic residues required for membrane binding. However, the loop region is not visible in the electron density. If residues W1325 and Y1329 indeed participate in membrane binding, inverting the charge of the residues K1326, R1333, K1366 and K1400 should in principle also affect lipid binding. Indeed, floatation

experiments with the mutant protein Myo4p-GT_{K1326D,R1333D,K1366D,K1400D} showed almost no membrane association, confirming a role of the identified region in membrane binding.

It is important to note that these results do not exclude the existence of additional residues or regions, which might be involved in lipid interaction. Furthermore, the final proof whether the identified membrane-binding region of Myo4p influences localization of mRNAs *in vivo*, remains open.

2.22 Quantification of the Myo4p globular-tail-vesicle interaction

Quantitative biophysical analyses were used to characterize the interaction between the lipid vesicles and the Myo4p-GT. Therefore, SPR analyses were performed, in which vesicles were immobilized on a L1-chip (Biacore™), which carries carboxymethylated dextran fibers with covalently attached lipophilic groups. The lipophilic surface allows for a direct binding of lipid vesicles, which maintain an intact structure. Unfortunately, injection of the analyte (Myo4p-GT) did not result in a stable steady-state situation. Although single injections of the Myo4p-GT resulted in a saturation of the response signal, repeated injection of constant analyte concentrations led to continuously increasing response levels. Thus, the interaction failed to reach a steady-state level. Furthermore, the Myo4p-GT did not dissociate completely during the washing steps. In summary, the experimental setup was not suitable to quantify the interaction of the Myo4p-GT and the lipid vesicles.

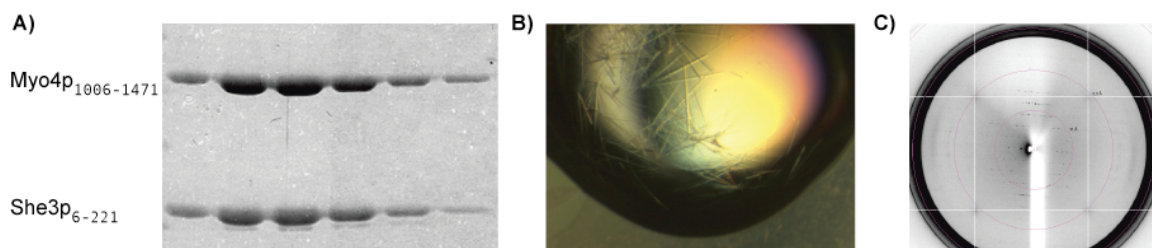
In a second approach, binding of Myo4p-GT to an enclosed lipid bilayer surface was analyzed using RfS (Reflectometric Interference Spectroscopy, in collaboration with the laboratory of Prof. Piehler at the University of Frankfurt). In these experiments, the vesicles were attached to a clean glass surface, resulting in the formation of a continuous phospholipid surface. In RfS, complex formation between two molecules is detected from an increase of the surface thickness by measuring the interference of reflected light from interfaces with different refractive indices. In short, any change of the optical thickness leads to linear changes in the interference spectrum, which can be detected by the intensity of the reflected light.

Although the lipid composition was the same as in the previous described floatation assay (chapter 2.19 and 4.10.3), no binding of the Myo4p-GT to the lipid surface could be detected by RfS. One potential reason for the failure to detect Myo4p-GT binding to the lipid surface might be the lack of surface curvature (in contrast to the vesicles used in floatation experiments). Another possible explanation is that the affinity of the Myo4p-GT to the membrane mixtures might be weak, resulting in signals below the detection limit of this assay. A third possibility is that the kinetics of this membrane binding is too slow to allow for a detectable interaction during the 30 s when Myo4p-GT is floated over the lipid surface.

In summary, it was not possible to quantify the interaction of the Myo4p-GT with the phospholipid vesicles.

2.23 Crystallization of the Myo4p-She3p complex

In order to analyze the Myo4p-She3p complex in more detail, crystallization experiments were performed. For co-crystallization of Myo4p and She3p, the She3p-Myo4p co-complexes were purified by size-exclusion chromatography (figure 2.20-A). Initial crystallization screens for the Myo4p-She3p complex were performed essentially as described for the Myo4p-GT (chapter 2.15), using an automated 96-well sitting drop format and commercially available crystallization screens. Crystal growth could be observed after 24 – 48 hours at 20°C only. Two-dimensional, needle shaped crystals could be observed in up to 15 different conditions, all forming hedgehog like structures. Refinements to improve the crystal quality included: streak seeding, reducing the speed of crystal growth by adding glycerol to the crystal setup or reducing the protein concentration, screens for optimized refinement conditions and the generation of cysteine-free protein fragments, respectively. Furthermore, attempts were made to generate stable dimeric forms of Myo4p either by introducing heterologous dimerization domains (the coiled-coil region from the yeast proteins Gcn4p and Myo2p) or via cysteine specific cross linking at the rod or coiled-coil region, using artificially introduced cysteine residues. In addition, great effort was made to optimize the N- and C-termini of protein constructs for crystallization (table 2.3). However, Myo4p fragments could not be shortened at their C-terminus, because deletion of helix 14 results in unstable protein. Since the She3p binding regions within the coiled-coil and the rod domain are located at the N-terminus of the Myo4p-tail, this domain could only be shortened to a point, where the She3p-binding is not affected. For She3p, attempts to optimize the N- and C-termini identified the residues 33-202 to be essential for stable complex formation with Myo4p. Finally, the most promising crystals were obtained with the fragments Myo4p₁₀₀₆₋₁₄₇₁ and She3p₆₋₂₂₁, using the following crystallization condition: 100 mM Hepes pH 7.5, 5 % (w/v) PEG 2000, 200 mM proline, 350 mM urea (figure 2.20-B). Using this setup, isolated crystals with a size of 300 µm x 20 µm x 20 µm could be obtained. The crystals were tested at beamline ID14-1 (ESRF, Grenoble, France) and showed anisotropic diffraction up to 5 Å in the best orientation (figure 2.20-C). However, all attempts to obtain high quality crystals were unsuccessful. Future steps to improve the crystal quality may include the use of eukaryotic expression systems and/or the investigation of homologous proteins from other species.

**Figure 2.20****Crystallization of the Myo4p-She3p complex**

A) The complex of Myo4p₁₀₀₆₋₁₄₇₁ and She3p₆₋₂₂₁ could be purified in high protein amounts. Shown is a coomassie stained PAGE after size exclusion chromatography, indicating pure proteins for crystallization. B) Crystals of the protein fragments Myo4p₁₀₀₆₋₁₄₇₁ and She3p₆₋₂₂₁ mainly have a long, needle-like structure. Crystals were grown in: 100 mM Hepes pH 7.5, 5 % (w/v) PEG 2000, 200 mM proline, 350 mM urea. C) Diffraction of crystals from Myo4p₁₀₀₆₋₁₄₇₁ and She3p₆₋₂₂₁ co-complex was anisotropic and had a maximum resolution of 5 Å in the best orientation.

Myo4p fragments	She3p fragments
Gcn4p ₂₄₂₋₂₇₁ -Myo4p _{1029-S}	She3p ₁₋₂₂₁
Myo2p ₁₀₀₈₋₁₀₈₈ -Myo4p ₁₀₄₂₋₁₄₇₁	She3p ₁₋₂₂₈
* Myo4p ₁₀₀₆₋₁₄₇₁	She3p ₁₋₂₃₁
Myo4p ₁₀₀₆₋₁₄₇₁ (C1113S)	She3p ₁₋₂₃₄
Myo4p ₁₀₀₆₋₁₄₇₁ (C1113S,C1288S)	She3p ₁₆₋₂₀₂
Myo4p ₁₀₀₆₋₁₄₇₁ (C1113S,C1288S,C1320S)	She3p ₁₆₋₂₂₁
Myo4p ₁₀₀₉₋₁₄₇₁	She3p ₃₋₂₂₈
Myo4p ₁₀₁₂₋₁₄₇₁	She3p ₃₋₂₃₁
Myo4p ₁₀₄₂₋₁₄₇₁	She3p ₃₃₋₂₀₂
Myo4p ₉₇₈₋₁₄₇₁	She3p ₃₃₋₂₂₁
Myo4p ₉₇₈₋₁₄₇₁ (C1113S,C1288S,C1320S)	She3p ₄₀₋₁₉₄ (C147S)
Myo4p ₉₉₆₋₁₀₇₂	She3p ₄₀₋₂₂₁
Myo4p ₉₉₆₋₁₄₂₀	She3p ₆₋₁₄₀
Myo4p ₉₉₆₋₁₄₆₃	She3p ₆₋₁₆₅
Myo4p ₉₉₆₋₁₄₆₇	She3p ₆₋₁₉₄
Myo4p ₉₉₆₋₁₄₇₁	She3p ₆₋₁₉₄ (C147S)
Myo4p _{C1042-1471} (C1113S,C1288S,C1320S)	She3p ₆₋₂₀₂
Myo4p _{CA1042-1471} (C1113S,C1288S,C1320S)	She3p ₆₋₂₁₁ (C147S)
Myo4p _{CC1042-1471} (C1113S,C1288S,C1320S)	* She3p ₆₋₂₂₁
	She3p ₆₋₂₂₈
	She3p ₆₋₂₃₁
	She3p ₆₋₂₃₄
	She3p ₈₈₋₁₉₄
	She3p ₉₋₁₉₄
	She3p ₉₋₁₉₄ (C147S)
	She3p ₉₋₂₂₁

Table 2.3**Protein fragments used in the co-crystallization of Myo4p and She3p**

An asterik highlights the protein fragments forming the most promising crystals so far.

3. Discussion

3.1 The oligomerization state of Myo4p

Cryo-EM studies on type-V myosins from vertebrates (Liu *et al.* 2006, Lu *et al.* 2006, Thirumurugan *et al.* 2006) showed that the coiled-coil region mediates efficient dimerization of the myosin. Based on this assumption, a model was designed how type-V myosins move along actin filaments using two motor domains in a coordinated manner (Veigel *et al.* 2005, Yildiz *et al.* 2003). Initial concerns regarding the multimerization state of Myo4p came up from the observation that its predicted coiled-coil region is surprisingly short compared to other type-V myosins (figure 2.6). Using analytical ultracentrifugation, the present study demonstrated that the Myo4p-tail alone is strictly monomeric in solution (figure 2.6). Since this fragment includes the entire predicted coiled-coil region, it can be assumed that the full-length motor protein is monomeric, too. In parallel to this work, two other groups also described the monomeric state of Myo4p, using either AUC or biochemical analyses (Dunn *et al.* 2007, Hodges *et al.* 2008). Altogether, the finding that Myo4p is not capable to form stable dimers was rather surprising. Before, it was assumed that one general characteristic, defining type-V myosins is their constitutive dimeric state.

The monomeric form of Myo4p is in agreement with results from previous *in vitro*-motility assays, which demonstrated that Myo4p is a non-processive motor (Dunn *et al.* 2007, Reck-Peterson *et al.* 2001). However, studies analyzing the *in vivo*-motility of Myo4p revealed a rather processive movement (Bertrand *et al.* 1998, Lange *et al.* 2008). Since the current model proposes that type-V myosins have to be dimeric for a processive movement, the question arises how to explain the discrepancy that monomeric Myo4p is catalyzing a processive movement within the cell? In principle, there are three different possibilities: i) monomeric Myo4p might be able to catalyze processive movements *in vivo* by an unknown mechanism, ii) several monomeric Myo4p molecules might be accumulated in the cargo complex, warranting a permanent actin binding and allowing for a processive movement even if individual Myo4p molecules drop down from the filament, or iii) the motor might oligomerize due to cargo binding. Below is a brief assessment of these three possibilities for Myo4p function.

- i) One important surface loop (loop 2) was identified within the motor domain of type-V myosins, which helps to keep the motor attached to the actin filaments. This loop 2 exhibits a positively net charge and is localized adjacent to the ATP binding region (Coureux *et al.* 2003). Previous experiments revealed that loop 2 has no influence on ATP binding or the catalytic activity, but supports the attachment of the motor to the negatively charged actin filament, especially during the weak binding-state. Therefore, the function of loop 2 is most likely to prevent a dissociation of the motor from the filament, especially at increased salt

concentrations (Yengo and Sweeney 2004). In contrast, within the motor domain of Myo4p this conserved loop 2 has no net charge, leading to a reduced affinity of the motor to the filament (Krementsova *et al.* 2006). Since Myo4p is rather weakly bound to the actin filament, a processive movement of individual Myo4p monomers along the actin filament is rather unlikely. In summary, the lack of positively charged residues at loop 2 in combination with the observed lack of processivity *in vitro* seems to exclude the possibility that monomeric Myo4p molecules catalyze a processive movement (Krementsova *et al.* 2006).

ii) A cargo-mediated accumulation of several monomeric Myo4p molecules is supported by recent data for the RNA-binding protein She2p. From the crystal structure and *in vitro*-binding experiments it was suggested that She2p forms a stable homodimer and interacts with individual mRNA localization elements in a molar ratio of 1:1 or 1:2 (Gonsalvez *et al.* 2003, Niessing *et al.* 2004). Recently, Marisa Müller from our laboratory revealed that She2p is present as a tetramer with a head to head orientation of two dimers in solution (Müller *et al.* Submitted). In case such a She2p tetramer is the functional species during the transport, it is possible that this tetramer might bind to several She3p molecules simultaneously.

This assumption is further supported by recently published live cell imaging experiments. Here, the Jansen group revealed that at least two different mRNAs are transported within the same translocation complex. Since only two mRNAs were analyzed at a certain time, it is very likely that the amount of in parallel transported mRNAs within one translocation complex is even higher (Lange *et al.* 2008). Both, the She2p tetramer and the increased number of RNAs per transport complex indicate that there might be several motor proteins incorporated within individual transport complexes. Chartrand *et al.* also suggested that four Myo4p molecules might be involved in the translocation of ASH1 mRNA since all four localization elements are sufficient to mediate mRNA transport (Chartrand *et al.* 2002).

Furthermore, Myo4p mediates the inheritance of cortical ER by transporting large ER tubules into the bud (Estrada *et al.* 2003, Schmid *et al.* 2006). So far it is still unclear how Myo4p is linked to the ER surface (see also chapter 3.7.1). However, it is likely that the ER tubules contain several binding sites for the motor complex and therefore it is tempting to speculate that multiple Myo4p molecules participate in the transport of the individual tubules. The attachment of multiple motor proteins might ensure a permanent connection of the transport complex to the actin filament, even if single Myo4p molecules fall off. Class-VI myosins were also shown to be present in a monomeric state. For this myosin subclass, it was shown using cross-linking experiments that Myo-VI undergoes cargo-mediated dimerization, and this dimerization was necessary for the catalytic activity (Spudich *et al.* 2007). Whether this is also true for the monomeric Myo4p remains elusive.

iii) Although the possibility that multiple monomeric Myo4p molecules in the cargo complex enable processive movement can not be ruled out (ii), the data from the present work rather indicate a cargo-induced dimerization of the motor protein. The artificially dimerized Myo4p

constructs (Myo4p-GST and Myo4p-GCN4) were shown to interact efficiently with She3p in pull-down and SPR experiments (figures 2.8 and 2.9). Furthermore, complexes of these proteins with She3p showed an approximately 10 fold increased complex stability compared to Myo4p fragments lacking the coiled-coil domain (compare figures 2.4 and 2.8). With the help of the laboratory of Prof. Jansen it could also be shown that an overexpressed Myo4p-GST fragment interferes with She3p binding to endogenous Myo4p. This interference was indirectly observed by impaired bud localization of She3p (Heuck *et al.* 2007). Therefore, an interaction of dimeric Myo4p-tail fragments with She3p is also compatible with results from *in vivo* studies.

For Myo2p it was shown that the coiled-coil region is capable to efficiently dimerize the motor protein (Dunn *et al.* 2007). A hybrid of Myo2p and Myo4p, in which the rod and the globular tail of Myo4p is linked to the coiled-coil region of Myo2p (Myo2p-4p, figure 3.1), should consequently form dimeric motor proteins. In a *myo4Δ* strain, this hybrid protein was able to translocate She3p towards the bud tip (Heuck *et al.* 2007). This experiment shows that a dimerization of Myo4p is also compatible with cargo translocation.

In addition to the arguments resulting from the *in vitro*- and *in vivo*-interaction studies with She3p, a dimerization of Myo4p is also in agreement with the catalytic activity of the Myo4p-motor domain. Using *in vitro* processivity assays, the laboratory of Kathleen Trybus (University of Vermont) showed that a hybrid motor, containing the Myo4p motor domain fused to the lever arm and the coiled-coil domain of murine MyoVa (Myo4p-Va, figure 3.1), is able to move processively along actin filaments at low salt concentrations (Krementsova *et al.* 2006).

Although the results discussed above using heterologous-dimerization domains suggest a dimer formation of Myo4p within the transport complex, it should be mentioned that Myo4p might form oligomers higher than dimers within the co-complexes. However, no oligomeric state higher than a dimer was described for type-V myosins so far (Vale 2003). Regardless whether Myo4p is present as a dimer or a higher oligomer in the complexes with She3p, no oligomerization of Myo4p occurs prior complex formation. In the yeast cell, Myo4p is present at concentrations of about 120 nM, when an average yeast cell volume of 30 μm^3 is assumed (Ghaemmaghami *et al.* 2003, Tyson *et al.* 1979) and therefore in a range at which Myo4p is strictly monomeric (figure 2.6). However, within the co-complex, Myo4p oligomerization has a stabilizing effect. This conclusion is based on the observation that a proteolytic cleavage of the Myo4p-GST fragment after complex formation results in the disassembly of the complexes during pull-down reactions (figure 2.9).

Arguments against a She3p-mediated dimerization of Myo4p came from recent studies with a Myo4p hybrid construct, in which the Myo4p-tail domain was linked to the MyoVa motor (MyoVa-

4p, figure 3.1). This hybrid protein is monomeric in solution as revealed by analytical ultracentrifugation experiments (Hodges *et al.* 2008). The monomeric state of this hybrid protein is in agreement with the results presented here, indicating that the coiled-coil region of Myo4p is not capable to dimerize the motor protein (figure 2.6). In AUC experiments with full-length She3p and the MyoVa-4p hybrid, a complex of one molecule She3p and one molecule of the MyoVa-4p hybrid was determined (Hodges *et al.* 2008). However, to approve these results it is indispensable to compare the sedimentation profiles of the complex with the respective profiles of the individual proteins. Unfortunately, the study from Hodges *et al.* did not include analyses to characterize the sedimentation properties of She3p. However, preliminary AUC experiments in collaboration with Dr. Klaus Richter from the department of Chemistry of the Technical University of Munich revealed that the sedimentation profile of isolated She3p-N is consistent with a dimeric form but seems to exclude the existence of monomeric She3p-N (data not shown). If these preliminary results are true and She3p is indeed present in a dimeric state, the existence of complexes formed by one molecule She3p and one molecule Myo4p seem to be rather unlikely. It is still possible that the She3p-N and the full-length She3p behave differently in complexes with Myo4p. But since the N-terminus of She3p was shown to be sufficient to catalyze the inheritance of cortical ER *in vivo* (Estrada *et al.* 2003) this interpretation is also rather unlikely. The differences in the mentioned studies might be partially explained by the protein fragments used in both studies and suggest a different behavior of the C-terminal Myo4p fragments and the MyoVa-4p hybrid-protein or the She3p-N and the full-length She3p.

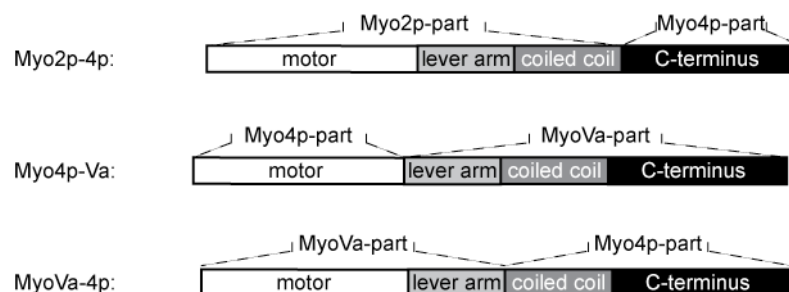


Figure 3.1

Cartoon representation of the Myo4p-hybrid proteins

Myo4p-hybrid proteins were described in the following publications: Myo4p-2p (Heuck *et al.* 2007), MyoVa-4p (Krementsova *et al.* 2006), and Myo4p-Va (Hodges *et al.* 2008).

In summary, the oligomeric state of Myo4p in the complexes with She3p is still under debate. While the results presented in this thesis strongly suggest that stable complexes between Myo4p and She3p require Myo4p dimerization, no direct data is available showing that Myo4p dimerization is required for transport activity of the motor-protein complex. To tackle this problem, *in vitro* processivity assays with full-length Myo4p and stoichiometric amounts of She3p will be necessary. Unfortunately, attempts to prepare full-length Myo4p with recombinant expression systems were not successful so far. In *E. coli* no expression of the full-length Myo4p was

observed, while experiments with the baculovirus-expression system ended up with a weak production of unstable/degrading Myo4p.

3.2 Structure of the Myo4p-She3p complex – an experimental outlook

Attempts to generate diffraction-quality crystals of the Myo4p-She3p complex were not successful so far. However, high resolution structural information on the Myo4p-She3p complex would help to clarify the questions concerning the oligomeric state of Myo4p within the complex (chapter 3.1).

During this thesis work, co-complex crystals were generated with a maximal resolution of 5 Å. This indicates that the proteins generally tend to crystallize and represents therefore a promising starting point. One of the bottlenecks for crystallization is the identification of optimal protein fragments. For Myo4p, two binding sites to She3p could be identified. Unfortunately, both She3p binding sites are not located within the highly ordered, globular part of the Myo4p-tail, but at the rather non-conserved, partially unstructured rod-region and the coiled-coil (figure 2.3 and 2.17). For She3p, a N- and C-terminal truncation of the constructs led to the identification of a minimal Myo4p binding region, including the residues 33-202 of the She3p sequence. However, the use of this fragment in crystallization experiments did not improve crystal quality. In total, various combinations of about 45 different protein fragments were tested in the crystallization experiments (table 2.3). It is rather unlikely that further variations of the protein fragments will improve crystal quality. Potential future strategies should consequently have their focus on the crystallization of homologous proteins from related species or the expression of the protein fragments in eukaryotic cells (yeast- or insect-expression systems). An additional possibility is the use of a Myo4p-tail fragment that lacks the globular tail in the crystallization experiments.

3.3 Two binding regions of Myo4p interact with She3p

By characterizing the interaction of She3p and Myo4p it was determined that She3p binds to two different regions of Myo4p. One binding region is located within the coiled-coil and the second within the rod region. Both regions bind to She3p individually and with comparable affinities of approximately $K_d = 500$ nM (figure 2.3). However, for efficient complex formation She3p has to interact with both regions of Myo4p, since the entire Myo4p-tail fragment binds to the adapter protein with a considerably higher affinity of $K_d = 50$ nM (figure 2.1). This conclusion is further supported by *in vivo*-interference studies. Here, the overexpression of the Myo4p-tail fragment had a strong negative effect on the Myo4p-driven localization of She3p. However, the effect was only moderate for the Myo4p-RGT and the Myo4p-GST, respectively (Heuck *et al.* 2007).

The phenomenon that type-V myosins bind to their adapter proteins via multiple binding sites was already observed for the interaction of Melanophilin to MyoVa. Melanophilin binds in parallel to two binding sites of MyoVa, one located within the coiled-coil region and the other at the globular-tail domain (Au and Huang 2002, Fukuda and Kuroda 2004, Wu *et al.* 2002). The parallel binding to two regions is likely to increase the strength and the specificity for a given interaction.

No type-V myosins are present in plants, but the homologous class-XI myosins are closely related (Richards and Cavalier-Smith 2005, Vale 2003). Similar to the interference effects observed for the Myo4p-tail, two recent studies on Myo-XI revealed that overexpressed C-terminal fragments are only localized correctly, if they contain the coiled-coil region (Li and Nebenfuhr 2007, Reisen and Hanson 2007). These results suggest that Myo-XI-dependent complex assembly uses a similar mechanism as observed for Myo4p and She3p. Also for mouse MyoVa, interference experiments suggest a scenario comparable to the complex formation by Myo4p-tail (Yoshimura *et al.* 2006). In hippocampal neurons the overexpression of various MyoVa-tail fragments suppressed translocation of specific mRNA transcripts only in the case that these fragments contained the coiled-coil region.

The mouse *MyoVa* gene contains seven exons (A to G), from which three (B, D and F) are alternatively spliced. This results in a tissue-specific target pattern of MyoVa and increases the flexibility for cargo transport (Seperack *et al.* 1995). None of the alternatively spliced exons within the *MyoVa* gene are part of the globular-tail domain. Instead, they are located in the coiled-coil region. Therefore, cargo-binding regions at the coiled-coil seem to represent a general property of type-V myosins and may help to stabilize the dimeric state. One example for specific exon usage within the coiled-coil domain is the role of exon B for the interaction with the dynein light chain (DLC) and mRNA (Hodi *et al.* 2006, Salerno *et al.* 2008). DLC binds directly to exon B and thereby increases the coiled-coil formation efficiency of MyoVa (Hodi *et al.* 2006). This might suggest a similar function for DLC and She3p to strengthen the dimeric state of the motor protein. It should be remembered that complexes of She3p with the Myo4p-tail and with Myo4p fragments that contain an artificial dimerization domain showed similar stabilities in the range of minutes, whereas complexes formed with the coiled-coil lacking Myo4p-RGT revealed a stability of only 5 s (compare results figure 2.1, 2.4 and 2.8).

The She3p-binding site within the rod region was located to an area around the residues 1056 and 1057 of the Myo4p sequence (figure 2.5). Secondary structure predictions and sequence alignments indicate that the rod region is rather unstructured and only weakly conserved, compared to other regions of the protein (figure 2.17). Since protein-interaction surfaces are

often highly conserved (Ma *et al.* 2003), it is likely that the mode of interaction between the rod region of Myo4p and She3p follows a rather unique, unusual mechanism.

3.4 Importance of complex stability for directional transport

Time-lapse microscopy revealed that the Myo4p-driven transport of the *ASH1* mRNA towards the bud tip is completed after approximately 2 minutes (Bertrand *et al.* 1998, Lange *et al.* 2008). In the present study, a complex half-life for the interaction of Myo4p with She3p of about 50 seconds was measured (figure 2.1). Of course this value represents only an approximation for the *in vivo* situation, since the experiments were performed *in vitro* with recombinant proteins. When considering that multiple Myo4p motors have been suggested to participate in the transport of cargo complexes (see chapter 3.1), the measured complex half-life of 50 s is likely to be sufficient to complete the cargo translocation *in vivo*. On one hand, transport complexes are only transiently assembled to allow for an efficient de-masking of the mRNAs, making them available for translation. On the other hand, their stability needs to be sufficient to guarantee efficient transport. Consequently, a balance between stability and flexibility has to exist.

ASH1 mRNA contains four localization elements (Gonsalvez *et al.* 2005). Each of these elements is sufficient for bud localization, but with increasing element numbers, the transport becomes more efficient (Chartrand *et al.* 2002). It is tempting to speculate that multiple localization elements recruit multiple motors, resulting in increased translocation efficiency. *IST2* mRNA, which is also translocated by Myo4p, contains only one localization element (Olivier *et al.* 2005). In case mRNAs with one localization element are linked to only one motor protein complex, they are more likely to dissociate from the actin filament. Therefore, it is not surprising that *IST2* mRNA is less efficiently transported (Juschke *et al.* 2005).

3.5 The Myo4p globular-tail domain is conserved in terms of fold but not function

The functions of the globular-tail domains of Myo4p and Myo2p are rather distinct. In Myo2p, the globular-tail domain represents a general landing platform for a number of different adapter proteins (Beach *et al.* 2000, Casavola *et al.* 2008, Fagarasanu *et al.* 2006, Ishikawa *et al.* 2003, Lipatova *et al.* 2008, Pashkova *et al.* 2006, Schott *et al.* 1999, Tang *et al.* 2003), while the globular-tail domain of Myo4p seems to be required for the anchoring of the transport complex at the bud tip (figure 2.12). Therefore, it is remarkable that both domains form very similar structures. The RMSD value for the whole globular-tail domains between Myo4p and Myo2p is 8.4 Å, while the individual subdomains are almost identical with RMSD values of 1.5 Å and 3.0 Å, respectively (figure 2.16). The overall folds of the globular-tail domains of Myo4p and Myo2p seem to be stabilized by conserved, buried residues (table 2.2). Therefore, it is likely that this

conserved architecture is also present in other type-V myosins, suggesting a high conservation of the globular-tail fold. Indeed, comparing the sequences of the globular-tail domains from Myo4p and Myo2p reveals that both domains share 28 % identical residues while 50 % have conservative amino acid exchanges. These values are very similar when comparing the Myo4p globular-tail sequence with different type-V myosins from higher eukaryotes.

Sequence alignments between Myo4p, Myo2p, and human MYOVIa revealed differences between their globular-tail domains (figure 2.16 and 2.17). A surface plot of this alignment onto the Myo4p-GT structure shows that only a minority of the highly conserved residues is exposed to the surface (table 2.2). It is widely accepted that residues, which mediate protein-protein contacts are conserved between different species (Ma *et al.* 2003). Since most of the conserved residues in the Myo4p globular-tail are not surface exposed, they are likely to mediate intramolecular contacts. Thereby, they might stabilize the compact fold of the globular-tail domain, rather than mediating cargo recognition. It is tempting to speculate that the globular domain of the type-V myosins evolved towards a general landing platform for a number of different cargo adapters. If true, an increased surface variability should provide the potential to establish diverse cargo interaction sites.

The main difference between the structural arrangements of the globular tails of Myo4p and Myo2p is the orientation of the subdomains I and II relative to each other (figure 2.16). Interference experiments with the Myo2p globular tail revealed interesting insights in the interdependency of both domains (chapter 1.8). In these experiments, Myo2p-tail fragments were overexpressed in yeast cells. If these overexpressed domains bind efficiently to selected cargo molecules, these cargoes should no longer be available for the binding to endogenous, full-length Myo2p motor and should subsequently not be incorporated into functional transport complexes. The overexpression of the entire globular-tail domain resulted in cell lethality. This is most likely due to failures in the transport of secretory vesicles (Reck-Peterson *et al.* 1999). More interesting were results from experiments, in which both subdomains I and II are overexpressed simultaneously. In contrast to the overexpression of the entire globular-tail domain these cells are viable, indicating a different cargo-binding pattern of the entire globular tail compared with the individual subdomains. This result was rather surprising since the two subdomains were shown to interact closely *in vitro* (Pashkova *et al.* 2005). These cells were defective in the transport of the vacuole but not of secretory vesicles. Surprisingly, the vacuole transport was not affected by an exclusive overexpression of subdomain I, although this domain contains all vacuole binding sites (Pashkova *et al.* 2005). These experiments suggest that the binding of some adapter proteins might require both subdomains.

Li *et al.* suggested for type-XI myosins that two alternative orientations of both subdomains might explain these distinguishable phenotypes. They propose that adapter proteins prefer certain orientations for their binding to the globular-tail domain (Li and Nebenfuhr 2007). However, this is a rather unlikely situation for Myo4p. Both subdomains I and II include parts of helix H6 as an integral structural element (figure 2.15 and 2.16). Since this helix forms a continuous intersection, it prevents the formation of alternative arrangements. By analyzing the Myo4p-GT structure, one notices that the loop region connecting the helices H6 and H7 is rather short. Therefore, it is unlikely that this loop can form a flexible hinge that allows switching between two alternative conformations. Furthermore, the interface between subdomain I and II of the Myo4p-GT is quite large (1190 Å² if the bracket loop is included in the calculation and 1095 Å² without) and mainly hydrophobic. This large contact area also argues against alternative orientations. Consistently, recombinant expression of the individual Myo4p subdomains in *E. coli* resulted in insoluble, degrading proteins (data not shown). It is interesting to speculate that instability of the individually expressed subdomains might be the simple reason for the results observed in the interference assay with Myo2p.

In summary, the existence of two alternative conformations between subdomain I and II is unlikely for Myo4p. Since the structural geometry between the globular-tail domains of Myo2p and Myo4p is very similar, this assumption might be extended to all type-V myosins.

Vertebrate type-V myosins are auto-inhibited in a cargo-free situation, (figure 1.3) (Li *et al.* 2006, Liu *et al.* 2006, Thirumurugan *et al.* 2006). If autoinhibited, the myosins are in a folded conformation, in which the globular-tail domain mediates direct contacts to the motor domain. *In vitro* studies demonstrated that binding of the globular-tail domain to the motor region regulates the catalytic ATPase activity of the myosin (Li *et al.* 2006). Upon cargo binding the folded conformation is released and the catalytic activity is restored. Since Myo4p alone is monomeric and thus non-processive under physiological conditions, this type of autoinhibition is most probably not required. The region that mediates the interaction between the motor and the tail domain was mapped for the mouse MyoVa globular tail to the residues K1706 and K1779 of the MyoVa sequence (Li *et al.* 2008). These positively charged residues are highly conserved throughout various species, but not in the Myo4p globular-tail sequence (the corresponding residues are C1320 and A1390). Again, the missing conservation of these regulatory residues highlights the special situation for the Myo4p globular tail and furthermore indicates that Myo4p is not regulated via autoinhibition.

3.6 The globular-tail domain as a peripheral membrane-binding domain

Peripheral membrane proteins interact with the lipid bilayer mainly via three different mechanisms: i) by a specific recognition of certain phospholipid head groups, ii) by electrostatic

interactions with the negatively charged membrane surface or iii) via the penetration of the lipid bilayer (Lemmon 2008). In this context it is important to mention that the participation of any of these association types might vary dramatically between different membrane binding proteins.

Within the present work, it was shown that the globular-tail domain of Myo4p binds directly to lipid vesicles in floatation experiments (figure 2.18). Furthermore, with the help of the Myo4p-GT crystal structure, the region of Myo4p that mediates the vesicle contact was mapped to the residues W1325 and Y1329 (figure 2.19). Three lysine residues and one arginine surround the residues W1325 and Y1329. Thus, one potential mechanism by which the globular-tail domain achieves its peripheral membrane association is that the positively charged residues mediate electrostatic interactions with the lipid surface, bringing the aromatic residues in proximity to the hydrophobic part of the membrane. Subsequently, the aromatic residues might penetrate the lipid bilayer. A direct vesicle association of Myo4p was previously described in a large scale interaction study. This interaction was strengthened if the vesicles contain phosphatidylinositol-3,5-bisphosphate (Zhu *et al.* 2001). Potentially, the globular-tail domain mediates the lipid binding observed in these previous experiments.

The residues W1325 and Y1329 are located on top of helix H9. A helical localization represents a rather unusual geometry for a peripheral membrane-binding domain. Most of the so far defined peripheral membrane interaction motives like the C1 domain (Colon-Gonzalez and Kazanietz 2006), the PH domain (Lemmon and Ferguson 2000) or the FYVE domain (Kutateladze 2006) recognize specific membrane components via defined structural elements (Lemmon 2008). Furthermore, they penetrate the membrane with residues that are located within flexible loop regions (figure 3.2) (Dumas *et al.* 2001, Macedo-Ribeiro *et al.* 1999, Zhang *et al.* 1995). Nevertheless, the Epsin-N-terminal homology (ENTH) domain represents an example for proteins, in which helical regions are directly involved in membrane association (figure 3.2). Similar to Myo4p, these protein domains were described to bind specifically to certain phosphatidylinositol derivatives (Ford *et al.* 2002, Ford *et al.* 2001, Legesse-Miller *et al.* 2006, Stahelin *et al.* 2003, Zhu *et al.* 2001).

In Myo4p, the region identified to be membrane associated includes only two residues that might penetrate the lipid bilayer directly and keep the protein attached to the membrane. An assessment of the examples listed in figure 3.2 indicates that also within these domains only few residues directly penetrate the membrane.

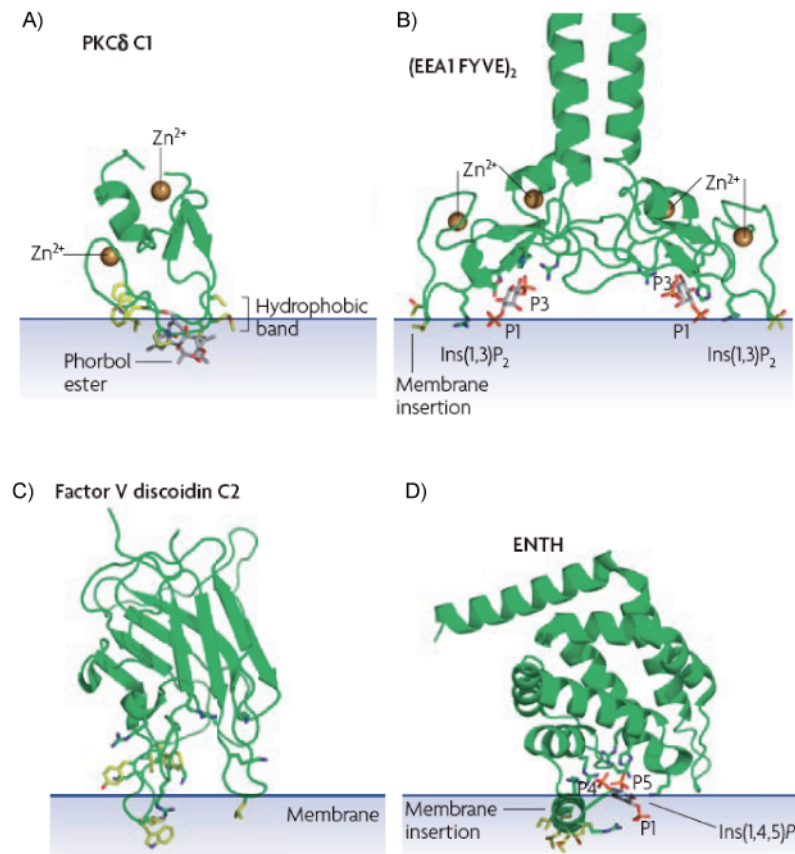


Figure 3.2

Representation of four different peripheral associated membrane domains

Positively charged residues, which mediate electrostatic interactions with the negatively charged membrane surface are highlighted in stick representation. Yellow colored residues directly penetrate the lipid bilayer. Shown are: A) The protein kinase δ (PKC δ) C1 domain (PDB code 1PTR, Zhang *et al.* 1995), B) the C-terminal region of the early endosome autoantigen (EEA) bound to inositol 1,3-bisphosphate (PDB code 1JOC, Dumas *et al.* 2001), C) the membrane-binding C2 domain of human coagulation factor V (PDB code 1CZS Macedo-Ribeiro *et al.* 1999) and D) Epsin N-terminal homology (ENTH) domain of epsin bound to Ins(1,4,5)P₃. (PDB code 1H0A, Ford *et al.* 2002). Picture was taken from Lemmon 2008 (Lemmon 2008).

Despite the results from the floatation experiments, attempts to quantify the Myo4p-membrane interaction with either SPR or RfS spectrometry were not successful (chapter 2.22). SPR experiments with an L1 chip and immobilized vesicles as ligand might have failed due to problems with the experimental setup. But if the Myo4p-GT membrane association observed in the floatation experiments is real, why could no lipid interaction be observed for the globular tail in the RfS experiments? First of all, the experimental setups are quite different between the floatation assay and the RfS experiment. Before the proteins were centrifuged for floatation, they were incubated with the membranes for approximately 30 min. In case such a long incubation time is necessary to generate stable membrane contacts, the rather dynamic situation in the RfS experiment would not allow for binding events. Here, the Myo4p globular-tail domain was floated

over the surface, allowing every molecule an approximately 30 s contact time with the membrane. *In vivo*, the translocation particles that are transported towards the bud tip seem to have a considerable longer membrane contact time. Experiments tracking individual Myo4p translocation particles *in vivo* revealed that Myo4p driven mRNP transport follows a straight bud directed movement in the mother cell. Later in the bud, translocation speed decreases and the movement is restricted to the cortex. Generally, at the bud tip the movements resembled a diffusion-like search for an anchoring point, indicating that the attachment to membranes might require a longer contact time (Lange *et al.* 2008).

One general problem towards the identification of peripheral membrane proteins is that most of the already characterized domains bind to membranes with a quite low affinity, while some are not even able to mediated membrane association on their own (Lemmon 2008). Therefore, these proteins require additional factors to mediate stable membrane binding, like dimerization or the recruitment of additional membrane binding domains (Klein *et al.* 1998, Seaman and Williams 2002). The potential dimerization of Myo4p in the complex with She3p (as discussed in chapter 3.1) might play a role in the membrane association. In case the binding of individual, monomeric Myo4p-GT molecules to membranes is not sufficient to mediate stable membrane binding, the dimerization of the motor could increase its affinity for membranes as observed for other peripheral membrane proteins (Klein *et al.* 1998).

Within the globular-tail domain, the dilute (DIL) region was identified as a conserved sequence that defines the class of type-V myosins. DIL regions are also found in proteins like Unc-104 and AF-6, a putative target for Ras proteins (Kuriyama *et al.* 1996, Ponting 1995). In Myo4p, the DIL region includes the residues 1300 to 1400. The identified membrane-binding region of Myo4p is formed by the aromatic residues W1325 and Y1329 and is part of the DIL domain (figure 2.19). Since neither the Myo2p globular tail nor the MyoVa globular tail (data not shown) showed a stable membrane association during floatation experiments, it remains to be shown whether membrane binding constitutes a more general feature of DIL domain-containing proteins. Furthermore, Unc-104 was shown to bind directly to lipid vesicles, however this binding is mainly mediated via a PH domain rather than the DIL region (Klopfenstein *et al.* 2002).

As it will be discussed in the following chapter, one potential function for the membrane association of Myo4p might be the anchoring of its cargo at the bud tip. If this is the case, the Myo4p membrane interaction requires a slow off rate, rather than a fast on rate. In the floatation assay, in which equilibrium is observed after 16 hours of centrifugation, the membrane association has to be stable for this entire period of time (figure 2.18). So, membrane association by the Myo4p-GT seems to represent a rather static event. Overexpression of the Myo4p-GT domain *in vivo* results in a random localization of that domain throughout the whole cytoplasm (Reck-Peterson *et al.* 1999). This indicates that Myo4p seem to require a long and static

membrane contact in order to mediate direct binding, as achieved by Myo4p accumulation at the bud tip.

3.7 The function of the globular-tail domain

Most type-V myosins like yeast Myo2p and vertebrate MyoVa interact with their cargoes mainly through binding sites located within the globular-tail domain. The globular tail of Myo2p for example binds to several different adapter proteins, linking the motor to a variety of different cargoes (chapter 1.5.3). In contrast, the only identified cargo-adapter protein for Myo4p is She3p (see chapter 1.7.1 and 1.7.2). The present work reveals that the interaction between both proteins does not require the globular-tail domain (figure 2.3). The first indication that the globular-tail domains of Myo2p and Myo4p fulfill different functions came from *in vivo*-localization studies for both domains, performed by Reck-Peterson and colleagues (Reck-Peterson *et al.* 1999). An overexpression of the Myo4p globular tail leads to a random distribution throughout the entire cytoplasm. In contrast, the Myo2p globular-tail domain localizes to the bud tip after overexpression. This bud-tip localization is most likely due to an interaction of the Myo2p globular tail with already localized adapter proteins. This result further suggests that the Myo4p globular tail is not binding to additionally localized adapter proteins that have not been identified to date (Reck-Peterson *et al.* 1999).

3.7.1 On cortical ER inheritance

What is the function of the Myo4p globular tail if not the binding to adapter proteins? To answer this question, the role of this domain for both Myo4p functions, i.e. the cortical ER inheritance and mRNA transport, was investigated. Surprisingly, cells expressing the Myo4p Δ GT in a Δ *myo4* background showed no difference in the inheritance of the cortical ER compared to wild-type cells (figure 2.10). This result reveals insights into the mechanisms of ER transport by Myo4p. First, the globular-tail domain itself is not binding to a yet unidentified further ER-adapter protein. Second, the previously identified membrane binding of Myo4p (Zhu *et al.* 2001), which is most probably mediated by the residues W1325 and Y1329 of the globular-tail domain (chapter 2.20), has no effect on ER transport.

It is already known that the RNA binding protein She2p is not required for ER inheritance (Estrada *et al.* 2003), although it associates with the ER independently of Myo4p and She3p (Schmid *et al.* 2006). Recent data from the laboratory of Prof. Jansen strongly suggest a direct association of She2p with ER membranes (M. Schmid & R.-P. Jansen: personal communication). Consequently, an interaction of She2p and She3p could potentially form an alternative connection of the motor complex to the ER. This linkage might explain why a lack of the globular-tail domain had no influence on ER inheritance. However, in control experiments with *myo4* Δ GT

cells, in which the She2p binding domain of She3p (Böhl *et al.* 2000) was removed, effective ER transport was also observed (Estrada *et al.* 2003, and own observation). This result makes a potential “cross linking” of the motor complex via She2p unlikely. However, the possibility that both types of ER tethering are redundant and only one of them is sufficient for ER inheritance cannot be excluded.

The N-terminus of She3p is the only identified adapter that is required for the cortical ER transport (Estrada *et al.* 2003). Therefore it was interesting to see that the She3p-N fragment showed no direct membrane association in floatation experiments (figure 2.18). This result may suggest the existence of a yet unidentified component within the ER membrane, which mediates the linkage of the organelle to the motor complex.

Myosin-dependent ER transport is mainly restricted to yeast and plant cells, while microtubules represent the major ER tracks in animal cells (Du *et al.* 2004). However, MyoVa-lacking mice have no smooth ER in the dendritic spines of Purkinje cells, suggesting also a role of this motor in ER transport (Bridgman 1999, Takagishi *et al.* 1996). Furthermore, it was described that in *Xenopus*-egg extracts the ER-network formation depends on microtubules. However, myosin-V dependent transport can compensate the network formation if the microtubules are blocked in these cells (Wollert *et al.* 2002). These examples indicate that a type-V myosin-dependent ER transport takes place in vertebrate cells and is eventually driven by similar molecular mechanisms as the inheritance of cortical ER in yeast.

3.7.2 On mRNA transport

Although *myo4ΔGT* cells showed a normal cortical ER inheritance (figure 2.10), the localized translation of *ASH1* mRNA was clearly affected in these cells (figure 2.11). The yeast strains used in the experiments carried the adenine synthetase *ADE2* gene behind the *HO*-promoter region. Consequently, the *ADE2* gene is not expressed in the presence of Ash1p and therefore depends on the correct distribution of *ASH1* mRNA (chapter 2.13). Obviously, this experiment is unsuitable to distinguish between potential defects occurring either during the transport, in the translational control or by the anchoring of the mRNP at the bud tip. The previous chapter described that a Myo4p fragment lacking the globular-tail domain efficiently catalyzes the cortical ER inheritance. Therefore it is unlikely that impaired catalytic activity of the motor protein fragment is the reason for the defective localized mRNA translation. Furthermore, the efficient ER transport indicates that also *in vivo* the globular tail is not required for the binding of Myo4p to She3p (compare figure 2.3 and 2.10). Because She3p seems to bind efficiently to Myo4pΔGT, it is most likely that also She3p-bound She2p and its target mRNAs are efficiently captured by Myo4p, lacking the globular-tail domain. Furthermore, a hybrid protein that links She2p and

She3p covalently with each other (in this construct She2p is connected to the C-terminus of She3p-N) is still able to mediate essentially the same function as both proteins individually (Du *et al.* 2008). Since the interaction between She3p and She2p itself tolerates such significant alterations, a deletion of the Myo4p globular-tail domain is unlikely to impair the She3p-She2p interaction.

Is translational control affected in Myo4p complexes lacking the globular-tail domain? The proteins Puf6p and Khd1p are described to prevent *ASH1*-mRNA translation during the transport event and bind directly to the mRNA and furthermore to ribosomal initiation factors (Deng *et al.* 2008, Gu *et al.* 2004, Irie *et al.* 2002, Paquin *et al.* 2007). However, none of these proteins was shown to interact with the globular-tail domain of Myo4p or the Myo4p-interaction partner She3p. In summary, it can be assumed that translational control is unlikely to be regulated by Myo4p or the globular-tail domain.

Phosphorylation was shown to be important for the regulation of transport events mediated by Myo2p and Myo4p. For instance, the protein phosphatase Ptc1p is involved in the localization of almost all Myo2p dependent cargoes (Jin *et al.* 2008). However, the effects mediated by Ptc1p seem to be indirect, since the adapter proteins of Myo2p are destabilized in $\Delta ptc1$ cells. In addition, the Myo2p tail domain itself contains phosphorylation sites in the amino acid region 1132-1135 (Legesse-Miller *et al.* 2006) that potentially regulate the binding of adapter proteins to the globular tail.

$\Delta ptc1$ cells showed also a slight translocation defect for the cortical ER and *ASH1* mRNA (Jin *et al.* 2008). Since the ER transport in *myo4 Δ GT* cells is not affected, a role of the globular tail in this signaling pathway is rather unlikely. Furthermore, the amino acid residues 1132-1135 of the Myo2p sequence (the phosphorylation site) are not conserved between Myo2p and Myo4p. All these arguments suggest that the defective mRNA transport in *myo4 Δ GT* cells is unlikely due to a deficiency of phosphorylation. In contrast, phosphorylation was shown for Khd1p and Puf6p to occur at the bud tip, leading to an onset of translation of the transported mRNA (Deng *et al.* 2008, Paquin *et al.* 2007). Therefore, phosphorylation seems to be required for the regulation of translational control rather than for the motor activity in mRNA transport.

3.7.3 Anchoring at the bud tip

In enterochromaffin cells, MyoVa was described to have a role in the exocytosis of secretory vesicles (Desnos *et al.* 2007). Overexpression of the MyoVa globular tail in these cells resulted in a reduced number of secretory vesicles, which are attached to the plasma membrane and MyoVa silencing decreased exocytosis in these cells. The attachment of MyoVa at exocytotic sites seems to involve binding of the motor to integrated-membrane proteins like Syntaxin-1, which

binds to the neck region of MyoVa (Toonen *et al.* 2006, Watanabe *et al.* 2005). Since the anchoring of Myo4p at the bud tip depends at least partially on the globular-tail domain, this attachment is likely to follow a different mechanism.

ASH1 mRNA that is artificially tethered to She2p is efficiently transported into the daughter cell but fails to be properly anchored at the bud tip (Gonsalvez *et al.* 2004). Furthermore, anchoring at the bud tip is a quite complex process that requires additional mRNA binding proteins (Trautwein *et al.* 2004), active translation of the mRNA transcripts (Gonzalez *et al.* 1999) and eventually a molecular remodelling of the Myo4p-She3p-She2p heterotrimeric complex (Gonsalvez *et al.* 2004). Mutations affecting cortical-ER inheritance to the bud (*sec3Δ*, and *srp101Δ*) also affect asymmetric mRNA localization (Aronov *et al.* 2007). In addition to all these aspects does the globular-tail domain of Myo4p also have a function in retaining the motor protein at the bud tip. Cells, which express Myo4p Δ GT, have a considerably reduced amount of the motor protein localized at the bud tip and show impaired *ASH1*-mRNA translation in the bud (figures 2.11 and 2.12). In summary, several mechanisms seem to work in parallel to mediate efficient anchoring of the transport complex at the bud tip.

3.8 Summary

To date, only little is known about the mechanisms by which motor proteins achieve specific cargo interactions. In particular, few information are available on the structural basis of myosin-cargo interactions and quantitative aspects of complex formation. This work aimed at the multidisciplinary characterization of molecular principles underlying motor-cargo recognition. In order to reach this goal, the complex formation between the type-V myosin Myo4p from budding yeast and its adapter She3p was analyzed. Since this interaction belongs to one of the best-characterized transport events, it is a well-suited model to tackle structural and mechanistic questions.

In this study, the interaction of the Myo4p-She3p complex was quantified by Surface-Plasmon Resonance revealing an equilibrium-dissociation constant of approximately 50 nM and a half-live time of approximately 52 s. *In vivo*, individual transport complexes of Myo4p and She3p require up to 2 minutes to reach their site of destination (Bertrand *et al.* 1998, Lange *et al.* 2008). Since multiple Myo4p-She3p complexes have been suggested to be present in transport particles, this complex stability might be sufficient to allow for efficient cargo translocation. Nevertheless, it also indicates that the assembly of transport complexes represents a balance between stability of the complexes and the release of the individual components. The present work also revealed that Myo4p alone is strictly monomeric. Since this is a rather unusual characteristic for type-V myosins, this finding leads to the question how the monomeric motor catalyzes processive movement *in vivo*. Experiments using fusion proteins of the Myo4p-tail to heterologous dimerization domains suggest that Myo4p is transferred into the dimeric state upon binding to She3p. This dimerization might trigger motor activation.

It has been suggested that the globular-tail domain of type-V myosins generally functions as a cargo-binding domain. In contrast, the present results show that She3p does not bind to the globular tail but to the rather unstructured rod region and the coiled-coil domain of Myo4p. *In vivo* experiments revealed that the globular tail is dispensable for the inheritance of the cortical ER. It is however required for the localized translation of *ASH1* mRNA, most likely by helping to anchor the motor complex at the bud tip. Consistently, floatation experiments with the globular tail and membrane vesicles revealed a direct lipid association, suggesting bud anchoring through direct membrane association. The crystal structure of the globular-tail domain was solved at 2.3 Å resolution and used to identify the region, which mediates lipid association. Structure-based mutational analyses resulted in the identification of a membrane-binding surface. Comparison of the structure with the recently published structure of the Myo2p globular tail revealed high similarities of the overall fold but a low sequence conservation of surface-exposed residues. This low surface conservation of the globular-tail domain might indicate the evolutionary adaptation of type-V myosins towards the binding of a large number of different cargoes, including proteins or membranes.

4. Materials and Methods

4.1 Consumables

All common chemicals were obtained from Merck (Darmstadt, Germany), Roth (Karlsruhe, Germany) and Sigma (Deisenhofen, Germany), unless stated otherwise. Enzymes and nucleotides for molecular biology as well as markers and loading dyes for electrophoresis were ordered by MBI Fermentas (St. Leon-Rot, Germany) or New England Biolabs (Frankfurt, Germany). Components to prepare media for bacteria and yeast growth were obtained from BD (Heidelberg, Germany) and Sigma. Chromatographic materials and columns as well as materials for western blots were purchased from GE Healthcare (Freiburg, Germany). Lipids were obtained from Avanti-Polar-Lipids (Alabaster, USA), Roth and Sigma. Crystallization screens and crystallization tools were obtained from Hampton Research (Aliso Viejo, USA) and Qiagen (Hilden, Germany). Finally, oligonucleotides for cloning were ordered by Thermo Scientific Electron Corporation (Ulm, Germany).

4.2 Plasmid DNA

4.2.1 Purchased plasmids

Name	Appication	Source
pGEX-6P-1	Bacterial expression	GE Healthcare
pET28a	Bacterial expression	Novagen (Schwalbach,Germany)
pYM17	Genomic yeast tagging	(Janke <i>et al.</i> 2004)
pYM19	Genomic yeast tagging	(Janke <i>et al.</i> 2004)

4.2.2 Plasmids for *E. coli* expression (biochemical characterization)

	Insert	Vector	Template	Primer	Mut. Primer	Enzyme
P002	She3p-N	pET 28a	genomic DNA			
P007	Myo4p-tail	pGEX-6P-1	<i>genomic DNA</i>	O002/O004		BamHI/XhoI
P129	Myo4p-CC	pGEX-6P-1	<i>genomic DNA</i>	O001/O124		BamHI/XhoI
P022	Myo4p-GT	pGEX-6P-1	<i>genomic DNA</i>	O013/O004		BamHI/XhoI
P010	Myo4p-RGT	pGEX-6P-1	<i>genomic DNA</i>	O005/O004		BamHI/XhoI
P131	Myo4p-GCN4	pGEX-6P-1	<i>genomic DNA</i>	O125/O004	O126/O127	BamHI/XhoI
P050	Myo2p-GT ₍₁₀₈₄₋₁₅₇₅₎	pGEX-6P-1	<i>genomic DNA</i>	O027/O086		BamHI/XhoI
P134	Myo4p-tail _{F1056R, I1057R}	pGEX-6P-1	<i>genomic DNA</i>	O002/O004	O98/O99	NdeI/SpeI
P161	Myo4p-GT _{F1379D, Y1381D}	pGEX-6P-1	<i>genomic DNA</i>	O013/O004	O158/O157	NsiI/XhoI
P170	Myo4p-GT _{W1325D, Y1329D}	pGEX-6P-1	<i>genomic DNA</i>	O013/O004	O165/O166	BamHI/XhoI
P173	Myo4p-GT _{R1333D}	pGEX-6P-1	<i>genomic DNA</i>	O013/O004	O169/O170	BamHI/XhoI
P175	Myo4p-GT _{R1333D, K1366D}	pGEX-6P-1	<i>P173</i>	O013/O004	O171/O172	BamHI/XhoI
P176	Myo4p-GT _{K1326D, R1333D, K1366D}	pGEX-6P-1	<i>P175</i>	O013/O004	O173/O174	BamHI/XhoI
P177	Myo4p-GT _{K1326D, R1333D, K1366D, K1400D}	pGEX-6P-1	<i>P176</i>	O013/O004	O175/O176	BamHI/XhoI

4.2.3 Plasmids for *E. coli* expression (crystallization)

	Insert	Vector	Template	Primer	Mut. Primer	Enzyme
P131	Gcn4p ²⁴²⁻²⁷¹ -Myo4p ¹⁰²⁹⁻¹⁴⁷¹	pGEX-6P-1	genomic DNA	O125/O004	O126/O127	BamHI/XhoI
P038	Myo2p ¹⁰⁰⁸⁻¹⁰⁸⁸ -Myo4p ¹⁰⁴²⁻¹⁴⁷¹	pET 28a	genomic DNA	O015/O004		SacI/XhoI
P048	Myo4p ¹⁰⁰⁶⁻¹⁴⁷¹	pGEX-6P-1	genomic DNA	O037/O004		BamHI/XhoI
P077	Myo4p ¹⁰⁰⁶⁻¹⁴⁷¹ (C1113S)	pGEX-6P-1	genomic DNA	O037/O004	O054/O055	BamHI/XhoI
P079	Myo4p ¹⁰⁰⁶⁻¹⁴⁷¹ (C1113S,C1288S)	pGEX-6P-1	P077	O037/O004	O056/O057	BamHI/XhoI
P081	Myo4p ¹⁰⁰⁶⁻¹⁴⁷¹ (C1113S,C1288S,C1320S)	pGEX-6P-1	P079	O037/O004	O058/O059	BamHI/XhoI
P064	Myo4p ¹⁰⁰⁹⁻¹⁴⁷¹	pGEX-6P-1	genomic DNA	O046/O004		BamHI/XhoI
P065	Myo4p ¹⁰¹²⁻¹⁴⁷¹	pGEX-6P-1	genomic DNA	O047/O004		BamHI/XhoI
P010	Myo4p ¹⁰⁴²⁻¹⁴⁷¹	pGEX-6P-1	genomic DNA	O005/O004		BamHI/XhoI
P007	Myo4p ⁹⁷⁸⁻¹⁴⁷¹	pGEX-6P-1	genomic DNA	O002/O004		BamHI/XhoI
P133	Myo4p ⁹⁷⁸⁻¹⁴⁷¹ (C1113S,C1288S,C1320S)	pGEX-6P-1	P081			NdeI/SpeI
P030	Myo4p ⁹⁹⁶⁻¹⁰⁷²	pGEX-6P-1	genomic DNA	O003/O018		BamHI/XhoI
P033	Myo4p ⁹⁹⁶⁻¹⁴²⁰	pGEX-6P-1	genomic DNA	O003/O021		BamHI/XhoI
P035	Myo4p ⁹⁹⁶⁻¹⁴⁶³	pGEX-6P-1	genomic DNA	O003/O020		BamHI/XhoI
P037	Myo4p ⁹⁹⁶⁻¹⁴⁶⁷	pGEX-6P-1	genomic DNA	O003/O019		BamHI/XhoI
P008	Myo4p ⁹⁹⁶⁻¹⁴⁷¹	pGEX-6P-1	genomic DNA	O003/O004		BamHI/XhoI
P117	Myo4p ^{C1042-1471} (C1113S,C1288S,C1320S)	pGEX-6P-1	P081	O115/O004		BamHI/XhoI
P118	Myo4p ^{CA1042-1471} (C1113S,C1288S,C1320S)	pGEX-6P-1	P081	O116/O004		BamHI/XhoI
P116	Myo4p ^{CC1042-1471} (C1113S,C1288S,C1320S)	pGEX-6P-1	P081	O114/O004		BamHI/XhoI
P023	She3p ¹⁻²²¹	pGEX-6P-1	genomic DNA	O006/O012		BamHI/XhoI
P018	She3p ¹⁻²²⁸	pGEX-6P-1	genomic DNA	O006/O011		BamHI/XhoI
P015	She3p ¹⁻²³¹	pGEX-6P-1	genomic DNA	O006/O010		BamHI/XhoI
P012	She3p ¹⁻²³⁴	pGEX-6P-1	genomic DNA	O006/O007		BamHI/XhoI
P043	She3p ¹⁶⁻²⁰²	pGEX-6P-1	genomic DNA	O022/O024		BamHI/XhoI
P039	She3p ¹⁶⁻²²¹	pGEX-6P-1	genomic DNA	O22/O012		BamHI/XhoI
P019	She3p ³⁻²²⁸	pGEX-6P-1	genomic DNA	O008/O011		BamHI/XhoI
P016	She3p ³⁻²³¹	pGEX-6P-1	genomic DNA	O008/O010		BamHI/XhoI
P066	She3p ³³⁻²⁰²	pGEX-6P-1	genomic DNA	O023/O024		BamHI/XhoI
P040	She3p ³³⁻²²¹	pGEX-6P-1	genomic DNA	O023/O012		BamHI/XhoI
P076	She3p ⁴⁰⁻¹⁹⁴ (C147S)	pGEX-6P-1	P072	O050/O051		BamHI/XhoI
P068	She3p ⁴⁰⁻²²¹	pGEX-6P-1	genomic DNA	O050/O012		BamHI/XhoI
P084	She3p ⁶⁻¹⁴⁰	pGEX-6P-1	genomic DNA	O009/O068		BamHI/XhoI
P083	She3p ⁶⁻¹⁶⁵	pGEX-6P-1	genomic DNA	O009/O067		BamHI/XhoI
P070	She3p ⁶⁻¹⁹⁴	pGEX-6P-1	genomic DNA	O009/O051		BamHI/XhoI
P074	She3p ⁶⁻¹⁹⁴ (C147S)	pGEX-6P-1	P072	O009/O051		BamHI/XhoI
P041	She3p ⁶⁻²⁰²	pGEX-6P-1	genomic DNA	O009/O024		BamHI/XhoI
P072	She3p ⁶⁻²¹¹ (C147S)	pGEX-6P-1	genomic DNA	O009/O012	O052/O053	BamHI/XhoI
P024	She3p ⁶⁻²²¹	pGEX-6P-1	genomic DNA	O009/O012		BamHI/XhoI
P020	She3p ⁶⁻²²⁸	pGEX-6P-1	genomic DNA	O009/O011		BamHI/XhoI
P017	She3p ⁶⁻²³¹	pGEX-6P-1	genomic DNA	O009/O010		BamHI/XhoI
P014	She3p ⁶⁻²³⁴	pGEX-6P-1	genomic DNA	O009/O007		BamHI/XhoI
P088	She3p ⁸⁸⁻¹⁹⁴	pGEX-6P-1	genomic DNA	O070/O051		BamHI/XhoI
P071	She3p ⁹⁻¹⁹⁴	pGEX-6P-1	genomic DNA	O049/O051		BamHI/XhoI
P075	She3p ⁹⁻¹⁹⁴ (C147S)	pGEX-6P-1	P072	O009/O051		BamHI/XhoI
P067	She3p ⁹⁻²²¹	pGEX-6P-1	genomic DNA	O049/O012		BamHI/XhoI

4.3 E. coli strains

Strain	Essential genotype	Source
XL-1 blue	recA1 endA1 gyrA96 thi-1 hsdR17 supE44 relA1 lac [<i>F'</i> pro AB lac ^f ZΔ M15 Tn10 (<i>Tet</i> ^r)]	Stratagene; La Jolla, USA
BL21 (DE3)	B F ⁻ ompT hsdS(<i>r_B</i> m _B) dcm+ Tet ^r galλ. (DE3) EndA Hte [argU ileY leuW Cam ^r]	Stratagene; La Jolla, USA
B834 (DE3)	F ⁻ ompT gal met <i>r_B</i> m _B	Novagen; Schwalbach, Germany

4.4 S. cerevisiae strains

Strain	Essential genotype	Source
Y18	<i>MAT a; URA3::HMG1-GFP;</i>	(Schmid <i>et al.</i> 2006)
Y21	<i>MAT a; URA3::HMG1-GFP; HIS3::MYO4-9Myc</i>	this study
Y22	<i>MAT a; URA3::HMG1-GFP; HIS3::MYO4-1090stop-9Myc</i>	this study
Y28	<i>MAT a; trp1-1; leu2-3; his3-11; ura3; ade2-1; HO-ADE2, HO-CAN1</i>	(Jansen <i>et al.</i> 1996)
Y29	<i>MAT a; trp1-1; leu2-3; his3-11; ura3; ade2-1; HO-ADE2, HO-CAN1, HIS3::MYO4-9Myc</i>	this study
Y30	<i>MAT a; trp1-1; leu2-3; his3-11; ura3; ade2-1; HO-ADE2, HO-CAN1; HIS3::MYO4-1090stop-9Myc</i>	this study
Y32	<i>MAT a; trp1-1; leu2-3; his3-11; leu; ura3; ade2-1; HO-ADE2, HO-CAN1; MYO4::URA3</i>	(Jansen <i>et al.</i> 1996)
Y42	<i>MAT a; trp1-1; leu2-3; his3-11; ura3; ade2-1; HO-ADE2, HO-CAN1; HIS3::MYO4-9Myc; CloNat::SHE2-6HA</i>	this study
Y43	<i>MAT a; trp1-1; leu2-3; his3-11; ura3; ade2-1; HO-ADE2, HO-CAN1; HIS3::MYO4-1090stop-9Myc; CloNat::SHE2-6HA</i>	this study

4.5 Oligonucleotides

Primer for biochemical characterization		Primer for complex crystallization	
O001	5' aaaggatcccaaaaagaagtgaagaacggaatattagg 3'	O002	5' aaaggatccaagcaaaggcaagagtacg 3'
O002	5' aaaggatccaagcaaaggcaagagtacg 3'	O003	5' aaaggatccaagctgaagacgttacaagttg 3'
O004	5' aaactcgagttattttctgctcaatttataat 3'	O004	5' aaactcgagttattttctgctcaatttataat 3'
O005	5' aaaggatccagattaagtgatgaagtcaaa 3'	O005	5' aaaggatccagattaagtgatgaagtcaaa 3'
O013	5' aaaggatccctagtcattgaattcgtaga 3'	O006	5' aaaggatccatgctgaccaggataatacc 3'
O027	5' ggggatccatgctgctggcaccgttact 3'	O007	5' ggactcgagtactgctcaattttga 3'
O086	5' gcactcgagttagtgccgtcttgaacgac 3'	O008	5' aaaggatcccaggataataccagacttct 3'
O124	5' aaactcgagttatctgaagttgttacc 3'	O009	5' aaaggatccaccagacttctcaagcaag 3'
O125	5' aaaggatcccgtgcgagaagttgcaaaga 3'	O010	5' ggactcgagttatttgaatcctttctgttc 3'
O126	5' agaaattagttggcgaacgcatgcaaagttggctgctat 3'	O011	5' ggactcgagtacttttctgtttccagagattt 3'
O127	5' atagcagccaaactttgcatgctgccaactaatttct 3'	O012	5' ggactcgagttacaaatcttccagagtcatt 3'
O157	5' aagtactattcgatgattgggatgcttgaatccagcc 3'	O015	5' ggagagctcagattaagtgatgaagtcaaa 3'
O158	5' ggctggattcaaggcatccaatcatcgaatagtaactt 3'	O018	5' gaactcgagttaatagcagaatatgtggtggtgaa 3'
O165	5' tgcctcgctaaatgataagtaggggatgaagtgatgataaat 3'	O019	5' aaactcgagttatttataattttactgacagt 3'
O166	5' atttctatccactcatcccatactatcatttaacgctgggaca 3'	O020	5' gaactcgagttactgacagtagctaaagccctc 3'
O171	5' aagatattacagttggacataagcaacttgaac 3'	O021	5' gaactcgagttattctttgatcagcttagc 3'
O172	5' gttcaagttgcttatgccaactgtaataatctt 3'	O022	5' aaaggatcccctcaccataatattttatggca 3'
O173	5' cccgcttaaatgggattatgggtacgaagtg 3'	O023	5' aaaggatccagaataacctccagccaaaat 3'
O174	5' cactcgtaccataatccaatttaacgctggg 3'	O024	5' ggactcgagttatgaactgatctgaaccata 3'
O175	5' tacaagcctgtaacgatggcgaagctggagta 3'	O037	5' aaaggatccaatactttaacaagaagaatgcc 3'

Primer for biochemical characterization		Primer for complex crystallization	
O176	5' tactccagcttcgccatcgcttagcaggcttgta 3'	O046	5' aaaggatccaacaagaagaatgccttgaag 3'
		O047	5' aaaggatccaatgccttgaaggagagaaaa 3'
		O049	5' aaaggatccacttctcaagcaagttggca 3'
		O050	5' aaaggatccgcctcatctcgagagtcatt 3'
		O051	5' ggactcgagtaatttgattacttaactctaa 3'
		O052	5' gccattgaacaatcttctctgaaaaattgcaa 3'
		O053	5' ttgcaatttttcagaggaagattgtcaatggc 3'
		O054	5' atggacctgaattcttacacattagaa 3'
		O055	5' ttctaattgtgaagaattcagggtccat 3'
		O056	5' gatgctgtctgtctaaattcaagt 3'
		O057	5' aactgaaatttagacaagacagcatc 3'
		O058	5' ctaataaccaaatctcccgcgttaa 3'
		O059	5' atttaacgcgggagatttggtattag 3'
		O067	5' ggactcgagtattgtgactccaataatgaatt 3'
		O068	5' ggactcgagtaagaatttttcgccaatttact 3'
		O070	5' aaaggatccttaaatctgctgaagaacgag 3'
		O114	5' aaaggatcctgtttagattaagtgatgaagtcaaa 3'
		O115	5' aaaggatcctgtagattaagtgatgaagtcaaa 3'
		O116	5' aaaggatcctgtgcaagattaagtgatgaagtcaaa 3'
		O125	5' aaaggatcccgtgagaaagttgcaaaga 3'
		O126	5' agaaattagttggcgaacgcatgcaaagttggctgctat 3'
		O127	5' atagcagccaaactttgcatcggttcgccaactaatttct 3'

Primer used for homologous recombination in yeast

O195	5' atgataaagtgaaaggttgggaatcgcaggacaacaagtaaaaccgaagcgtacgctgcaggctcgac 3'
O196	5' atacagaggcttagctactgtcagtaaaattataaaattagacagaaaacgtacgctgcaggctcgac 3'
O197	5' tatatgatatacatatatacatatagggcgtatatttactttgttcacatgaattcgagctcg 3'
O208	5' ttgatgtgtcgtactactaaatggcatgacaaatttgtaaattgaaaaaccgtacgctgcaggctcgac3'
O209	5' tattaactagtgtactatttgctcttttgagctaaaaactgaaggccatcgatgaattcgagctcg 3'

4.6 Antibodies

Name	Source	Dilution	Supplier
Alexa®488 anti-mouse-IgG	goat	1:250 (IF)	MoBiTec (Göttingen, Germany)
anti-HA (16B12)	mouse	1:1000 (IF)	HISS Diagnostics GmbH
anti-HA (3F10)	rat	1:1000 (Western)	Roche (Mannheim, Germany)
anti-myc (9E10)	mouse	1:50(IF,Western)	E. Kremmer (Helmholtz-Center Munich)
anti-mouse-IgG-HRP	goat	1:3000 (Western)	BioRad (Munich, Germany)
anti-rat-IgG-HRP	rabbit	1:10000 (Western)	Abcam (Cambridge, USA)

4.7 Molecular biology

4.7.1 Standard cloning methods

Standard methods for molecular biology like PCR, restriction digestion, ligation and the separation of DNA fragments were generally performed as indicated in Sambrook *et al.* (Sambrook and Russel 2000). Enzymes and buffers were used as recommended by the manufacturer. Purification of DNA products was performed using the NucleoSpin Extract II Kit (Macherey and Nagel, Dueren, Germany). Cleaved vector DNA was additionally treated with calf intestinal alkaline phosphatase (CIAP). Point mutations were introduced by PCR-based mutagenesis (Ho *et al.* 1989).

4.7.2 Transformation of *E. coli* and isolation of plasmid DNA

Preparation of chemically competent bacteria was performed according to Hanahan *et al.* (Hanahan 1983). The cells were aliquoted, flash frozen in liquid nitrogen and stored at -80°C. Transformation of plasmid DNA was essentially performed as described in Sambrook *et al.* (Sambrook and Russel 2000). Plasmid DNA was isolated from 5 ml overnight cultures using the NucleoSpin-Plasmid Kit (Macherey-Nagel). DNA sequencing to confirm the correctness of the plasmid DNA was performed by Medigenomix (Medigenomix, Martinsried, Germany).

4.7.3 Transformation of yeast cells

The protocol to transform PCR products for homologous recombination was adapted from Knop *et al.* (Knop *et al.* 1999). For ClonNAT (Werner BioAgents, Jena, Germany) selection, transformed cells were incubated at 30°C over night in YPD medium (chapter 4.11.1) before plating. Colonies were streaked out to single colonies on selection plates. Correct integration was analysed by western blot after alkaline yeast-cell lysis (Knop *et al.* 1999) and PCR.

4.7.4 Isolation of yeast genomic DNA

10 ml of a stationary yeast culture were sedimented, washed with 0.5 ml water and resuspended in 200 µl breaking buffer. Subsequently, 200 µl phenol/chloroform/isoamyl alcohol (24:24:1) and glass beads were added. The reaction was vortexed for 5 minutes, mixed with 200 µl TE buffer and centrifuged for 5 minutes at 16000 g at RT. The DNA containing aqueous phase was isolated and ethanol precipitated.

Breaking buffer: 2 % (v/v) Triton X-100, 1 % (v/v) SDS, 100 mM NaCl, 10 mM Tris-HCl pH 8.0, 1 mM EDTA pH 8.0

TE buffer: 10 mM Tris pH 7.5, 1 mM EDTA

4.8 Protein analysis

4.8.1 Protein separation by SDS-PAGE

Protein samples were analyzed by SDS-PAGE on 15 % polyacrylamide gels as described by Laemmli *et al.* (Laemmli 1970) using the vertical Mini-PROTEAN 3 System (Bio-Rad, Munich, Germany). Samples were mixed with loading dye and boiled for 2 minutes. After separation, gels were either stained with Coomassie-staining solution and discolored with water or applied to western blot analysis.

Coomassie staining solution: 50 % (v/v) ethanol, 7 % (v/v) acetic acid, 0.2 % Coomassie Brilliant blue R-250

4.8.2 Western blot

After SDS-PAGE, proteins were transferred onto a PVDF membrane (Millipore, Billerica, MA, USA), using the wet-blot method. The blotting procedure was performed at 4°C for 2 hours at 60 V. After transfer, the membrane was blocked with TBS-T containing 10 % milk powder, before the primary antibody (dissolved in TBS-T containing 2 % milk powder) was added and incubated overnight at 4°C. The membrane was washed 3 times for 5 minutes with TBS-T at RT and afterwards incubated with secondary antibody dissolved in TBS-T containing 2 % milk powder for 1h at RT. Visualization was performed using an ECL-Kit (Thermo-Scientific), followed by exposure of the membrane to light-sensitive films (GE Healthcare). The films were developed using a Kodak Xomat M35 developing machine.

Blot buffer: 10 mM NaHCO₃, 3 mM NaCO₃

TBS-T: 10 mM Tris HCl pH 8.0, 150 mM NaCl, 0,05 % Tween

4.9 Protein expression, purification and crystallization

4.9.1 Recombinant protein expression in *E. coli*

To overexpress recombinant proteins, competent *E. coli* BL21 (DE3) cells were transformed with plasmid DNA carrying the gene of interest. Cells were grown at 37°C in LB medium with the appropriate antibiotics to an OD₆₀₀ of 0.6-0.8. Cells were cooled down to 18°C and expression was induced by the addition of 0.2 mM IPTG. After growing for 12-16 hours at 18°C, cells were harvested by centrifugation at 4°C. Pellets were dissolved in lysis buffer, frozen in liquid N₂, and stored at -80°C.

LB medium: 1 % (w/v) tryptone, 0.5 % (w/v) yeast extract, 0.5 % (w/v) NaCl

Lysis buffer: 20 mM Tris, pH 7.5, 500 mM NaCl, 1 mM EDTA and 1 mM DTT

4.9.2 Selenomethionine labeling

To generate selenomethionine labeled protein, overexpression was performed with the *E. coli* strain B834 (DE3). Cells were grown in minimal medium, containing SeMet and the appropriate antibiotic. The overall procedure was identical to point 4.9.1.

Minimal media: 7,5 mM (NH₄)₂SO₄, 8,5 mM NaCl, 55 mM KH₂PO₄, 100 mM K₂HPO₄, 1 mM MgSO₄, 20 mM glucose, 1 mg/l CaCl₂, 1 mg/l FeCl₂, 1 µg/l of the following trace element: Cu²⁺; Mn²⁺; Zn²⁺; MoO₄²⁻, 1 mg/l Thiamine, 1 mg/l Biotin, 100 mg/l of the following amino acids (L-alanine, L-arginine, L-aspartic acid, L-cysteine, L-glutamate, L-glycine, L-histidine, L-isoleucine, L-leucine, L-lysine, L-phenylalanine, L-proline, L-serine, L-threonine, L-tyrosine, L-valine, SeMet)

4.9.3 Purification of Myo4p fragments

Myo4p fragments were expressed as GST-fusion proteins. Cells were resuspended in Lysis buffer and disrupted by sonification. Cell debris was removed by centrifugation. For purification, the respective supernatant was loaded onto a 5 ml HiTrap-GST column, equilibrated with the corresponding lysis buffer. After extensive washing with buffer-AM4, the column was floated with 6 ml buffer-AM4 containing 15 mg/ml Precision protease (GE Healthcare) and stored for 8 hours at 4°C. Cleaved protein was eluted with buffer-AM4 and directly applied to a MonoSP-HiTrap column for all Myo4p fragments containing the rod region and otherwise to a MonoQ-HiTrap column. Ion-exchange chromatography was performed using the Äkta System (GE Healthcare). Prior to protein loading, the ion exchange columns were equilibrated with the respective buffer-AM4 and protein was eluted with a gradient of 20 column volumes ranging from buffer-AM4 to buffer-BM4. The pooled peak fractions (the flow-through for the rod lacking Myo4p fragments) were concentrated using centrifugal filter devices (Millipore) and loaded onto a Superdex S200 16/60 size exclusion chromatography column, equilibrated with the buffer-AM4. SeMet-containing Myo4p-GT protein was purified as the wild-type protein, but all buffers were additionally degassed before use and contained 2 mM DTT.

Buffer-AM4: 10 mM Tris, pH 8.25, 200 mM NaCl and 1 mM DTT

Buffer-BM4: 10 mM Tris, pH 8.25, 1 M NaCl and 1 mM DTT

Lysis buffer: 20 mM Tris, pH 7.5, 500 mM NaCl, 1 mM EDTA and 1 mM DTT

4.9.4 Purification of She3p fragments

She3p fragments used for crystallization were expressed as GST-fusion proteins and essentially purified as the Myo4p fragments, using the buffer conditions mentioned below. After affinity purification, She3p fragments were loaded onto a MonoQ-HiTrap column.

For affinity chromatography of His-tagged She3p-N the protein was loaded onto a HisTrap column, equilibrated with Ni-lysis buffer. After extensive washing, protein was eluted with Ni-elution buffer. Subsequently, the protein was dialysed against 1.5 l of buffer-AS3. Cation-exchange chromatography was performed as described for She3p-GST fusion proteins.

Buffer-AS3: 10 mM Tris, pH 6.5, 100 mM NaCl and 1 mM DTT

Buffer-BS3: 10 mM Tris, pH 6.5, 1 M NaCl and 1 mM DTT

Lysis buffer: 20 mM Tris, pH 7.5, 500 mM NaCl, 1 mM EDTA and 1 mM DTT

Ni-elution buffer: 20 mM Tris, pH 7.5, 500 mM NaCl, 1 mM EDTA and 250 mM Imidazole

Ni-lysis buffer: 20 mM Tris, pH 7.5, 500 mM NaCl, 1 mM EDTA and 15 mM Imidazole

4.9.5 Crystallization and structure determination of the Myo4p-GT

After size exclusion chromatography, the protein solution was concentrated to 20 mg/ml using centrifugal filter devices (Millipore). The protein was crystallized by hanging drop vapour diffusion technique by mixing 1 μ l protein (20 - 12 mg/ml) and 1 μ l of reservoir solution at 20°C. Prior data collection, crystals were incubated for 2 minutes in cryoprotectant, mounted in nylon loops, and flash frozen in liquid nitrogen. Single wavelength anomalous dispersion (SAD) experiments were recorded at beamline X12 (DESY, Hamburg, detector type MAR CCD 225mm) with SeMet-containing crystals at the K absorption edge to 0.97776 Å. Data from 240 images (1 ° rotation) was integrated and scaled with XDS and XSCALE (Kabsch 1993). The Atomic positions for 14 Selenium atoms were located with SHELXD (Schneider and Sheldrick 2002). Native data were recorded at ID14-1 (ESRF, Grenoble France, detector type ADSC Q210 CCD) with a wavelength of 0.933 Å to a resolution of 2.3 Å. Data from 190 images (1 ° rotation) were integrated and scaled with Mosflm and SCALA (Collaborative Computational Project 1994, Leslie 1992). Phases to 2.3 Å were obtained with SHARP (Bricogne *et al.* 2003), using the anomalous and the native data set and phase extension. Resulting phases were used for automated building with ArpWarp (Perrakis *et al.* 1999). The model was manually completed using COOT. Refinement of the native data was performed with Refmac (Murshudov *et al.* 1997, Terwilliger 2002), using Twin-Lattice Symmetry (TLS, dividing each monomer in 2 domains) and Non-Crystallographic Symmetry (NCS). The final model was analyzed using SFCHECK (Vaguine *et al.* 1999)

Cryoprotectant: reservoir solution containing 20 % Ethylenglycol

Reservoir solution: 100 mM Hepes pH 8.5, 20 % PEG 3350, 150 mM HCO₂Na and 10 mM K₂Pt(CN)₄

4.9.6 Crystallization of the Myo4p-She3p complex

After proteins were purified individually, they were mixed with an excess of Myo4p and applied to a Superdex S200 16/60 size exclusion column. The complex was analyzed by SDS-PAGE, concentrated to 4 mg/ml using centrifugal filter devices (Millipore) and used in crystallization experiments. Initial screens were performed as sitting drop vapour diffusion experiments using the Hydra-II-robot system (Thermo Scientific) and commercially available crystallization screen in a 96 well format. The total reservoir volume was 80 μ l and 0.5 μ l of protein solution were mixed with 0.5 μ l of reservoir solution. Crystallization plates were incubated at 4°C and 20°C. Hanging drop vapour diffusion experiments were used to refine individual conditions. Here, 1 μ l protein was mixed with 1 μ l of the respective reservoir solution.

4.10 In vitro characterization of the Myo4p-tail function

4.10.1 Ni-pull down

50 μ g of each analyzed protein were incubated with 50 μ l of Ni-Sepharose for 1 hour in reaction buffer. Afterwards, the sepharose was washed five times with 200 μ l reaction buffer, followed by a final wash step with 50 μ l. Proteins were eluted with 50 μ l of elution buffer. For visualization: 1/10 of the input, 1/5 of the final wash, and 1/5 of the elution fraction was analyzed by SDS-PAGE and Coomassie staining.

Elution buffer: 20 mM Tris-HCl (pH 7.5), 200 mM NaCl, and 750 mM Imidazole

Reaction buffer: 20 mM Tris-HCl (pH 7.5), 200 mM NaCl, and 15 mM Imidazol

4.10.2 Surface Plasmon-Resonance

4.10.2.1 Myo4p-She3p-N interaction

All SRP experiments were performed using a Biacore 3000 system (GE Healthcare). She3p-N was attached to a CM5 chip surface (GE Healthcare) to signal levels below 200 RU by standard amine coupling. Myo4p fragments were applied in running buffer with the following concentration ranges: Myo4p-tail, 11 nM to 700 nM; Myo4p-GT, 1 μ M to 5 μ M, Myo4p-RGT, 170 nM to 5.5 μ M; Myo4p-CC, 88 nM to 5.6 μ M; Myo4p-GCN4, 27 nM to 860 nM; Myo4p-GST, 36 nM to 1.2 μ M. Equilibrium dissociation constants were derived from steady-state measurements, applying the Langmuir isotherm ($R_{eq} = K_A c R_{max} / (1 + c K_A)$), with R_{eq} : steady state binding level, K_A : association constant, c : analyte concentration, R_{max} : maximal binding level). $R_{max1/2}$ values were determined by using three independent measurements.

Running buffer: 10 mM Hepes, pH 7.5, 200 mM NaCl, and 50 mM EDTA

4.10.2.2 Myo4p-GT vesicle interaction

Vesicles were attached to a L1 chip surface (GE Healthcare) to signal levels below 300 RU by floating over the surface. Myo4p-GT was applied in running buffer with a concentration range from 100 nM to 3 μ M.

4.10.3 Floatation assay with ER-like protein-free liposomes

4.10.3.1. Preparation of protein free Liposomes

Liposomes containing the following lipid composition were prepared according to Qbadou *et al.* (Qbadou *et al.* 2003): Ergosterol 16 %, Phosphatidylcholine PC 40 %, Phosphatidylethanolamine PE 24 %, Phosphatidylserine PS 10 %, Phosphatidylinositol PI 10 %. Lipids were solved in chloroform/methanol and mixed in a darkened, evacuated round bottom flask. The mixture was dried by rotary evaporation and the lipid film was dissolved to a final total concentration of 10 mg/ml in degassed liposome buffer. To create unilamellar liposomes, the lipids were passed 20 times through a 400 nm pore polycarbonate filter membrane mounted in an extruder (Avestin, Mannheim, Germany). Liposomes were aliquoted, shock frozen in liquid N₂ and stored at – 80°C.

Liposome buffer: 20 mM HEPES pH 7.4, 100 mM NaCl

4.10.3.2 In vitro binding and floatation of liposomes

100 μ g of proteins were mixed with 1 mg of liposomes and filled up to 250 μ l with binding buffer. The mixture was incubated for 15 minutes at RT followed by 10 minutes on ice. Afterwards, the reaction was mixed with 3 ml binding buffer containing 70 % sucrose and transferred to the bottom of a SW40 ultraclear polycarbonate tube (Beckman, Krefeld, Germany). The sample-containing fraction was covered with 3 ml of binding buffer, each containing 50 %, 40 % and 0 % sucrose, respectively. After centrifugation to equilibrium (22000 rpm, 16.5 h, 4°C, SW40 rotor (Beckman)) the gradient was harvested from top to bottom in 1 ml fractions. Fractions were TCA precipitated, dissolved in 50 μ l HU-buffer and 1/5 of each fraction was analyzed by SDS-PAGE and coomassie staining.

Binding buffer: 50 mM Hepes/KOH pH 7.5, 150 mM KOAc, 1 mM MgOAc₂, 1mM EDTA, 1mM DTT

HU-buffer: 8 M Urea, 5 % (w/v) SDS, 200 mM Tris pH 6.8, 1 mM EDTA, 0,1 % (w/v) Bromphenolblue, 1,5 % (w/v) DTT

4.10.4 Reflectometric Interference Spectroscopy

The lipid composition and preparation was identical to chapter 4.10.3.1. To generate vesicles, the lipid mixture was sonified until the solution became clear. Subsequently the lipids were applied to a RfS setup (AG Piehler) and floated over a clean glass surface. The formation of a

unilaminar surface was observed via the RfS signal. The Myo4p-GT fragment was applied in liposome buffer with concentrations ranging from 500 nM to 3 μ M.

Liposome buffer: 20 mM HEPES pH 7.4, 100 mM NaCl

4.11. Fluorescence microscopy

4.11.1 Preparation of cells for Immunofluorescence microscopy

YPD or SDC media with the appropriate amino-acid mix were inoculated with a single yeast colony and incubated at 30°C. For Immunofluorescence, cells of a logarithmically growing cultures were fixed by adding 3.7 % formaldehyde to the growing culture and further incubation for 1 hour at 30°C while shaking. Cells were sedimented and washed three times with spheroplasting buffer. Spheroblasts were made by adding 500 μ l spheroplasting buffer containing 100 μ g/ml Zymolyase T100 (USBioLogical, Swampscott, USA) and 0.2 % β -Mercaptoethanol and incubation for 45 minutes at 30°C. Spheroplasts were washed and finally resuspended in 200 μ l spheroplasting buffer. The cell suspension was stored in aliquots at -80°C or used directly.

SCD: 0.67 % (w/v) yeast nitrogen base, 2 % glucose, amino acid supplement mixture

Spheroplasting buffer: 1.2 M Sorbitol, 0.1 M K_3PO_4 (pH 7.4), and 0.5 mM $MgCl_2$

YPD: 1 % yeast extract, 2 % peptone, 2 % glucose

4.11.2 Preparation of cells for fluorescence microscopy

To visualize GFP signals, cells were grown as described earlier (chapter 4.11.1). After reaching logarithmic phase, one ml of the culture was incubated with 500 μ l paraformaldehyde solution, mixed gently and incubated at RT for 10 minutes. Afterwards the cells were sedimented and the pellet was dissolved in 1x PBS and either directly used in fluorescence microscopy or stored at 4°C.

Paraformaldehyde solution: 10 % (w/v) Paraformaldehyde, 15 mM NaOH, 150 mM K_3PO_4

4.11.3 Fluorescence microscopy

Multi-well slides (Neolab) used for immunofluorescence microscopy were coated with 0.02 % Poly-L-Lysine (Sigma) for 5 minutes and washed with distilled water. A drop of the cell suspension was applied onto each well and incubated for 5 minutes. Cells were blocked for 5 minutes with block buffer. A dilute solution of the primary antibody in block buffer was put onto each well and incubated for 2 hours in a wet chamber. Afterwards, the wells were washed three times with washing buffer and subsequently incubated with diluted secondary antibodies in a darkened wet chamber for 1 hour. After another three rounds of washing, nuclei were stained with DAPI-Stain Solution (SIGMA) and cells were mounted in mounting buffer. Cells were

inspected with an Olympus BX60 fluorescence microscope (Olympus) and a 100x NA 1.3 DIC oil objective. Images were acquired using an ORCA ER CCD camera (Hamamatsu Photonics) controlled by Openlab 4.01 software (Improvision).

Block buffer: 1x PBS, 1 % BSA

Mounting solution 1x PBS, 80 % glycerol

PBS: 150 mM NaCl, 3 mM KCl, 12 mM Na₃PO₄ (pH 7.4)

Washing buffer 1x PBS, 1 % BSA, 0.1 % Triton X-100

4.12. Bioinformatics

4.12.1 Homology searches and alignments

DNA and protein sequences were found using the NCBI database (<http://www.ncbi.nlm.nih.gov>). Homology searches were performed using the NCBI Basic Local Alignment Search Tool (BLAST) server (<http://www.ncbi.nlm.nih.gov/BLAST>). Multiple sequence alignments were performed with JPred (Cole *et al.* 2008, <http://www.compbio.dundee.ac.uk/~www-jpred/>) and visualized with the program CLC-free-workbench (CLCbio, Alfortville, France).

4.12.2 Protein parameters

Physical and chemical parameters of the recombinant proteins were calculated with the program ProtParam (Wilkins *et al.* 1999, www.expasy.org/tools/protparam.html), the coiled-coil-formation propability was determined by the program COILS (Lupas *et al.* 1991, http://www.ch.embnet.org/software/COILS_form.html) and the hydrophobicity prediction by the program ProtScale (Wilkins *et al.* 1999) <http://ca.expasy.org/tools/protscale.html>) using the amino acid scale by Kyte & Doolittle (Kyte and Doolittle 1982). All programs are available via the ExPASy Proteomics Server (<http://ca.expasy.org/sitemap.html>).

4.12.3 Structure visualization and analysis

Calculations of buried surface areas of the molecule were performed with Surface (Collaborative Computational Project 1994). Superposition of two homologous structures and RMSD calculation was performed with LSQMAN (Uppsala software factory, <http://xray.bmc.uu.se/usf/>). Calculation and representation of the electrostatic surface was done with CCP4mg (Potterton *et al.* 2002). Images of the crystal structures were prepared with PyMol (DELANO, Palo Alto, USA) and Chimera (Pettersen *et al.* 2004).

5. Literature

- Alberts, B., Johnson, A., Lewis, J., Raff, M., Roberts, C. & Walter, P. (2003) *Molekularbiologie der Zelle* (Wiley-VCH).
- Altmann, K., Frank, M., Neumann, D., Jakobs, S. & Westermann, B. (2008) "The class V myosin motor protein, Myo2, plays a major role in mitochondrial motility in *Saccharomyces cerevisiae*" *J Cell Biol* **181**: 119-30.
- Angenstein, F., Evans, A. M., Ling, S. C., Settlege, R. E., Ficarro, S., Carrero-Martinez, F. A., Shabanowitz, J., Hunt, D. F. & Greenough, W. T. (2005) "Proteomic characterization of messenger ribonucleoprotein complexes bound to nontranslated or translated poly(A) mRNAs in the rat cerebral cortex" *J Biol Chem* **280**: 6496-503.
- Aronov, S., Gelin-Licht, R., Zipor, G., Haim, L., Safran, E. & Gerst, J. E. (2007) "mRNAs encoding polarity and exocytosis factors are cotransported with the cortical endoplasmic reticulum to the incipient bud in *Saccharomyces cerevisiae*" *Mol Cell Biol* **27**: 3441-55.
- Asakura, T., Sasaki, T., Nagano, F., Satoh, A., Obaishi, H., Nishioka, H., Imamura, H., Hotta, K., Tanaka, K., Nakanishi, H. & Takai, Y. (1998) "Isolation and characterization of a novel actin filament-binding protein from *Saccharomyces cerevisiae*" *Oncogene* **16**: 121-30.
- Au, J. S. & Huang, J. D. (2002) "A tissue-specific exon of myosin Va is responsible for selective cargo binding in melanocytes" *Cell Motil Cytoskeleton* **53**: 89-102.
- Ayscough, K. R. (2005) "Coupling actin dynamics to the endocytic process in *Saccharomyces cerevisiae*" *Protoplasma* **226**: 81-8.
- Beach, D. L., Thibodeaux, J., Maddox, P., Yeh, E. & Bloom, K. (2000) "The role of the proteins Kar9 and Myo2 in orienting the mitotic spindle of budding yeast" *Curr Biol* **10**: 1497-506.
- Bement, W. M., Hasson, T., Wirth, J. A., Cheney, R. E. & Mooseker, M. S. (1994) "Identification and overlapping expression of multiple unconventional myosin genes in vertebrate cell types" *Proc Natl Acad Sci U S A* **91**: 6549-53.
- Berg, J. S., Powell, B. C. & Cheney, R. E. (2001) "A millennial myosin census" *Mol Biol Cell* **12**: 780-94.
- Bertrand, E., Chartrand, P., Schaefer, M., Shenoy, S. M., Singer, R. H. & Long, R. M. (1998) "Localization of *ASH1* mRNA particles in living yeast" *Mol Cell* **2**: 437-45.
- Bi, E., Maddox, P., Lew, D. J., Salmon, E. D., McMillan, J. N., Yeh, E. & Pringle, J. R. (1998) "Involvement of an actomyosin contractile ring in *Saccharomyces cerevisiae* cytokinesis" *J Cell Biol* **142**: 1301-12.
- Bobola, N., Jansen, R. P., Shin, T. H. & Nasmyth, K. (1996) "Asymmetric accumulation of Ash1p in postanaphase nuclei depends on a myosin and restricts yeast mating-type switching to mother cells" *Cell* **84**: 699-709.
- Böhl, F., Kruse, C., Frank, A., Ferring, D. & Jansen, R. P. (2000) "She2p, a novel RNA-binding protein tethers *ASH1* mRNA to the Myo4p myosin motor via She3p" *Embo J* **19**: 5514-24.
- Bricogne, G., Vornrhein, C., Flensburg, C., Schiltz, M. & Paciorek, W. (2003) "Generation, representation and flow of phase information in structure determination: recent developments in and around SHARP 2.0" *Acta Crystallogr D Biol Crystallogr* **59**: 2023-30.

- Bridgman, P. C. (1999) "Myosin Va movements in normal and dilute-lethal axons provide support for a dual filament motor complex" *J Cell Biol* **146**: 1045-60.
- Casavola, E. C., Catucci, A., Bielli, P., Di Pentima, A., Porcu, G., Pennestri, M., Cicero, D. O. & Ragnini-Wilson, A. (2008) "Ypt32p and Mlc1p bind within the vesicle binding region of the class V myosin Myo2p globular tail domain" *Mol Microbiol* **67**: 1051-66.
- Catlett, N. L., Duex, J. E., Tang, F. & Weisman, L. S. (2000) "Two distinct regions in a yeast myosin-V tail domain are required for the movement of different cargoes" *J Cell Biol* **150**: 513-26.
- Chang, W., Zaarour, R. F., Reck-Peterson, S., Rinn, J., Singer, R. H., Snyder, M., Novick, P. & Mooseker, M. S. (2008) "Myo2p, a class V myosin in budding yeast, associates with a large ribonucleic acid-protein complex that contains mRNAs and subunits of the RNA-processing body" *RNA* **14**: 491-502.
- Chartrand, P., Meng, X. H., Huttelmaier, S., Donato, D. & Singer, R. H. (2002) "Asymmetric sorting of ash1p in yeast results from inhibition of translation by localization elements in the mRNA" *Mol Cell* **10**: 1319-30.
- Cheney, R. E., O'Shea, M. K., Heuser, J. E., Coelho, M. V., Wolenski, J. S., Espreafico, E. M., Forscher, P., Larson, R. E. & Mooseker, M. S. (1993) "Brain myosin-V is a two-headed unconventional myosin with motor activity" *Cell* **75**: 13-23.
- Cole, C., Barber, J. D. & Barton, G. J. (2008) "The Jpred 3 secondary structure prediction server" *Nucleic Acids Res* **36**: W197-201.
- Collaborative Computational Project (1994) "The CCP4 suite: programs for protein crystallography" *Acta Crystallogr D Biol Crystallogr* **50**: 760-3.
- Colon-Gonzalez, F. & Kazanietz, M. G. (2006) "C1 domains exposed: from diacylglycerol binding to protein-protein interactions" *Biochim Biophys Acta* **1761**: 827-37.
- Cope, M. J., Whisstock, J., Rayment, I. & Kendrick-Jones, J. (1996) "Conservation within the myosin motor domain: implications for structure and function" *Structure* **4**: 969-87.
- Correia, S. S., Bassani, S., Brown, T. C., Lise, M. F., Backos, D. S., El-Husseini, A., Passafaro, M. & Esteban, J. A. (2008) "Motor protein-dependent transport of AMPA receptors into spines during long-term potentiation" *Nat Neurosci* **11**: 457-66.
- Cosma, M. P. (2004) "Daughter-specific repression of *Saccharomyces cerevisiae* HO: *ASH1* is the commander" *EMBO Rep* **5**: 953-7.
- Coureux, P. D., Wells, A. L., Menetrey, J., Yengo, C. M., Morris, C. A., Sweeney, H. L. & Houdusse, A. (2003) "A structural state of the myosin V motor without bound nucleotide" *Nature* **425**: 419-23.
- DeLano, W. L. (2002) "The PyMOL Molecular Graphics System".
- Deng, Y., Singer, R. H. & Gu, W. (2008) "Translation of *ASH1* mRNA is repressed by Puf6p-Fun12p/eIF5B interaction and released by CK2 phosphorylation" *Genes Dev* **22**: 1037-50.
- Desnos, C., Huet, S., Fanget, I., Chapuis, C., Bottiger, C., Racine, V., Sibarita, J. B., Henry, J. P. & Darchen, F. (2007) "Myosin va mediates docking of secretory granules at the plasma membrane" *J Neurosci* **27**: 10636-45.

- Drubin, D. G., Miller, K. G. & Botstein, D. (1988) "Yeast actin-binding proteins: evidence for a role in morphogenesis" *J Cell Biol* **107**: 2551-61.
- Du, T. G., Jellbauer, S., Müller, M., Schmid, M., Niessing, D. & Jansen, R. P. (2008) "Nuclear transit of the RNA-binding protein She2 is required for translational control of localized *ASH1* mRNA" *EMBO Rep* **9**: 781-7.
- Du, Y., Ferro-Novick, S. & Novick, P. (2004) "Dynamics and inheritance of the endoplasmic reticulum" *J Cell Sci* **117**: 2871-8.
- Dumas, J. J., Merithew, E., Sudharshan, E., Rajamani, D., Hayes, S., Lawe, D., Corvera, S. & Lambright, D. G. (2001) "Multivalent endosome targeting by homodimeric EEA1" *Mol Cell* **8**: 947-58.
- Dunn, B. D., Sakamoto, T., Hong, M. S., Sellers, J. R. & Takizawa, P. A. (2007) "Myo4p is a monomeric myosin with motility uniquely adapted to transport mRNA" *J Cell Biol* **178**: 1193-206.
- Espindola, F. S., Espreafico, E. M., Coelho, M. V., Martins, A. R., Costa, F. R., Mooseker, M. S. & Larson, R. E. (1992) "Biochemical and immunological characterization of p190-calmodulin complex from vertebrate brain: a novel calmodulin-binding myosin" *J Cell Biol* **118**: 359-68.
- Espreafico, E. M., Cheney, R. E., Matteoli, M., Nascimento, A. A., De Camilli, P. V., Larson, R. E. & Mooseker, M. S. (1992) "Primary structure and cellular localization of chicken brain myosin-V (p190), an unconventional myosin with calmodulin light chains" *J Cell Biol* **119**: 1541-57.
- Estrada de Martin, P., Du, Y., Novick, P. & Ferro-Novick, S. (2005) "Ice2p is important for the distribution and structure of the cortical ER network in *Saccharomyces cerevisiae*" *J Cell Sci* **118**: 65-77.
- Estrada de Martin, P., Novick, P. & Ferro-Novick, S. (2005) "The organization, structure, and inheritance of the ER in higher and lower eukaryotes" *Biochem Cell Biol* **83**: 752-61.
- Estrada, P., Kim, J., Coleman, J., Walker, L., Dunn, B., Takizawa, P., Novick, P. & Ferro-Novick, S. (2003) "Myo4p and She3p are required for cortical ER inheritance in *Saccharomyces cerevisiae*" *J Cell Biol* **163**: 1255-66.
- Evangelista, M., Pruyne, D., Amberg, D. C., Boone, C. & Bretscher, A. (2002) "Formins direct Arp2/3-independent actin filament assembly to polarize cell growth in yeast" *Nat Cell Biol* **4**: 260-9.
- Fagarasanu, A., Fagarasanu, M., Eitzen, G. A., Aitchison, J. D. & Rachubinski, R. A. (2006) "The peroxisomal membrane protein Inp2p is the peroxisome-specific receptor for the myosin V motor Myo2p of *Saccharomyces cerevisiae*" *Dev Cell* **10**: 587-600.
- Ford, M. G., Mills, I. G., Peter, B. J., Vallis, Y., Praefcke, G. J., Evans, P. R. & McMahon, H. T. (2002) "Curvature of clathrin-coated pits driven by epsin" *Nature* **419**: 361-6.
- Ford, M. G., Pearse, B. M., Higgins, M. K., Vallis, Y., Owen, D. J., Gibson, A., Hopkins, C. R., Evans, P. R. & McMahon, H. T. (2001) "Simultaneous binding of PtdIns(4,5)P₂ and clathrin by AP180 in the nucleation of clathrin lattices on membranes" *Science* **291**: 1051-5.

- Fukuda, M. & Itoh, T. (2004) "Slac2-a/melanophilin contains multiple PEST-like sequences that are highly sensitive to proteolysis" *J Biol Chem* **279**: 22314-21.
- Fukuda, M. & Kuroda, T. S. (2004) "Missense mutations in the globular tail of myosin-Va in dilute mice partially impair binding of Slac2-a/melanophilin" *J Cell Sci* **117**: 583-91.
- Ghaemmaghani, S., Huh, W. K., Bower, K., Howson, R. W., Belle, A., Dephoure, N., O'Shea, E. K. & Weissman, J. S. (2003) "Global analysis of protein expression in yeast" *Nature* **425**: 737-41.
- Golemis, E. & Adams, P. (2005) *Protein-Protein Interactions: A Molecular Cloning Manual* (Cold Spring Harbor Laboratory Press).
- Gomes, A. Q., Ali, B. R., Ramalho, J. S., Godfrey, R. F., Barral, D. C., Hume, A. N. & Seabra, M. C. (2003) "Membrane targeting of Rab GTPases is influenced by the prenylation motif" *Mol Biol Cell* **14**: 1882-99.
- Gonsalvez, G. B., Lehmann, K. A., Ho, D. K., Stanitsa, E. S., Williamson, J. R. & Long, R. M. (2003) "RNA-protein interactions promote asymmetric sorting of the *ASH1* mRNA ribonucleoprotein complex" *RNA* **9**: 1383-99.
- Gonsalvez, G. B., Little, J. L. & Long, R. M. (2004) "*ASH1* mRNA anchoring requires reorganization of the Myo4p-She3p-She2p transport complex" *J Biol Chem* **279**: 46286-94.
- Gonsalvez, G. B., Urbinati, C. R. & Long, R. M. (2005) "RNA localization in yeast: moving towards a mechanism" *Biol Cell* **97**: 75-86.
- Gonzalez, I., Buonomo, S. B., Nasmyth, K. & von Ahsen, U. (1999) "*ASH1* mRNA localization in yeast involves multiple secondary structural elements and Ash1 protein translation" *Curr Biol* **9**: 337-40.
- Gu, W., Deng, Y., Zenklusen, D. & Singer, R. H. (2004) "A new yeast PUF family protein, Puf6p, represses *ASH1* mRNA translation and is required for its localization" *Genes Dev* **18**: 1452-65.
- Haarer, B. K., Petzold, A., Lillie, S. H. & Brown, S. S. (1994) "Identification of MYO4, a second class V myosin gene in yeast" *J Cell Sci* **107 (Pt 4)**: 1055-64.
- Hales, C. M., Vaerman, J. P. & Goldenring, J. R. (2002) "Rab11 family interacting protein 2 associates with Myosin Vb and regulates plasma membrane recycling" *J Biol Chem* **277**: 50415-21.
- Hanahan, D. (1983) "Studies on transformation of *Escherichia coli* with plasmids" *J Mol Biol* **166**: 557-80.
- Hasegawa, Y., Irie, K. & Gerber, A. P. (2008) "Distinct roles for Khd1p in the localization and expression of bud-localized mRNAs in yeast" *RNA* **14**: 2333-47.
- Heuck, A., Du, T. G., Jellbauer, S., Richter, K., Kruse, C., Jaklin, S., Müller, M., Buchner, J., Jansen, R. P. & Niessing, D. (2007) "Monomeric myosin V uses two binding regions for the assembly of stable translocation complexes" *Proc Natl Acad Sci U S A* **104**: 19778-83.
- Hirokawa, N. (1998) "Kinesin and dynein superfamily proteins and the mechanism of organelle transport" *Science* **279**: 519-26.

- Hirokawa, N., Pfister, K. K., Yorifuji, H., Wagner, M. C., Brady, S. T. & Bloom, G. S. (1989) "Submolecular domains of bovine brain kinesin identified by electron microscopy and monoclonal antibody decoration" *Cell* **56**: 867-78.
- Ho, S. N., Hunt, H. D., Horton, R. M., Pullen, J. K. & Pease, L. R. (1989) "Site-directed mutagenesis by overlap extension using the polymerase chain reaction" *Gene* **77**: 51-9.
- Hodges, A. R., Kremetsova, E. B. & Trybus, K. M. (2008) "She3p binds to the rod of yeast myosin V and prevents it from dimerizing, forming a single-headed motor complex" *J Biol Chem* **283**: 6906-14.
- Hodi, Z., Nemeth, A. L., Radnai, L., Hetenyi, C., Schlett, K., Bodor, A., Perczel, A. & Nyitray, L. (2006) "Alternatively spliced exon B of myosin Va is essential for binding the tail-associated light chain shared by dynein" *Biochemistry* **45**: 12582-95.
- Hook, P. & Vallee, R. B. (2006) "The dynein family at a glance" *J Cell Sci* **119**: 4369-71.
- Huang, J. D., Mermall, V., Strobel, M. C., Russell, L. B., Mooseker, M. S., Copeland, N. G. & Jenkins, N. A. (1998) "Molecular genetic dissection of mouse unconventional myosin-VA: tail region mutations" *Genetics* **148**: 1963-72.
- Huckaba, T. M., Gay, A. C., Pantalena, L. F., Yang, H. C. & Pon, L. A. (2004) "Live cell imaging of the assembly, disassembly, and actin cable-dependent movement of endosomes and actin patches in the budding yeast, *Saccharomyces cerevisiae*" *J Cell Biol* **167**: 519-30.
- Inoue, A. & Ikebe, M. (2003) "Characterization of the motor activity of mammalian myosin VIIA" *J Biol Chem* **278**: 5478-87.
- Inoue, A., Saito, J., Ikebe, R. & Ikebe, M. (2002) "Myosin IXb is a single-headed minus-end-directed processive motor" *Nat Cell Biol* **4**: 302-6.
- Irie, K., Tadauchi, T., Takizawa, P. A., Vale, R. D., Matsumoto, K. & Herskowitz, I. (2002) "The Khd1 protein, which has three KH RNA-binding motifs, is required for proper localization of *ASH1* mRNA in yeast" *Embo J* **21**: 1158-67.
- Ishikawa, K., Catlett, N. L., Novak, J. L., Tang, F., Nau, J. J. & Weisman, L. S. (2003) "Identification of an organelle-specific myosin V receptor" *J Cell Biol* **160**: 887-97.
- Iwaki, M., Tanaka, H., Iwane, A. H., Katayama, E., Ikebe, M. & Yanagida, T. (2006) "Cargo-binding makes a wild-type single-headed myosin-VI move processively" *Biophys J* **90**: 3643-52.
- Janke, C., Magiera, M. M., Rathfelder, N., Taxis, C., Reber, S., Maekawa, H., Moreno-Borchart, A., Doenges, G., Schwob, E., Schiebel, E. & Knop, M. (2004) "A versatile toolbox for PCR-based tagging of yeast genes: new fluorescent proteins, more markers and promoter substitution cassettes" *Yeast* **21**: 947-62.
- Jansen, R. P., Dowzer, C., Michaelis, C., Galova, M. & Nasmyth, K. (1996) "Mother cell-specific HO expression in budding yeast depends on the unconventional myosin myo4p and other cytoplasmic proteins" *Cell* **84**: 687-97.
- Jin, Y., Eves, P. T., Tang, F. & Weisman, L. S. (2008) "PTC1 Is Required for Vacuole Inheritance and Promotes the Association of the Myosin-V Vacuole-specific Receptor Complex" *Mol Biol Cell*.

- Juschke, C., Wachter, A., Schwappach, B. & Seedorf, M. (2005) "SEC18/NSF-independent, protein-sorting pathway from the yeast cortical ER to the plasma membrane" *J Cell Biol* **169**: 613-22.
- Kabsch, W. (1993) "Automatic processing of rotation diffraction data from crystals of initially unknown symmetry and cell constants." *J Appl Cryst* . 795-800.
- Kaksonen, M., Sun, Y. & Drubin, D. G. (2003) "A pathway for association of receptors, adaptors, and actin during endocytic internalization" *Cell* **115**: 475-87.
- Kanai, Y., Dohmae, N. & Hirokawa, N. (2004) "Kinesin transports RNA: isolation and characterization of an RNA-transporting granule" *Neuron* **43**: 513-25.
- Kantardjieff, K. A. & Rupp, B. (2003) "Matthews coefficient probabilities: Improved estimates for unit cell contents of proteins, DNA, and protein-nucleic acid complex crystals" *Protein Sci* **12**: 1865-71.
- Kini, A. R. & Collins, C. A. (2001) "Modulation of cytoplasmic dynein ATPase activity by the accessory subunits" *Cell Motil Cytoskeleton* **48**: 52-60.
- Klein, D. E., Lee, A., Frank, D. W., Marks, M. S. & Lemmon, M. A. (1998) "The pleckstrin homology domains of dynamin isoforms require oligomerization for high affinity phosphoinositide binding" *J Biol Chem* **273**: 27725-33.
- Klopfenstein, D. R., Tomishige, M., Stuurman, N. & Vale, R. D. (2002) "Role of phosphatidylinositol(4,5)bisphosphate organization in membrane transport by the Unc104 kinesin motor" *Cell* **109**: 347-58.
- Knop, M., Siegers, K., Pereira, G., Zachariae, W., Winsor, B., Nasmyth, K. & Schiebel, E. (1999) "Epitope tagging of yeast genes using a PCR-based strategy: more tags and improved practical routines" *Yeast* **15**: 963-72.
- Komaba, S., Inoue, A., Maruta, S., Hosoya, H. & Ikebe, M. (2003) "Determination of human myosin III as a motor protein having a protein kinase activity" *J Biol Chem* **278**: 21352-60.
- Komili, S., Farny, N. G., Roth, F. P. & Silver, P. A. (2007) "Functional specificity among ribosomal proteins regulates gene expression" *Cell* **131**: 557-71.
- Kon, T., Nishiura, M., Ohkura, R., Toyoshima, Y. Y. & Sutoh, K. (2004) "Distinct functions of nucleotide-binding/hydrolysis sites in the four AAA modules of cytoplasmic dynein" *Biochemistry* **43**: 11266-74.
- Koning, A. J., Lum, P. Y., Williams, J. M. & Wright, R. (1993) "DiOC6 staining reveals organelle structure and dynamics in living yeast cells" *Cell Motil Cytoskeleton* **25**: 111-28.
- Krementsov, D. N., Krementsova, E. B. & Trybus, K. M. (2004) "Myosin V: regulation by calcium, calmodulin, and the tail domain" *J Cell Biol* **164**: 877-86.
- Krementsova, E. B., Hodges, A. R., Lu, H. & Trybus, K. M. (2006) "Processivity of chimeric class V myosins" *J Biol Chem* **281**: 6079-86.
- Krendel, M. & Mooseker, M. S. (2005) "Myosins: tails (and heads) of functional diversity" *Physiology (Bethesda)* **20**: 239-51.
- Kukimoto-Niino, M., Sakamoto, A., Kanno, E., Hanawa-Suetsugu, K., Terada, T., Shirouzu, M., Fukuda, M. & Yokoyama, S. (2008) "Structural basis for the exclusive specificity of Slac2-a/melanophilin for the Rab27 GTPases" *Structure* **16**: 1478-90.

- Kuriyama, M., Harada, N., Kuroda, S., Yamamoto, T., Nakafuku, M., Iwamatsu, A., Yamamoto, D., Prasad, R., Croce, C., Canaani, E. & Kaibuchi, K. (1996) "Identification of AF-6 and canoe as putative targets for Ras" *J Biol Chem* **271**: 607-10.
- Kutateladze, T. G. (2006) "Phosphatidylinositol 3-phosphate recognition and membrane docking by the FYVE domain" *Biochim Biophys Acta* **1761**: 868-77.
- Kyte, J. & Doolittle, R. F. (1982) "A simple method for displaying the hydropathic character of a protein" *J Mol Biol* **157**: 105-32.
- Laemmli, U. K. (1970) "Cleavage of structural proteins during the assembly of the head of bacteriophage T4" *Nature* **227**: 680-5.
- Lange, S., Katayama, Y., Schmid, M., Burkacky, O., Brauchle, C., Lamb, D. C. & Jansen, R. P. (2008) "Simultaneous transport of different localized mRNA species revealed by live-cell imaging" *Traffic* **9**: 1256-67.
- Lapierre, L. A., Kumar, R., Hales, C. M., Navarre, J., Bhartur, S. G., Burnette, J. O., Provance, D. W., Jr., Mercer, J. A., Bahler, M. & Goldenring, J. R. (2001) "Myosin vb is associated with plasma membrane recycling systems" *Mol Biol Cell* **12**: 1843-57.
- Lawrence, C. J., Dawe, R. K., Christie, K. R., Cleveland, D. W., Dawson, S. C., Endow, S. A., Goldstein, L. S., Goodson, H. V., Hirokawa, N., Howard, J., Malmberg, R. L., McIntosh, J. R., Miki, H., Mitchison, T. J., Okada, Y., Reddy, A. S., Saxton, W. M., Schliwa, M., Scholey, J. M., Vale, R. D., Walczak, C. E. & Wordeman, L. (2004) "A standardized kinesin nomenclature" *J Cell Biol* **167**: 19-22.
- Legesse-Miller, A., Zhang, S., Santiago-Tirado, F. H., Van Pelt, C. K. & Bretscher, A. (2006) "Regulated phosphorylation of budding yeast's essential myosin V heavy chain, Myo2p" *Mol Biol Cell* **17**: 1812-21.
- Lemmon, M. A. (2008) "Membrane recognition by phospholipid-binding domains" *Nat Rev Mol Cell Biol* **9**: 99-111.
- Lemmon, M. A. & Ferguson, K. M. (2000) "Signal-dependent membrane targeting by pleckstrin homology (PH) domains" *Biochem J* **350 Pt 1**: 1-18.
- Leslie, A. G. W. (1992) "Recent changes to the MOSFLM package for processing film and image plate data" *Joint CCP4 + ESF-EAMCB Newsletter on Protein Crystallography* **29**.
- Li, J. F. & Nebenfuhr, A. (2007) "Organelle targeting of myosin XI is mediated by two globular tail subdomains with separate cargo binding sites" *J Biol Chem* **282**: 20593-602.
- Li, X. D., Jung, H. S., Mabuchi, K., Craig, R. & Ikebe, M. (2006) "The globular tail domain of myosin Va functions as an inhibitor of the myosin Va motor" *J Biol Chem* **281**: 21789-98.
- Li, X. D., Jung, H. S., Wang, Q., Ikebe, R., Craig, R. & Ikebe, M. (2008) "The globular tail domain puts on the brake to stop the ATPase cycle of myosin Va" *Proc Natl Acad Sci U S A* **105**: 1140-5.
- Lipatova, Z., Tokarev, A. A., Jin, Y., Mulholland, J., Weisman, L. S. & Segev, N. (2008) "Direct interaction between a myosin V motor and the Rab GTPases Ypt31/32 is required for polarized secretion" *Mol Biol Cell* **19**: 4177-87.

- Lippincott, J. & Li, R. (1998) "Sequential assembly of myosin II, an IQGAP-like protein, and filamentous actin to a ring structure involved in budding yeast cytokinesis" *J Cell Biol* **140**: 355-66.
- Liu, J., Taylor, D. W., Kremmentsova, E. B., Trybus, K. M. & Taylor, K. A. (2006) "Three-dimensional structure of the myosin V inhibited state by cryoelectron tomography" *Nature* **442**: 208-11.
- Long, R. M., Gu, W., Lorimer, E., Singer, R. H. & Chartrand, P. (2000) "She2p is a novel RNA-binding protein that recruits the Myo4p-She3p complex to *ASH1* mRNA" *Embo J* **19**: 6592-601.
- Long, R. M., Gu, W., Meng, X., Gonsalvez, G., Singer, R. H. & Chartrand, P. (2001) "An exclusively nuclear RNA-binding protein affects asymmetric localization of *ASH1* mRNA and Ash1p in yeast" *J Cell Biol* **153**: 307-18.
- Long, R. M., Singer, R. H., Meng, X., Gonzalez, I., Nasmyth, K. & Jansen, R. P. (1997) "Mating type switching in yeast controlled by asymmetric localization of *ASH1* mRNA" *Science* **277**: 383-7.
- Longtine, M. S. & Bi, E. (2003) "Regulation of septin organization and function in yeast" *Trends Cell Biol* **13**: 403-9.
- Lopez de Heredia, M. & Jansen, R. P. (2004) "mRNA localization and the cytoskeleton" *Curr Opin Cell Biol* **16**: 80-5.
- Lu, H., Kremmentsova, E. B. & Trybus, K. M. (2006) "Regulation of myosin V processivity by calcium at the single molecule level" *J Biol Chem* **281**: 31987-94.
- Lupas, A., Van Dyke, M. & Stock, J. (1991) "Predicting coiled coils from protein sequences" *Science* **252**: 1162-4.
- Ma, B., Elkayam, T., Wolfson, H. & Nussinov, R. (2003) "Protein-protein interactions: structurally conserved residues distinguish between binding sites and exposed protein surfaces" *Proc Natl Acad Sci U S A* **100**: 5772-7.
- Macedo-Ribeiro, S., Bode, W., Huber, R., Quinn-Allen, M. A., Kim, S. W., Ortel, T. L., Bourenkov, G. P., Bartunik, H. D., Stubbs, M. T., Kane, W. H. & Fuentes-Prior, P. (1999) "Crystal structures of the membrane-binding C2 domain of human coagulation factor V" *Nature* **402**: 434-9.
- Mallik, R. & Gross, S. P. (2004) "Molecular motors: strategies to get along" *Curr Biol* **14**: R971-82.
- Matthews, B. W. (1968) "Solvent content of protein crystals" *J Mol Biol* **33**: 491-7.
- Mehta, A. D., Rock, R. S., Rief, M., Spudich, J. A., Mooseker, M. S. & Cheney, R. E. (1999) "Myosin-V is a processive actin-based motor" *Nature* **400**: 590-3.
- Mercer, J. A., Seperack, P. K., Strobel, M. C., Copeland, N. G. & Jenkins, N. A. (1991) "Novel myosin heavy chain encoded by murine dilute coat colour locus" *Nature* **349**: 709-13.
- Miki, H., Okada, Y. & Hirokawa, N. (2005) "Analysis of the kinesin superfamily: insights into structure and function" *Trends Cell Biol* **15**: 467-76.
- Moseley, J. B. & Goode, B. L. (2006) "The yeast actin cytoskeleton: from cellular function to biochemical mechanism" *Microbiol Mol Biol Rev* **70**: 605-45.

- Munchow, S., Sauter, C. & Jansen, R. P. (1999) "Association of the class V myosin Myo4p with a localised messenger RNA in budding yeast depends on She proteins" *J Cell Sci* **112** (Pt **10**): 1511-8.
- Murshudov, G. N., Vagin, A. A. & Dodson, E. J. (1997) "Refinement of macromolecular structures by the maximum-likelihood method" *Acta Crystallogr D Biol Crystallogr* **53**: 240-55.
- Naisbitt, S., Valtschanoff, J., Allison, D. W., Sala, C., Kim, E., Craig, A. M., Weinberg, R. J. & Sheng, M. (2000) "Interaction of the postsynaptic density-95/guanylate kinase domain-associated protein complex with a light chain of myosin-V and dynein" *J Neurosci* **20**: 4524-34.
- Nascimento, A. A., Amaral, R. G., Bizario, J. C., Larson, R. E. & Espreafico, E. M. (1997) "Subcellular localization of myosin-V in the B16 melanoma cells, a wild-type cell line for the dilute gene" *Mol Biol Cell* **8**: 1971-88.
- Niessing, D., Huttelmaier, S., Zenklusen, D., Singer, R. H. & Burley, S. K. (2004) "She2p is a novel RNA binding protein with a basic helical hairpin motif" *Cell* **119**: 491-502.
- O'Connell, C. B. & Mooseker, M. S. (2003) "Native Myosin-IXb is a plus-, not a minus-end-directed motor" *Nat Cell Biol* **5**: 171-2.
- Olivier, C., Poirier, G., Gendron, P., Boisgontier, A., Major, F. & Chartrand, P. (2005) "Identification of a conserved RNA motif essential for She2p recognition and mRNA localization to the yeast bud" *Mol Cell Biol* **25**: 4752-66.
- Paquin, N., Menade, M., Poirier, G., Donato, D., Drouet, E. & Chartrand, P. (2007) "Local activation of yeast *ASH1* mRNA translation through phosphorylation of Khd1p by the casein kinase Yck1p" *Mol Cell* **26**: 795-809.
- Park, H., Li, A., Chen, L. Q., Houdusse, A., Selvin, P. R. & Sweeney, H. L. (2007) "The unique insert at the end of the myosin VI motor is the sole determinant of directionality" *Proc Natl Acad Sci U S A* **104**: 778-83.
- Park, H., Ramamurthy, B., Travaglia, M., Safer, D., Chen, L. Q., Franzini-Armstrong, C., Selvin, P. R. & Sweeney, H. L. (2006) "Full-length myosin VI dimerizes and moves processively along actin filaments upon monomer clustering" *Mol Cell* **21**: 331-6.
- Pashkova, N., Catlett, N. L., Novak, J. L. & Weisman, L. S. (2005) "A point mutation in the cargo-binding domain of myosin V affects its interaction with multiple cargoes" *Eukaryot Cell* **4**: 787-98.
- Pashkova, N., Catlett, N. L., Novak, J. L., Wu, G., Lu, R., Cohen, R. E. & Weisman, L. S. (2005) "Myosin V attachment to cargo requires the tight association of two functional subdomains" *J Cell Biol* **168**: 359-64.
- Pashkova, N., Jin, Y., Ramaswamy, S. & Weisman, L. S. (2006) "Structural basis for myosin V discrimination between distinct cargoes" *Embo J* **25**: 693-700.
- Pelham, R. J., Jr. & Chang, F. (2001) "Role of actin polymerization and actin cables in actin-patch movement in *Schizosaccharomyces pombe*" *Nat Cell Biol* **3**: 235-44.
- Peng, Y. & Weisman, L. S. (2008) "The cyclin-dependent kinase Cdk1 directly regulates vacuole inheritance" *Dev Cell* **15**: 478-85.

- Perrakis, A., Morris, R. & Lamzin, V. S. (1999) "Automated protein model building combined with iterative structure refinement" *Nat Struct Biol* **6**: 458-63.
- Pettersen, E. F., Goddard, T. D., Huang, C. C., Couch, G. S., Greenblatt, D. M., Meng, E. C. & Ferrin, T. E. (2004) "UCSF Chimera--a visualization system for exploratory research and analysis" *J Comput Chem* **25**: 1605-12.
- Ponting, C. P. (1995) "AF-6/cno: neither a kinesin nor a myosin, but a bit of both" *Trends Biochem Sci* **20**: 265-6.
- Post, P. L., Bokoch, G. M. & Mooseker, M. S. (1998) "Human myosin-IXb is a mechanochemically active motor and a GAP for rho" *J Cell Sci* **111** (Pt 7): 941-50.
- Post, P. L., Tyska, M. J., O'Connell, C. B., Johung, K., Hayward, A. & Mooseker, M. S. (2002) "Myosin-IXb is a single-headed and processive motor" *J Biol Chem* **277**: 11679-83.
- Potterton, E., McNicholas, S., Krissinel, E., Cowtan, K. & Noble, M. (2002) "The CCP4 molecular-graphics project" *Acta Crystallogr D Biol Crystallogr* **58**: 1955-7.
- Prinz, W. A., Grzyb, L., Veenhuis, M., Kahana, J. A., Silver, P. A. & Rapoport, T. A. (2000) "Mutants affecting the structure of the cortical endoplasmic reticulum in *Saccharomyces cerevisiae*" *J Cell Biol* **150**: 461-74.
- Provance, D. W., Jr., Wei, M., Ipe, V. & Mercer, J. A. (1996) "Cultured melanocytes from dilute mutant mice exhibit dendritic morphology and altered melanosome distribution" *Proc Natl Acad Sci U S A* **93**: 14554-8.
- Puthalakath, H., Villunger, A., O'Reilly, L. A., Beaumont, J. G., Coultas, L., Cheney, R. E., Huang, D. C. & Strasser, A. (2001) "Bmf: a proapoptotic BH3-only protein regulated by interaction with the myosin V actin motor complex, activated by anoikis" *Science* **293**: 1829-32.
- Qbadou, S., Tien, R., Soll, J. & Schleiff, E. (2003) "Membrane insertion of the chloroplast outer envelope protein, Toc34: constrains for insertion and topology" *J Cell Sci* **116**: 837-46.
- Reck-Peterson, S. L., Novick, P. J. & Mooseker, M. S. (1999) "The tail of a yeast class V myosin, myo2p, functions as a localization domain" *Mol Biol Cell* **10**: 1001-17.
- Reck-Peterson, S. L., Provance, D. W., Jr., Mooseker, M. S. & Mercer, J. A. (2000) "Class V myosins" *Biochim Biophys Acta* **1496**: 36-51.
- Reck-Peterson, S. L., Tyska, M. J., Novick, P. J. & Mooseker, M. S. (2001) "The yeast class V myosins, Myo2p and Myo4p, are nonprocessive actin-based motors" *J Cell Biol* **153**: 1121-6.
- Reinhard, J., Scheel, A. A., Diekmann, D., Hall, A., Ruppert, C. & Bahler, M. (1995) "A novel type of myosin implicated in signalling by rho family GTPases" *Embo J* **14**: 697-704.
- Reisen, D. & Hanson, M. R. (2007) "Association of six YFP-myosin XI-tail fusions with mobile plant cell organelles" *BMC Plant Biol* **7**: 6.
- Richards, T. A. & Cavalier-Smith, T. (2005) "Myosin domain evolution and the primary divergence of eukaryotes" *Nature* **436**: 1113-8.
- Rogers, S., Wells, R. & Rechsteiner, M. (1986) "Amino acid sequences common to rapidly degraded proteins: the PEST hypothesis" *Science* **234**: 364-8.

- Rogers, S. L., Karcher, R. L., Roland, J. T., Minin, A. A., Steffen, W. & Gelfand, V. I. (1999) "Regulation of melanosome movement in the cell cycle by reversible association with myosin V" *J Cell Biol* **146**: 1265-76.
- Roland, J. T., Lapierre, L. A. & Goldenring, J. R. (2009) "Alternative splicing in class v myosins determines association with rab10" *J Biol Chem* **284**: 1213-23.
- Sagot, I., Klee, S. K. & Pellman, D. (2002) "Yeast formins regulate cell polarity by controlling the assembly of actin cables" *Nat Cell Biol* **4**: 42-50.
- Sagot, I., Rodal, A. A., Moseley, J., Goode, B. L. & Pellman, D. (2002) "An actin nucleation mechanism mediated by Bni1 and profilin" *Nat Cell Biol* **4**: 626-31.
- Salerno, V. P., Calliari, A., Provance, D. W., Jr., Sotelo-Silveira, J. R., Sotelo, J. R. & Mercer, J. A. (2008) "Myosin-Va mediates RNA distribution in primary fibroblasts from multiple organs" *Cell Motil Cytoskeleton* **65**: 422-33.
- Sambrook, J. & Russel, D. W. (2000) *Molecular Cloning: A Laboratory Manual* (Cold Spring Harbor Laboratory).
- Schmid, M., Jaedicke, A., Du, T. G. & Jansen, R. P. (2006) "Coordination of endoplasmic reticulum and mRNA localization to the yeast bud" *Curr Biol* **16**: 1538-43.
- Schneider, T. R. & Sheldrick, G. M. (2002) "Substructure solution with SHELXD" *Acta Crystallogr D Biol Crystallogr* **58**: 1772-9.
- Schott, D., Ho, J., Pruyne, D. & Bretscher, A. (1999) "The COOH-terminal domain of Myo2p, a yeast myosin V, has a direct role in secretory vesicle targeting" *J Cell Biol* **147**: 791-808.
- Seaman, M. N. & Williams, H. P. (2002) "Identification of the functional domains of yeast sorting nexins Vps5p and Vps17p" *Mol Biol Cell* **13**: 2826-40.
- Sellers, J. R. & Veigel, C. (2006) "Walking with myosin V" *Curr Opin Cell Biol* **18**: 68-73.
- Seperack, P. K., Mercer, J. A., Strobel, M. C., Copeland, N. G. & Jenkins, N. A. (1995) "Retroviral sequences located within an intron of the dilute gene alter dilute expression in a tissue-specific manner" *Embo J* **14**: 2326-32.
- Shen, Z., Paquin, N., Forget, A. & Chartrand, P. (2009) "Nuclear Shuttling of She2p Couples *ASH1* mRNA Localization to its Translational Repression by Recruiting Loc1p and Puf6p" *Mol Biol Cell*.
- Shepard, K. A., Gerber, A. P., Jambhekar, A., Takizawa, P. A., Brown, P. O., Herschlag, D., DeRisi, J. L. & Vale, R. D. (2003) "Widespread cytoplasmic mRNA transport in yeast: identification of 22 bud-localized transcripts using DNA microarray analysis" *Proc Natl Acad Sci U S A* **100**: 11429-34.
- Sil, A. & Herskowitz, I. (1996) "Identification of asymmetrically localized determinant, Ash1p, required for lineage-specific transcription of the yeast HO gene" *Cell* **84**: 711-22.
- Smith, M. G., Swamy, S. R. & Pon, L. A. (2001) "The life cycle of actin patches in mating yeast" *J Cell Sci* **114**: 1505-13.
- Spudich, G., Chibalina, M. V., Au, J. S., Arden, S. D., Buss, F. & Kendrick-Jones, J. (2007) "Myosin VI targeting to clathrin-coated structures and dimerization is mediated by binding to Disabled-2 and PtdIns(4,5)P2" *Nat Cell Biol* **9**: 176-83.

- Stahelin, R. V., Long, F., Peter, B. J., Murray, D., De Camilli, P., McMahon, H. T. & Cho, W. (2003) "Contrasting membrane interaction mechanisms of AP180 N-terminal homology (ANTH) and epsin N-terminal homology (ENTH) domains" *J Biol Chem* **278**: 28993-9.
- Takagishi, Y., Oda, S., Hayasaka, S., Dekker-Ohno, K., Shikata, T., Inouye, M. & Yamamura, H. (1996) "The dilute-lethal (dl) gene attacks a Ca²⁺ store in the dendritic spine of Purkinje cells in mice" *Neurosci Lett* **215**: 169-72.
- Takizawa, P. A., Sil, A., Swedlow, J. R., Herskowitz, I. & Vale, R. D. (1997) "Actin-dependent localization of an RNA encoding a cell-fate determinant in yeast" *Nature* **389**: 90-3.
- Takizawa, P. A. & Vale, R. D. (2000) "The myosin motor, Myo4p, binds *ASH1* mRNA via the adapter protein, She3p" *Proc Natl Acad Sci U S A* **97**: 5273-8.
- Tang, F., Kauffman, E. J., Novak, J. L., Nau, J. J., Catlett, N. L. & Weisman, L. S. (2003) "Regulated degradation of a class V myosin receptor directs movement of the yeast vacuole" *Nature* **422**: 87-92.
- TerBush, D. R., Maurice, T., Roth, D. & Novick, P. (1996) "The Exocyst is a multiprotein complex required for exocytosis in *Saccharomyces cerevisiae*" *Embo J* **15**: 6483-94.
- Terwilliger, T. C. (2002) "Automated structure solution, density modification and model building" *Acta Crystallogr D Biol Crystallogr* **58**: 1937-40.
- Thirumurugan, K., Sakamoto, T., Hammer, J. A., 3rd, Sellers, J. R. & Knight, P. J. (2006) "The cargo-binding domain regulates structure and activity of myosin 5" *Nature* **442**: 212-5.
- Toonen, R. F., Kochubey, O., de Wit, H., Gulyas-Kovacs, A., Konijnenburg, B., Sorensen, J. B., Klingauf, J. & Verhage, M. (2006) "Dissecting docking and tethering of secretory vesicles at the target membrane" *Embo J* **25**: 3725-37.
- Trautwein, M., Dengjel, J., Schirle, M. & Spang, A. (2004) "Arf1p provides an unexpected link between COPI vesicles and mRNA in *Saccharomyces cerevisiae*" *Mol Biol Cell* **15**: 5021-37.
- Tyson, C. B., Lord, P. G. & Wheals, A. E. (1979) "Dependency of size of *Saccharomyces cerevisiae* cells on growth rate" *J Bacteriol* **138**: 92-8.
- Urbinati, C. R., Gonsalvez, G. B., Aris, J. P. & Long, R. M. (2006) "Loc1p is required for efficient assembly and nuclear export of the 60S ribosomal subunit" *Mol Genet Genomics* **276**: 369-77.
- Uyeda, T. Q., Abramson, P. D. & Spudich, J. A. (1996) "The neck region of the myosin motor domain acts as a lever arm to generate movement" *Proc Natl Acad Sci U S A* **93**: 4459-64.
- Vaguine, A. A., Richelle, J. & Wodak, S. J. (1999) "SFCHECK: a unified set of procedures for evaluating the quality of macromolecular structure-factor data and their agreement with the atomic model" *Acta Crystallogr D Biol Crystallogr* **55**: 191-205.
- Vale, R. D. (2003) "The molecular motor toolbox for intracellular transport" *Cell* **112**: 467-80.
- Vallee, R. B., Williams, J. C., Varma, D. & Barnhart, L. E. (2004) "Dynein: An ancient motor protein involved in multiple modes of transport" *J Neurobiol* **58**: 189-200.
- Vaughan, P. S., Leszyk, J. D. & Vaughan, K. T. (2001) "Cytoplasmic dynein intermediate chain phosphorylation regulates binding to dynactin" *J Biol Chem* **276**: 26171-9.

- Veigel, C., Schmitz, S., Wang, F. & Sellers, J. R. (2005) "Load-dependent kinetics of myosin-V can explain its high processivity" *Nat Cell Biol* **7**: 861-9.
- Villace, P., Marion, R. M. & Ortin, J. (2004) "The composition of Staufen-containing RNA granules from human cells indicates their role in the regulated transport and translation of messenger RNAs" *Nucleic Acids Res* **32**: 2411-20.
- Vreugde, S., Ferrai, C., Miluzio, A., Hauben, E., Marchisio, P. C., Crippa, M. P., Bussi, M. & Biffo, S. (2006) "Nuclear myosin VI enhances RNA polymerase II-dependent transcription" *Mol Cell* **23**: 749-55.
- Waddle, J. A., Karpova, T. S., Waterston, R. H. & Cooper, J. A. (1996) "Movement of cortical actin patches in yeast" *J Cell Biol* **132**: 861-70.
- Wang, F., Thirumurugan, K., Stafford, W. F., Hammer, J. A., 3rd, Knight, P. J. & Sellers, J. R. (2004) "Regulated conformation of myosin V" *J Biol Chem* **279**: 2333-6.
- Warrick, H. M. & Spudich, J. A. (1987) "Myosin structure and function in cell motility" *Annu Rev Cell Biol* **3**: 379-421.
- Watanabe, M., Nomura, K., Ohyama, A., Ishikawa, R., Komiya, Y., Hosaka, K., Yamauchi, E., Taniguchi, H., Sasakawa, N., Kumakura, K., Ushiki, T., Sato, O., Ikebe, M. & Igarashi, M. (2005) "Myosin-Va regulates exocytosis through the submicromolar Ca²⁺-dependent binding of syntaxin-1A" *Mol Biol Cell* **16**: 4519-30.
- Wei, Q., Wu, X. & Hammer, J. A., 3rd (1997) "The predominant defect in dilute melanocytes is in melanosome distribution and not cell shape, supporting a role for myosin V in melanosome transport" *J Muscle Res Cell Motil* **18**: 517-27.
- Wells, A. L., Lin, A. W., Chen, L. Q., Safer, D., Cain, S. M., Hasson, T., Carragher, B. O., Milligan, R. A. & Sweeney, H. L. (1999) "Myosin VI is an actin-based motor that moves backwards" *Nature* **401**: 505-8.
- Wiederkehr, A., De Craene, J. O., Ferro-Novick, S. & Novick, P. (2004) "Functional specialization within a vesicle tethering complex: bypass of a subset of exocyst deletion mutants by Sec1p or Sec4p" *J Cell Biol* **167**: 875-87.
- Wiederkehr, A., Du, Y., Pypaert, M., Ferro-Novick, S. & Novick, P. (2003) "Sec3p is needed for the spatial regulation of secretion and for the inheritance of the cortical endoplasmic reticulum" *Mol Biol Cell* **14**: 4770-82.
- Wilkins, M. R., Gasteiger, E., Bairoch, A., Sanchez, J. C., Williams, K. L., Appel, R. D. & Hochstrasser, D. F. (1999) "Protein identification and analysis tools in the ExPASy server" *Methods Mol Biol* **112**: 531-52.
- Wollert, T., Weiss, D. G., Gerdes, H. H. & Kuznetsov, S. A. (2002) "Activation of myosin V-based motility and F-actin-dependent network formation of endoplasmic reticulum during mitosis" *J Cell Biol* **159**: 571-7.
- Wu, X., Bowers, B., Rao, K., Wei, Q. & Hammer, J. A., 3rd (1998) "Visualization of melanosome dynamics within wild-type and dilute melanocytes suggests a paradigm for myosin V function *In vivo*" *J Cell Biol* **143**: 1899-918.
- Wu, X., Sakamoto, T., Zhang, F., Sellers, J. R. & Hammer, J. A., 3rd (2006) "*In vitro* reconstitution of a transport complex containing Rab27a, melanophilin and myosin Va" *FEBS Lett* **580**: 5863-8.

- Wu, X. S., Rao, K., Zhang, H., Wang, F., Sellers, J. R., Matesic, L. E., Copeland, N. G., Jenkins, N. A. & Hammer, J. A., 3rd (2002) "Identification of an organelle receptor for myosin-Va" *Nat Cell Biol* **4**: 271-8.
- Yengo, C. M. & Sweeney, H. L. (2004) "Functional role of loop 2 in myosin V" *Biochemistry* **43**: 2605-12.
- Yildiz, A., Forkey, J. N., McKinney, S. A., Ha, T., Goldman, Y. E. & Selvin, P. R. (2003) "Myosin V walks hand-over-hand: single fluorophore imaging with 1.5-nm localization" *Science* **300**: 2061-5.
- Yoshimura, A., Fujii, R., Watanabe, Y., Okabe, S., Fukui, K. & Takumi, T. (2006) "Myosin-Va facilitates the accumulation of mRNA/protein complex in dendritic spines" *Curr Biol* **16**: 2345-51.
- Zhang, G., Kazanietz, M. G., Blumberg, P. M. & Hurley, J. H. (1995) "Crystal structure of the cys2 activator-binding domain of protein kinase C delta in complex with phorbol ester" *Cell* **81**: 917-24.
- Zhu, H., Bilgin, M., Bangham, R., Hall, D., Casamayor, A., Bertone, P., Lan, N., Jansen, R., Bidlingmaier, S., Houfek, T., Mitchell, T., Miller, P., Dean, R. A., Gerstein, M. & Snyder, M. (2001) "Global analysis of protein activities using proteome chips" *Science* **293**: 2101-5.

Acknowledgment

Of course many people had their contribution to this work and I would thank especially ...

... Dierk Niessing for giving me the opportunity to do my thesis in his lab and for teaching me to interpret results in a constructive and positive way. I am very grateful for the excellent working conditions and atmosphere, from which I could benefit over the last three and a half years.

... Ralf-Peter Jansen for his accordance to advice my thesis and many tips, which helped me to benefit from his deep experience with the SHE machinery.

... Karl-Peter Hopfner for being the second examiner of my thesis.

... the entire Niessing lab for a nice and constructive atmosphere:

Sigrun, her golden hands are legendary to solve every cloning problems

Marisa, for nice discussions and critical comments on this thesis

Daniela, for her acceptance that I used her workplace in case mine was too overcrowded

and all the others for a really nice time ...

... Susi, Maria, Stephan and Tung for their patience to show me how to get familiar with yeast.

... Michael, who discovered the Myo4p-GT crystals during a practical course.

... my collaborators

Gabriele Möller and Jerzy Adamski, who enabled me almost unlimited Biacore access

Klaus Richter and Johannes Buchner for the AUC analyses

Friedrich Roder and Jacob Piehler for an interesting introduction into RfS

... Sabine, this work would never be possible without her, for many discussions, and proof readings but especially for her persistence to build me up again after exhausting days in the lab with all experiments going wrong.

... my whole family, especially my parents, for their support and the encouragement to continuously follow my way.

Curriculum Vitae

Name	Alexander Heuck
Date of birth	31.12.1980
Place of birth	Rodewisch
Nationality	German

Education and Qualifications

2005-2009	PhD thesis in the lab of Dr. D. Niessing (Gene Center Munich) <i>“Characterization of a myosin transport complex from yeast”</i>
2004-2005	Diploma thesis in the lab of Prof. Dr. S. Diekmann (Fritz-Lippmann Institute, Jena) <i>“In vitro interaction studies on proteins of the inner kinetochore”</i>
2000-2004	Study of biochemistry at the Friedrich Schiller University, Jena <i>Diploma</i>
1999-2000	Civil service at the hospital “Obergöltzsch Rodewisch”
1992-1999	Secondary school (J.-H. Pestalozzi school, Rodewisch) <i>Abitur (general university-entrance diploma)</i>
1987-1992	Primary school (G.-E. Lessing school, Lengenfeld)

Publications

Müller, M., Heuck, A. & Niessing, D. (2007) "Directional mRNA transport in eukaryotes: lessons from yeast" *Cell Mol Life Sci* 64: 171-80.

Heuck, A., Du, T. G., Jellbauer, S., Richter, K., Kruse, C., Jaklin, S., Müller, M., Buchner, J., Jansen, R. P. & Niessing, D. (2007) "Monomeric myosin V uses two binding regions for the assembly of stable translocation complexes" *Proc Natl Acad Sci U S A* 104: 19778-83.